Separation of Carboxylic Acids From Aqueous Fraction of Fast Pyrolysis Bio-Oils Using Nanofiltration and Reverse Osmosis Membranes

SEPARATION OF CARBOXYLIC ACIDS FROM AQUEOUS FRACTION OF FAST PYROLYSIS BIO-OILS USING NANOFILTRATION AND REVERSE OSMOSIS MEMBRANES

A Dissertation Presented

by

ACHYUTA VARA PRASADA RAO TEELLA

Submitted to the Graduate School of the

University of Massachusetts Amherst in partial fulfillment

of the requirements for the degree of

DOCTOR OF PHILOSOPHY

September 2011

Chemical Engineering

SEPARATION OF CARBOXYLIC ACIDS FROM AQUEOUS FRACTION OF FAST PYROLYSIS BIO-OILS USING NANOFILTRATION AND REVERSE OSMOSIS MEMBRANES

A Dissertation Presented

by

ACHYUTA VARA PRASADA RAO TEELLA

Approved as to style and content by:

_____
David M. Ford, Chair

_____
George W. Huber, Member

_____
Sankaran Thayumanavan, Member

_____
T. J. (Lakis) Mountziaris, Department Head
Chemical Engineering

ACKNOWLEDGEMENTS

I would like to express my deepest regard and appreciation to my advisor, Prof. David M. Ford, for his encouragement, guidance and support throughout my doctoral study. His patience, good humor and kindness have left a lasting impression on me.

I would like express my gratitude to Prof. George W. Huber and Prof. Sankaran Thayumanavan for being my committee membranes. Their flexibility, help, and suggestions during the course of this research have been greatly appreciated. I am greatly indebted to Dr. Suk Joon Yoo (John) for his help in building up our lab and for sharing all his experience and knowledge. I am also thankful to Dr. Asad Javaid for his invaluable suggestions in preparing my proposal. It was a wonderful experience working with him in the lab. I would like to thank Prof. Ford's entire group members for providing a friendly and fun environment in the group. I would also like to thank all the Chemical Engineering Department staff members who either directly or indirectly helped me in pursuit of my research.

I would like to thank all the people I met here at UMass that made my six years of stay happy and memorable. I owe a special gratitude to my parents, my sister Hyma, and my brothers Hari and Venu who always supported and believed in me. Their encouragement and unconditional love made possible what I have today. Lastly I would like to acknowledge my funding agencies. This work was supported by UMASS Chemical Engineering Department through start-up fund and by the U. S. Department of Energy Office of Energy Efficiency and Renewable Energy, under grant DE-FG36-08GO18212.

ABSTRACT

SEPARATION OF CARBOXYLIC ACIDS FROM AQUEOUS FRACTION OF FAST PYROLYSIS BIO-OILS USING NANOFILTRATION AND REVERSE OSMOSIS MEMBRANES

SEPTEMBER 2011

ACHYUTA VARA PRASADA RAO TEELLA, B.TECH., ANDHRA UNIVERSITY;

M.TECH., INDIAN INSTITUTE OF TECHNOLOGY, BOMBAY;

Ph.D., UNIVERSITY OF MASSACHUSETTS AMHERST

Directed by: Professor David M. Ford

There has been a growing interest in renewable sources of energy due to an increase in demand and potential shortages and environmental problems associated with fossil fuels. Bio-oils, complex liquid fuels produced from fast pyrolysis of biomass, have been recognized as one potential source of renewable energy. However, they cannot be utilized directly due to their high viscosity, corrosiveness, and high char content. Bio-oils readily phase separate into aqueous phase and organic phase upon addition of water. The aqueous fraction of bio oil (AFBO) is convenient to process and contains sugars, organic acids, hydroxyacetone, hydroxyacetaldehyde, furfural, phenols and other organic species that can potentially be converted to hydrogen, alkanes, aromatics, or olefins. However, the acidity of AFBO (pH ~2.5) is relatively high due to the presence of organic acids which can impose more demands on construction equipment of the vessels and the upgrading process. Removal of acids is essential to use AFBO as a commercial fuel or further upgrading into fuels or chemicals. Traditional separation techniques for the

removal of acids from AFBO, like ion exchange and distillation are not attractive due to practical limitations.

Membrane-based separations have been increasingly employed due to their inherent advantages over conventional separations methods. Pressure driven membrane processes like nanofiltration (NF) and reverse osmosis (RO) have been used in chemical, electronics, textile, petrochemical, pulp and paper, and food industries as well as for the treatment of municipal wastewater and landfill leachates. However, these processes are targeted for aqueous systems containing little or no organic solvents. The use of membranes to separate organic solvent solutions or organic-rich aqueous solutions is still at a very early stage.

The feasibility of removing small organic acids from the AFBO using NF and RO membranes was studied. Experiments were conducted with commercially available polymeric NF and RO membranes and aqueous solutions of increasing complexity, i.e. single solute solutions of acetic acid and glucose, binary solute solutions containing both acetic acid and glucose, and a model AFBO containing acetic acid, glucose, formic acid, hydroxyacetone, furfural, guaiacol, and catechol. Feed concentrations (up to 34 % solute by weight) close to those in real AFBO were chosen. These were generally at least an order of magnitude higher than previously studied in the literature for related membrane separations. Retention factors for single and binary solutions of acetic acid and glucose were promising so that the separation was expected to be feasible. However, all the membranes were irreversibly damaged when experiments were conducted with the model AFBO due to the presence of guaiacol in the feed solution. Experiments with model AFBO excluding guaiacol were also conducted. NF membranes showed retention factors of glucose greater than 80% and of acetic acid less than -15% when operated at transmembrane pressures near 60 bar. Finally, the solution-diffusion (SD)

model was applied to predict the permeate flux and solute retention and compared to the experimental results.

In another study, we explored the potential of nanocomposite membranes in gas separations. Solubility based membrane gas separation, in which the more soluble (and perhaps slower-diffusing) species preferentially permeates through the membranes, has received considerable attention due to both economic and environmental concerns. In this work, we synthesized organic-inorganic nanocomposite membranes by decorating the surfaces of commercially available alumina substrates with a selective organic material that is physically or chemically anchored to the porous surfaces. Hyperbranched melamine-based dendrimers and polydimethylsiloxane (PDMS) were used as filling agents. Separation factors for propane/nitrogen and carbon dioxide/methane were obtained for modified membranes. The separation performance of PDMS-alumina composite membranes was comparable to the currently best known polymers being used for this type of application.

TABLE OF CONTENTS

LIST OF TABLES

Table **Page**

LIST OF FIGURES

Figure **Page**

CHAPTER 1

INTRODUCTION

There is a growing interest in renewable sources of energy due to the economical, political and environmental issues associated with fossil fuels [1]. Biomass is the only renewable source of organic carbon. It is composed of polymers such as cellulose, hemicellulose and lignin. The employment of these lignocellulosics directly as chemical feedstock is difficult due to their complex structure, and thus they must be refined to forms that are easy and economical to use. One of the promising technologies is fast pyrolysis of biomass to liquid fuels [2-4]. In fast pyrolysis, bio-oil is produced by rapidly heating biomass to moderately high temperature (around 500 °C) in the absence of oxygen followed by rapid quenching of the resulting vapors. Bio-oil is a complex mixture of more than 300 compounds resulting from the depolymerization and fragmentation of lignocellulosics [4]. However, the direct use of bio-oil as a fuel is limited due to its poor fuel quality. The poor fuel quality of bio-oils is due to its high viscosity, corrosiveness and high char content. Bio-oil can be separated into two phases by using water extraction: the hydrophilic aqueous phase and the organophilic phase. Aqueous fraction of bio-oil (AFBO) contains compounds like levoglucosan and glucose along with organic acids and other low molecular weight hydrocarbons. The acidity (pH ~ 2.5) of AFBO is relatively high due to the presence of organic acids which can impose more demands processing equipment. Therefore removal of acids is essential to use AFBO as a commercial fuel or as an intermediate in the production of fuels and chemicals. Conventional acid removal methods are not attractive due to economical and practical concerns. Membrane separation technology can be used as an alternative for the deacidification of AFBO.

Membrane separation technology has been employed in wide range of applications and the number of such applications is growing rapidly. Today, membrane processes are used in chemical, petrochemical, water treatment, food, dairy, pharmaceutical, paper, textile and electronic industries [5, 6]. Membrane-based separations are often more capital and energy efficient when compared to well-established separation processes like distillation, adsorption and absorption.

Pressure driven membrane processes for liquid phase separations include microfiltration (MF), ultrafiltration (UF), nanofiltration (NF) and reverse osmosis (RO). These processes can be used to concentrate or purify a dilute (aqueous or non-aqueous) solution. Because of a driving force, i.e., the transmembrane pressure, the solvent and various solute molecules permeate through the membrane, while other molecules or particles are retained to various extents dependent on the structure of the membrane. Membranes used for MF and UF applications are typically porous and separation is accomplished by a size-sieving mechanism, where as NF and RO membranes have an essentially non-porous separating layer and separation is governed by a solution-diffusion mechanism.

Nanofiltration and reverse osmosis membranes for aqueous applications are quite similar in chemical composition and membrane preparation. However, mass transport in NF is more complicated than in RO because – in addition to solution-diffusion mechanism – size and charge exclusion are also usually involved. Ideally, polymeric membranes for NF and RO should be hydrophilic, resistant to chemicals, and microbial attack, and they should be mechanically, thermally, and structurally stable over the long period of operation. Most of commercial RO and NF membranes are polyamide-based thin film composites (TFCs). NF and RO are used when low molecular weight solutes such as inorganic salts or small organic molecules such as glucose,

and sucrose have to be separated from a solvent. The primary difference between NF and RO is the size of the dissolved contaminants that can be removed. NF membranes are typically used for bivalent hardness, calcium and magnesium plus sulphates and organics (sugars, dyes, and pesticides) removal. RO membranes are typically used for total dissolved solids (TDS) and monovalent ion removal (e.g., sea water and brackish water desalting, F^-, and Cl^- removal). However most of the applications are in water treatment, for drinking-water production [7], desalination [8], wastewater treatment [9] and process water recycling [10].

The use of membranes to separate organic solvent solutions is still at a very early stage. A difficult problem that prevented the utilization of NF and RO in organic solvents for a long time was the limited stability of polymeric NF and RO membranes, and the lack of ceramic nanofiltration membranes. For polymeric membranes various problems occurred: nonselective flux due to membrane swelling [11], zero flux due to membrane collapse [11], membrane deterioration [12], poor separation quality [13], etc. Developing membranes for processing organic solvent solutions is more challenging than conventional NF and RO membranes because different membranes must be developed for each type of solvent. The first solvent-permeable membrane is the Starmem® series of solvent-resistant membranes developed by W. R. Grace [14]. These membranes found their first large scale commercial use in the separation of methyl ethyl ketone-toluene solvent mixture from lube oil [15]. Development of such solvent resistant membranes is essential in expanding membrane technology to more important refining operations, such as fractionation of linear and branched paraffins, or the separation of benzene and other aromatics from paraffins and olefins in the gasoline pool.

The objective of this research was to implement membrane technology to reduce the acidity of AFBO, thus stabilizing it for long-term storage and further processing. The main goal

was to reject low molecular weight acids while retaining glucose and other heavier compounds. Different commercially available NF and RO membranes were examined for the separation. The effects of pretreatment, cross flow velocity, pressure and concentration on membrane performance were explored. Chemical compatibility of these membranes against different organic compounds was investigated.

The outline of this dissertation is as follows. Chapter II provides a background on fast pyrolysis bio-oil and review of membrane separations used for acid removal. Chapter III describes the experimental procedure for liquid permeation experiments and list of chromatographic analyses used. The results and discussion of these permeation experiments are given in Chapter IV. Chapter V details the comparison of experimental results with solution-diffusion (SD) model calculations for single solute solutions of glucose and acetic acid. Chapter VI details the background, experimental procedure and results and discussion of synthesis of organic-inorganic composite membranes and their gas permeance characteristics. Finally, Chapter VII discusses our major conclusions and gives the summary of the work conducted.

CHAPTER 2

LITERATURE REVIEW

2.1. Bio-oil

Biomass is one of the main renewable energy resources available and offers the only source of renewable solid, liquid and gaseous fuels [3, 16]. Biomass is composed of polymers such as cellulose, hemicellulose and lignin. The utilization of these lignocellulosics directly as chemical feedstock is difficult due to their complex structure, and thus they must be refined to more convenient forms.

One of the simplest refining technologies is fast pyrolysis [4, 17, 18]. Fast pyrolysis is a moderately high temperature (around 500 °C) process in which biomass is rapidly heated in the absence of oxygen and the resulting vapors are cooled to give a liquid product called bio-oil. Depending on its source, bio-oil typically contains organics (about 70-80 wt %) of varying polarity and water (about 20-30 wt %) [3, 19]. Organics include acids (formic, acetic, propanoic), aldehydes (acetaldehyde, hydroxyacetaldehyde), ketones (acetone, hydroxyacetone, hydroxybutanone), sugars (glucose, xylose, fructose), alcohols, esters, furans, furfurals, guaiacols, and some micron sized char particles. The low cost of bio-oil production by fast pyrolysis makes it a competitive technology compared to other biofuel technologies such as gasification and cellulosic ethanol [20-23]. However, the direct use of bio-oil as a replacement for petroleum derived liquid transportation fuel is limited due to its insolubility in petroleum derived fuels, corrosiveness, phase instability, high viscosity, and high char content. The composition of the bio-oil, storage conditions, and storage time affect the properties [24]. Further processing is necessary to stabilize or upgrade it.

Bio-oil can be separated into an aqueous phase and a heavier organic phase upon addition of water. The aqueous fraction of bio-oil (AFBO) contains sugars, organic acids, hydroxyacetone, hydroxyacetaldehyde, furfural, and small amounts of guaiacols that may be further upgraded to produce hydrogen, alkanes, aromatics, or olefins [25-28]. However, the acidity of AFBO is relatively high (pH ~ 2.5) due to the presence of organic acids, which can cause corrosion in downstream processing equipment that is made of low quality materials (e.g. carbon steel). Furthermore, the organic acids could be valuable byproducts if they could be separated and sold. Therefore, removal of acids is important to the use of AFBO as an intermediate in the production of fuels and chemicals.

2.2 Acid Removal by Traditional Methods

There are several possible techniques for the removal of acids from AFBO. A related separation, the removal of acetic acid from hemicellulosic hydrolysates (mixture of five and six carbon sugars obtained from hydrolysis of hemicellulose), has been done with ion exchange resins [29]. However, resin based separations have a number of limitations. The resins must be regenerated with stoichiometric amounts of bases to remove the acids. The pressure drop across the bed is usually high and pore diffusion is generally slow leading to increased processing time. In addition to ion exchange resins, several other methods such as extraction, neutralization, vacuum evaporation, charcoal adsorption, and over-liming have been applied to remove acetic acid from the hydrolysates. Parajo et al. [30], Mussatto and Roberto [31], and Huang et al. [32] provide detailed reviews of these methods. Separation of bio-oil components by distillation would be difficult because the oil decomposes to form coke and some light gases when heated to temperatures above 80^{o}C [18].

Membrane separation is an alternative technology to remove acids that does not require the use of stoichiometric reagents. For example, processes such as adsorptive membrane and membrane extraction were used to remove acetic acid from hydrolysates [33, 34]. However, the use of membrane separation in bio-energy, in particular for acid removal, is still in its infancy. Membrane separation technology, which is the focus of this study, is explained in detail in the next section.

2.3 Membrane Separation Technology

Membrane technologies have seen a major growth and increase in separation applications in the last 40 years. A membrane can be defined as a permselective barrier or interphase between two phases. Separation is achieved because of different permeation rates of species across the membrane. Membrane separation processes offer a number of significant benefits over conventional separation processes, like cryogenic distillation, absorption and adsorption. First, energy requirements, and in some cases also capital investment costs, are lower than those for traditional separation processes in important industrial applications. Second, the required process equipment is simple, compact, and relatively easy to operate and control. Furthermore, this equipment is modular and can be easily scaled up or operated at partial capacity. As a result, membrane separations have acquired a significant role in the industry.

The first recorded observation of a membrane phenomenon appears to have been by Abbe Nollet in 1748, who discovered osmosis in natural membranes. In 1855, Fick employed synthetic membranes, made from nitrocellulose, to develop his mathematical model of diffusion [35]. The first reference to a separation procedure by means of a membrane is Graham's use of dialyzer in 1854, to separate a solution into its components [36]. In 1863, his work on porous membranes led to Graham's law of diffusion and subsequently, in 1866, he gave the first

description of the "solution-diffusion" model for permeation of gases in nonporous membranes [37]. During the next 30 years, Traube and Pfeffer prepared artificial membranes and their research with osmotic phenomena led to the well known van't Hoff osmotic pressure relationship [38]. The first series of microfiltration membranes of graded pore size were synthesized by Bechhold in 1907. He first defined the relationship between the membrane performance and the physical properties such as pore size and surface tension [39]. Other early workers, especially, Zsigmondy and Bachmann [40], Elford [41], and Ferry [42] improved on Bechhold's technique and by the early 1930s microporous collodian membranes were commercially available. During the next 20 years, many other polymeric materials were found and tried in a substantial number of applications and subsequent studies were done about diffusion across various kinds of membranes with porous, non-porous, glassy and rubbery characteristics. By 1960, the elements of modern science had been developed and ample knowledge was available on the relationships between the structure and property in membranes. However, membranes were used in only a few laboratory and small, specialized industrial applications because they were unreliable, very slow, unselective and too expensive.

The breakthrough discovery that transformed membrane separation from laboratory to an industrial process was the development of defect-free, high-flux, asymmetric cellulose acetate reverse osmosis membranes by Loeb and Sourirajan in 1962 [43]. These membranes consist of an ultrathin dense top layer (thickness < 0.5 μm) on a much thicker (50 – 200 μm) but more permeable microporous sublayer, which provides the mechanical support. The flux of this reverse osmosis membrane was 10 times higher than that of any membrane available at that time and made reverse osmosis a practical method of desalting water.

The period from 1960 to 1980 produced a substantial change in the status of membrane technology. Several other membrane formation processes, including interfacial polymerization and multilayer composite casting and coating, were developed for making high performance membranes. Techniques for packaging membranes into large surface area modules, such as spiral-wound, hollow fiber, and plate-and-frame, were also developed, and advances were made in enhancing membrane stability. By 1980, microfiltration, ultrafiltration, reverse osmosis and electrodialysis were all well established with large plants installed worldwide.

The principal development in the 1980s was the work of Henis and Tripodi [44] that made industrial gas separation economically feasible. They coated an asymmetric polysulfone membrane with a very thin homogenous layer of silicone polymer with high gas permeability. Silicone is extremely permeable compared to polysulfone but has a much lower selectivity; thus, the coating did not substantially change the flux or selectivity through the defect-free portions of the polysulfone membrane. However, the coating plugged membrane defects in the membrane and eliminated convective flow through these defects. The silicone layer also protected the membrane during handling. The development of these composite membranes was a critical step in the installment by Monsanto of the first successful large scale gas separations plants for hydrogen/nitrogen separations. Considerable work is presently in progress in academic and industrial laboratories in order to improve the economics of existing membrane processes, as well as to extend the range of applications of this technology.

A membrane process, in its basic form, is illustrated in Figure 1. A feed stream is divided into two streams, i.e. permeate and retentate, and either of them can be the desired product. Two factors determine the performance or separation efficiency of a given membrane: flux and selectivity. Flux is defined as amount of material passing per unit area per unit time and hence

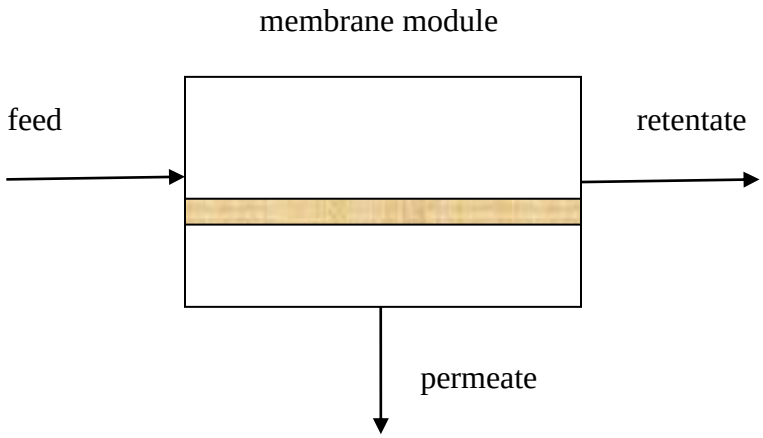

Figure 2-1 Schematic drawing of the basic membrane process

is a measure of throughput. Selectivity is generally expressed by one of the two parameters: retention or separation factor. Permeance and selectivity are dependent on membrane, process conditions and feed conditions. The ideal membrane should be mechanically, chemically and thermally resistant and the separation performance should not change after long term operation. Transport across a membrane is a non equilibrium process and occurs under an applied driving force. Driving forces can be gradients in pressure, activity (concentration), electric potential or temperature. The most general driving force in membrane separation is pressure difference. Pressure differences across the membrane can facilitate microfiltration, ultrafiltration, nanofiltration, reverse osmosis, gas separation, vapor permeation and pervaporation. Concentration differences across the membrane can facilitate dialysis and extraction, whereas temperature differences can facilitate distillation. Electrodialysis can also performed with the help of membranes when an electrical potential difference across the membrane is maintained.

Other than driving force, membranes are normally classified according to pore size or the size of the materials they are used to separate. Membranes with pore sizes of 5 μm or greater are particulate filters. Microfiltration membranes have pore sizes in the range of 100 – 5000 nm and are capable of removing suspended particles like blood cells and latex emulsions. Ultrafiltration membranes have pore sizes in the range of 2 – 100 nm and can remove large molecules like albumin or pepsin within this range. Nanofiltration membranes can separate small molecules like dissolved salts, dissociated acids and sugar, and have pore sizes in the range 1 – 2 nm. Reverse osmosis membranes separate ions like sodium and chloride on the molecular level and have pore sizes in the range of few Angstroms. Non-porous membranes are used for gas separation, vapor permeation, and pervaporation. A summary of driving forces and pore sizes associated with various membrane processes is given in Table 2-1.

Table 2-1 Classification of membrane separation processes

Process	Pore size	Driving force
Microfiltration	0.1 – 5 μm	ΔP, 1-2 bar
Ultrafiltration	0.002 – 0.1 μm	ΔP, 2-5 bar
Nanofiltration	1 – 2 nm	ΔP, 5-15 bar
Reverse osmosis	< 0.5 nm	ΔP, 15-100 bar
Gas separation	Non-porous	ΔP, 15-100 bar
Vapor permeation	Non-porous	Δp
Pervaporation	Non-porous	Δp
Dialysis	1 – 3 nm	Δc
Membrane extraction	Porous, hydrophobic	Δc
Membrane distillation	Porous, hydrophobic	ΔT
Electrodialysis	MWCO* < 200	ΔE

*Molecular Weight Cut-Off

2.3.1 Membrane Classification

A membrane can be thick or thin, homogenous or heterogeneous, symmetric or asymmetric, charged or uncharged, dense or porous, and solid or liquid. Membranes can also be classified by nature, i.e. natural biological or synthetic membranes. Synthetic membranes can be grouped according to their selective barrier, their structure and morphology and the membrane material [45]. The selective barrier – porous, nonporous, charged or with chemical affinity – determines the mode of permeation and separation. The principal types of membranes are shown schematically in Figure 2-2. Some major characteristics of those membranes are given below.

2.3.1.1 Selective Barrier Structure

Porous membranes have a rigid, well-defined static pore structure, which depending on the formation process can be highly connected and tortuous or non-connected and straight. Transport through porous membranes is by viscous flow or diffusion, and the selectivity is based on sieving mechanism. This implies that separation characteristics are mainly governed by membrane pore size and the effective size of the components in the feed, the type of material being crucial importance for chemical, thermal and mechanical stability but not for flux and retention. In general, porous membranes can exhibit very high fluxes. High selectivity can be obtained when solute size is large compared to the pore size in the membrane. Transport through nonporous (dense) membranes can be described by solution-diffusion mechanism [46]. Therefore, the intrinsic properties of the membrane material and the permeating species determine the extent of permeability and selectivity. Electrically charged membranes can be either porous or nonporous, but are commonly microporous, with fixed charge groups on the pore wall. Separation using charged membranes is achieved mainly by (Donnan) exclusion of

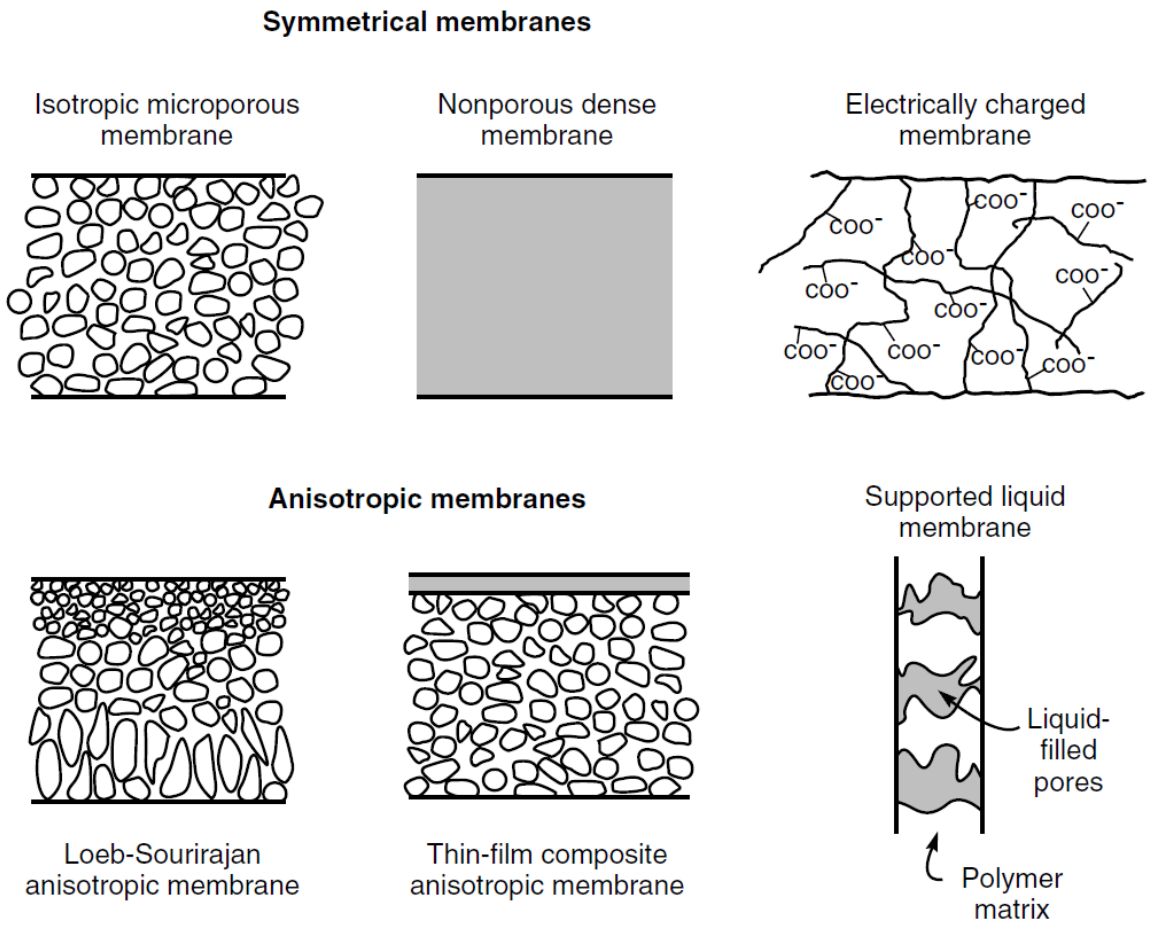

Figure 2-2 Schematic diagrams of the principal types of membranes [46]

ions of the same charge as the fixed ions of the membrane structure, and to a much lesser extent by the pore size. Hence, the separation is affected by the charge and concentration of ions in the solution. Finally, the molecules or moieties with specific affinity for components in the feed form the basis for carrier-mediated transport through the membrane [46].

2.3.1.2 Cross-section Structure

Isotropic (symmetric) membranes have a uniform chemical composition structure throughout the cross-section, and can be porous or dense. The transport resistance of species in these membranes is proportional to the total membrane thickness. A decrease in membrane thickness results in an increased permeation flux. As discussed in the section 2-1, an anisotropic (asymmetric) membrane has a thin dense or porous selective barrier, supported mechanically by a much thicker porous substructure. This type of morphology decreases the effective thickness of the surface layer, and the flux can be enhanced without changes in selectivity. Both the above-mentioned membranes can in principle be made from the same material. On the other hand, a thin film composite (TFC) membrane consists of different materials for the selective barrier and the support structure in contrast to integrally skinned anisotropic membrane (homogenous with respect to composition). The advantage of TFC membranes is that each layer can be optimized independently to achieve the desired membrane performance with regard to permeability, selectivity, and chemical and thermal stability. Other examples include pore filled or pore surface-coated composite membranes and mixed matrix membranes [47].

2.3.1.3 Membrane Materials

As mentioned earlier, membranes can be classified into two groups, i.e. biological and

synthetic membranes. Biological membranes are vital for life on the earth. Every cell is surrounded by a membrane, but these membranes differ fundamentally in structure, functionality etc. from synthetic membranes. Synthetic membranes can be divided further into organic (polymeric) and inorganic membranes. Both organic and inorganic membranes can be either dense or porous depending on the type of application. In principle, all materials that form sufficiently thin and stable films can be membranes. These include metal, glass, ceramic, and polymers as well as molecular monolayer of liquids. However, the most important class of membrane materials is organic, i.e. polymers or macromolecules.

2.3.2 Pressure Driven Membrane Processes

In pressure driven membrane processes a hydrostatic pressure applied on the feed solution at one side of the membrane provides the driving force to separate it into permeate and retentate. An overview of various pressure driven liquid phase membrane separation processes is given in Figure 2-3. The appropriate membrane processes for the removal of acids from AFBO are nanofiltration and reverse osmosis and are explained in detail below.

2.3.2.1 Reverse Osmosis

Osmosis is a natural process in which solvent molecules (usually water) pass through a semipermeable membrane (permeable to the solvent but not to the solute) from the side with lower solute concentration to that with higher solute concentration as shown in Figure 2-4. Solvent (water) flow continues until chemical potential equilibrium is established. At equilibrium, the pressure difference between the two sides of the membrane is equal to the osmotic pressure of the solution. If a hydrostatic pressure higher than the osmotic pressure is applied to the high concentration side, solvent (water) flow is reversed. This phenomenon is

	Microfiltration (MF)	**Ultrafiltration (UF)**	**Nanofiltration (NF)**	**Reverse Osmosis (RO)**
Permeability (l/h.m^2.bar)	> 1,000	10 – 1,000	1.5 – 30	0.05 – 1.5
Pressure (bar)	0.1 - 2	0.1 – 5	3 – 20	5 – 120
Pore size (nm)	100 – 10,000	2 – 100	0.5 – 2	< 0.5
Rejection				
• Monovalent ions	-	-	-	+
• Multivalent ions	-	-/+	+	+
• Small organic compounds	-	-	-/+	+
• Macromolecules	-	+	+	+
• Particles	+	+	+	+
Separation mechanism	Sieving	Sieving	Sieving Charge effects	Solution - Diffusion
Applications	Clarification; pretreatment; removal of bacteria	Removal of macromolecules, bacteria, viruses	Removal of (multivalent) ions and relatively small organics	Ultrapure water; desalination

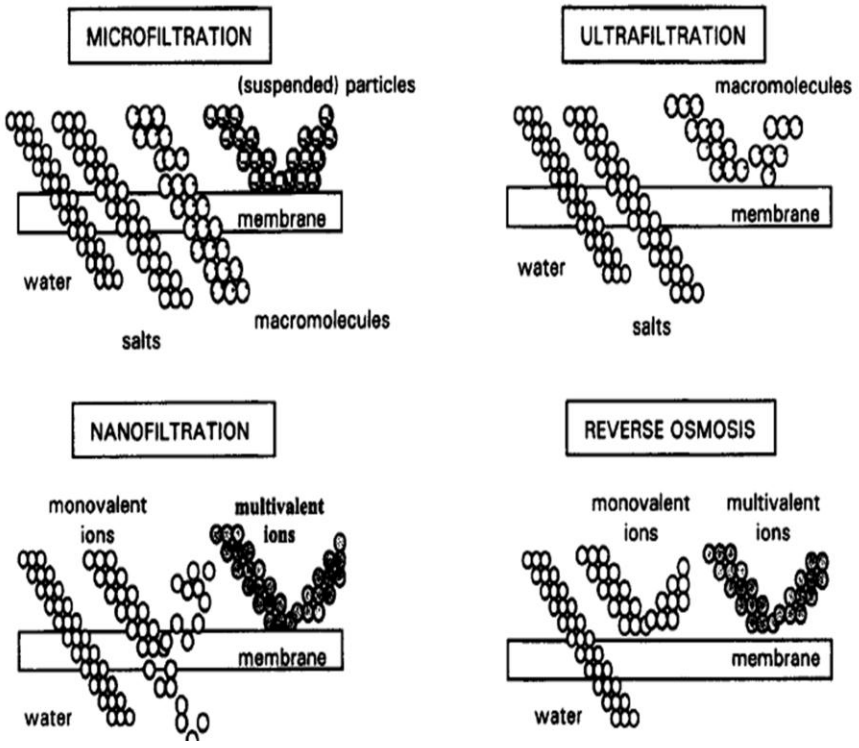

Figure 2-3 Classification of pressure driven liquid phase membrane processes. Reproduced from [48].

termed reverse osmosis (it has also been referred to as hyperfiltration). Reverse osmosis can be used to remove solutes such as dissolved monovalent ions from a solution. Chemical potential gradients across the membrane provide the driving forces for solute and solvent transport. Water (solvent) and solute permeate through RO membranes according to the solution-diffusion mechanism (described in detail in section 5.1.2.4) [46]. The effective water flux, J_w, through the membrane at constant temperature can be represented by the following equation

$$J_w = A(\Delta P - \Delta\pi) \tag{2-18}$$

where ΔP is the pressure difference across the membrane, $\Delta\pi$ is the osmotic pressure differential across the membrane, and A is water permeability coefficient. According to Equation (2-18), when $\Delta P < \Delta\pi$, water flows from the dilute to the concentrated side of the membrane by normal osmosis. When $\Delta P = \Delta\pi$, no flow occurs, and when $\Delta P > \Delta\pi$, water flows from the concentrated to the dilute side of the membrane. In practice, the membrane may be a little permeable to low molecular solutes (retention is always less than 100%). Hence, the real osmotic pressure difference across the membrane is $\sigma\Delta\pi$ where σ is the reflection coefficient. The value of A is approximately in the range of 6.10^{-5} – 3.10^{-3} $m^3/(m^2.hr.bar)$ for RO membranes while for NF membranes the permeabilities range from 3.10^{-3} – 2.10^{-2} $m^3/(m^2.hr.bar)$ [5].

The solute flux through the membrane is given by the following equation

$$J_s = B(C_{so} - C_{sl}) \tag{2-19}$$

where B is the solute permeability constant and C_{so} and C_{sl}, respectively, are the solute concentrations on the feed and permeate sides of the membrane. The value of B is in the range of 1.10^{-4} – 5.10^{-3} $m^3/(m^2.hr)$ for RO with NaCl as the solute with the lowest value for high retention membranes. For nanofiltration membranes the retention for the different salts may vary

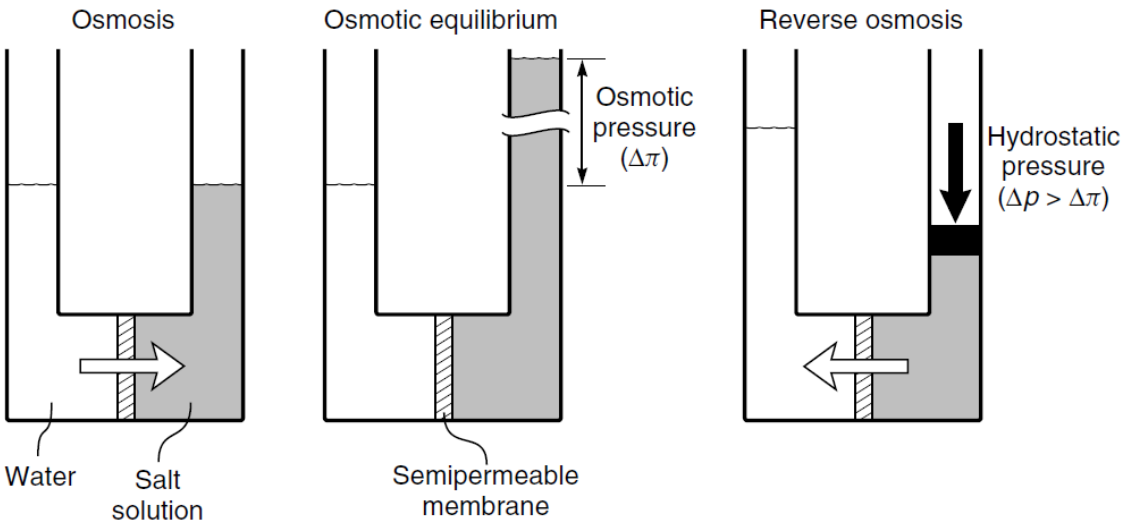

Figure 2-4 A schematic demonstration of the relationship between osmosis, osmotic equilibrium, and reverse osmosis [46]

considerably, e.g. the retention for NaCl may range from 5 to 95%.

The performance of reverse osmosis is directly dependent on the properties of the membrane material. More specifically, the structure of the membrane and the chemical nature of the membrane polymer are what govern the flux and retention properties of the RO system. A number of membrane materials and membrane preparation methods have been used to make reverse osmosis membranes. Two most common types of RO membranes, based on the kind of the polymer backbone, are cellulose acetate and aromatic polyamide [46].

Cellulose acetate (CA) membranes were the first commercially viable RO membranes developed by Reid and coworkers in 1959 [38, 49, 50]. Their films were 5 – 20 μm thick so fluxes were very low, but pressurizing the feed salt solution to 1000 psi, they obtained salt retentions of better than 98% in the permeate water. In 1963, Loeb and Sourirajan demonstrated asymmetric cellulose acetate membranes which exhibited remarkably high flux and good salt retention [43]. They used phase inversion process to prepare these membranes. Their membranes had 10 times the flux of the best membrane of Reid and Breton and equivalent retentions. CA membranes offer numerous advantages over other RO membranes on the market today. They are relatively easy to synthesize and have outstanding mechanical properties. They are also relatively resistant to attack by chlorine. However, their stability against chemicals, temperature and bacteria is very poor. Typical operating conditions of these membranes are over the pH range 4 to 6 and at a temperature below 30° C, thus avoiding hydrolysis of the polymer.

Asymmetric CA membranes were the dominant choice for RO membranes through the 1960s to the mid-1970s, until Cadotte, then at North Star Research, produced thin film composite (TFC) membranes using interfacial polymerization [51]. Interfacial composite membranes had extremely high salt retentions, combined with good water fluxes. Based on aromatic polyamides,

TFC membrane fluxes and retentions surpassed those of CA and currently are the industry standard for desalination applications. In addition to high flux and retention, TFC membranes are also stable over a larger pH and temperature range than CA [46]. However, one major drawback of polyamide membranes is their sensitivity to chlorine. TFC membranes undergo oxidative degradation when exposed to trace amounts of chlorine [52, 53]. The polyamide is believed to undergo ring chlorination, which disrupts the hydrogen bonding between the chains and degrades the polymer matrix [54]. Although various approaches have been investigated for producing chlorine resistant aromatic polyamide materials, the advantages have been limited since most approaches degrade membrane separation performance [55].

Reverse osmosis can be used in principle for a wide range of applications, which may be roughly grouped as solvent purification (where permeate is the product) and solute concentration (where retentate is the product). Most of the applications are in the purification of water, mainly the desalination of seawater and brackish water to produce drinking water [46]. Another important application is in the production of ultrapure water for the electronics, pharmaceutical, and power generation industries. RO processes for waste water treatment have been applied to the chemical, textile, petrochemical, pulp and paper, and food industries as well as for the treatment of municipal wastewater and landfill leachates [56, 57]. The applications of RO in the paper and pulp industry have been mainly for the removal of dissolved solids, organics, and color from wastewaters [58, 59]. A detailed review of reverse osmosis applications has been written by Williams et al. [60].

2.3.2.2 Nanofiltration

Nanofiltration (NF) is a relatively new category of pressure driven processes (3-20 bar) that lies between ultrafiltration (small particle removal) and reverse osmosis (salt removal) on

the membrane spectrum. The average pore size of NF membranes is around 2nm, which is between the size of RO and UF membranes. The size of the solute molecules that are retained and the range of operating pressures (5-20 bar) are also between those for RO (20-100 bar) and UF (1-5 bar). Therefore, NF membranes are ideally suited for rejecting organics such as lactose, glucose, and sucrose with molecular weights above 150 g/mol, and for rejecting multivalent ions.

Nanofiltration is closely related to RO, and is sometimes called 'loose RO'. Similar to RO most of the NF membranes are polyamide thin film composites (TFCs). However, the transport in NF membranes is more complex than in RO. In addition to solution-diffusion mechanism, size and charge exclusion are also usually involved. Commercially available polyamide NF membranes have a surface charge due to ionizable groups. e.g. carboxylic or sulfonic acid groups. The equilibrium between charged membrane and the bulk solution is characterized by an electrical potential called the Donnan potential. Ions smaller than the pore size are retained because of Donnan exclusion [61].

Reduction of hardness (i.e., Ca^{+2} and Mg^{+2}) and dissolved organics from drinking water are the most important applications of NF membranes [62, 63]. However, the selective properties of NF membranes make them appropriate for a wide range of unconventional applications. An important example is the recovery of heavy metals (e.g. Ni, Fe, Cu, Zn etc.) and reclamation of waste waters from textile mills and metal working plants [64, 65]. More recently, NF membranes have been adopted for use in the biotechnology and pharmaceutical industries for purification of small bioactive organic molecules such as antibiotics or separation of small organic components from biological liquids (e.g., lactic acid separation from fermentation broths [66, 67], amino acid removal from protein hydrolysates [68], or removal of organics from municipal wastewater [69, 70]).

In contrast to aqueous systems, the use of NF membranes in organic solvents is much more recent evolution. The first applications investigated in non aqueous media were not very successful. Membranes showed performance loss due to chemical instability of polymeric materials in organic solvents. Different problems occurred: zero flux due to membrane collapse, 'infinite' flux due to membrane swelling, membrane degradation, poor separation performance and the like. Due to recent advancements in membrane development, NF membranes are increasingly used for non aqueous applications [71]. Commercial solvent resistant nanofiltration (SRNF) membranes include Koch (MPF 44 and MPF 50), NF-PES-10, Starmem^{TM}, and N30F. However, some of these membranes showed visible defects after ten days exposure to one or more organic solvents and characteristics of all the membranes changed significantly after exposure to solvents [72, 73]. This means that these membranes should be denoted as semi-solvent-stable instated of solvent-stable. Researchers obtained insight into the interactions between membranes and solvents, which result in a performance that is totally different from the performance in water [74-76].

SRNF-membranes have a strong potential for a variety of applications ranging from pharmaceutical to chemical and food industries. Large-scale industrial applications of SRNF membranes have been in operation since 1998 [15], the best known being the MAX-DEWAX at the ExxonMobil refinery in Beaumont (Texas) for the recovery of dewaxing solvents from lube oil filtrates. The membrane used in this process was an asymmetric polyimide-based membrane, with a reported rejection for the lube oil greater than 95%. A typical application is the separation and purification of edible oil. Recently, several articles have published on the membrane applications in the edible oil industry for the solvent recovery (hexane, acetone, ethanol, and isoproponol) and oil refining process [77, 78]. In the pharmaceutical industry, drugs with

molecular weight (MW) higher than 300 g/mol could be recovered from solvents such as ethanol, ethyl acetate etc at room temperature by NF-based process [79]. A detailed list of applications is reviewed by Vandezande et al. [80]. Many more processes could be realized if stable membranes with high selectivities, competitive flux and sufficient long-term stability were available.

2.4 Acid Removal by Membrane Technology

The above characteristics of NF and RO would make them appropriate for removing small acids from AFBO while retaining larger species. There is some related membrane work in the literature. Han and Cheryan [81] were the first to use NF and RO membranes to separate acetic acid from glucose. The average observed retentions of acetic acid and glucose were 40% and 99% respectively. They also found that performance of membranes as measured by flux and retention of acetic acid is influenced by pressure, pH, concentration, temperature and the presence of other media components. Sagehashi et al [82] used RO membranes to separate phenols and furfurals from biomass-superheated steam pyrolysis-derived aqueous solution. They observed that almost all of the solutes were retained by the RO membrane. Weng et al [83] performed NF experiments to separate furans and carboxylic acids from sugars in dilute acid rice straw hydrolysates. The retention of the sugars was greater than 94% whereas negative retentions were observed with acetic acid and furan. However, in all the above studies, the concentrations of sugars, carboxylic acids, furans and phenols in the feed were very low (< 1wt %). The organic feed concentration in the aqueous phase of pyrolysis oil is significantly higher with organic concentrations above 30 wt % (see section 2.1). There are few studies published on NF using solutions at higher concentration (> 10 wt% or 100 g/L). Sjöman et al [84] studied the separation of xylose from glucose by NF from highly concentrated monosaccharide solutions. The total

concentration of sugars is varied up to 30 wt% and they observed a xylose/glucose separation factor over 2, but they didn't study the effect of the presence of other organic compounds. Weng et al [19] used NF membranes to separate acetic acid from xylose at high concentration of xylose (100 g/L) but relatively low concentration of acetic acid (10 g/L).

There are no published systematic investigations on NF and RO separations using high concentrations of sugars and other organic compounds that are directly relevant to pyrolysis bio-oils. Since the membrane performance depends on the solute concentration and the presence of other media components [84, 85], it is necessary to study the performance of NF and RO at realistic concentrations. This research aims at implementing membrane technology to reduce the acidity of AFBO, thus stabilizing it for long-term storage and further processing. The main goal is to reject low molecular weight acids while retaining glucose and other valuable, heavier compounds.

CHAPTER 3

EXPERIMENTAL PROCEDURE

This chapter describes the experimental procedure for liquid permeation experiments. Details of NF and RO membranes used and chromatographic analyses are also given.

3.1 Membranes and Chemicals

NF and RO flat sheet membranes were purchased from Wilkem Scientific (Pawtucket, RI). The information provided by the manufacturers is summarized in Table 3-1. All the membranes were supplied in a dry form except for MPF 34, which were supplied in a wet form in a 0.7 % Roccal preserving solution (0.7% benzalkonium chloride + 0.25% sodium metabisulfite in water). Desal DK and RO AG membranes are thin film composites (TFC) that have a three–layered structure comprising active, intermediate and backing layers. The active (top) layer of Desal DK membrane is a polyamide, with polysulfone as backing layer. The intermediate layer is a proprietary polymer. The layers in RO AG membranes have a similar composition. MPF 34 also consists of three layers, with a backing made of a polypropylene-polyethylene blend. The intermediate and top polymeric layers are a proprietary polymer. RO CE membranes are asymmetric membranes, with a continuous variation in structure across the membrane thickness, made of cellulose acetate. Since the MPF 34 membranes were supplied in wet form, these membranes were washed with distilled water before using them in our experiments.

D-glucose (anhydrous), acetic acid (glacial), phenol (laboratory grade), ethanol (200 proof), methanol (laboratory grade) were purchased from Fisher Scientific. Furfural (99 %),

Table 3-1
Membrane parameters. All data are from the manufacturers, except for the permeability values in parentheses that were measured in this work.

Membrane	Rejection	Polymer	Pure water permeability constant, A L/m^2-hr-bar	pH range @ 25 ºC
GE Osmonics Desal DK	98 % $MgSO_4$	Aromatic polyamide	5.44 (4.78)	2-11
Koch MPF 34	200 MWCO[a]	Proprietary	1.95 (1.71)	0-14
GE Osmonics RO AG	99.5 % NaCl	Aromatic polyamide	2.85 (2.87)	4-11
GE Osmonics RO CE	97% NaCl	Cellulose Acetate	1.38 (1.32)	2-8

[a] Molecular Weight Cut Off

formic acid (98%), catechol (99%), guaiacol (99%) were purchased from Acros and hydroxyacetone (technical) was purchased from TCI America. Aqueous solutions of model solutions were prepared using distilled water.

3.2 Permeation Set-up

A Sepa® CF II Med/High foulant lab scale cross-flow membrane filtration unit from GE Osmonics was used to carry out the permeation experiments. Figure 3-1 shows the schematic diagram of the experimental equipment. The Sepa® CF II unit has three major components: cell body, cell holder, and hydraulic hand pump. Precut rectangular membranes (19 cm × 14 cm) with an effective area of 137 cm^2 were installed in the cell body. Feed spacer and permeate carrier were installed on the bottom and top of the membrane respectively. The unit was pressurized using the hydraulic hand pump to a pressure greater than the expected feed pressure; double O-rings in the cell body provide a leak-proof seal. The feed stream was pumped using an Eldex Optos reciprocating pump from the feed vessel to the inlet. Flow continued through a manifold into the membrane cavity and then flowed tangentially across the membrane surface. The transmembrane pressure was monitored by two digital pressure gauges located on the inlet and outlet of the cell. A back pressure valve was mounted on the retentate outlet to control the transmembrane pressure. The permeate pressure was always atmospheric. All the experiments were conducted at room temperature (21 ± 1 °C) at constant cross flow velocity of 0.026 m/s and at different transmembrane pressures ranging from 5 to 58 bar. Both the permeate and the retentate were recycled to feed vessel. Permeate samples were collected at each pressure and timed to calculate permeation flux. At each flux measurement, a sample of permeate was taken for chemical analysis. The flux was obtained by

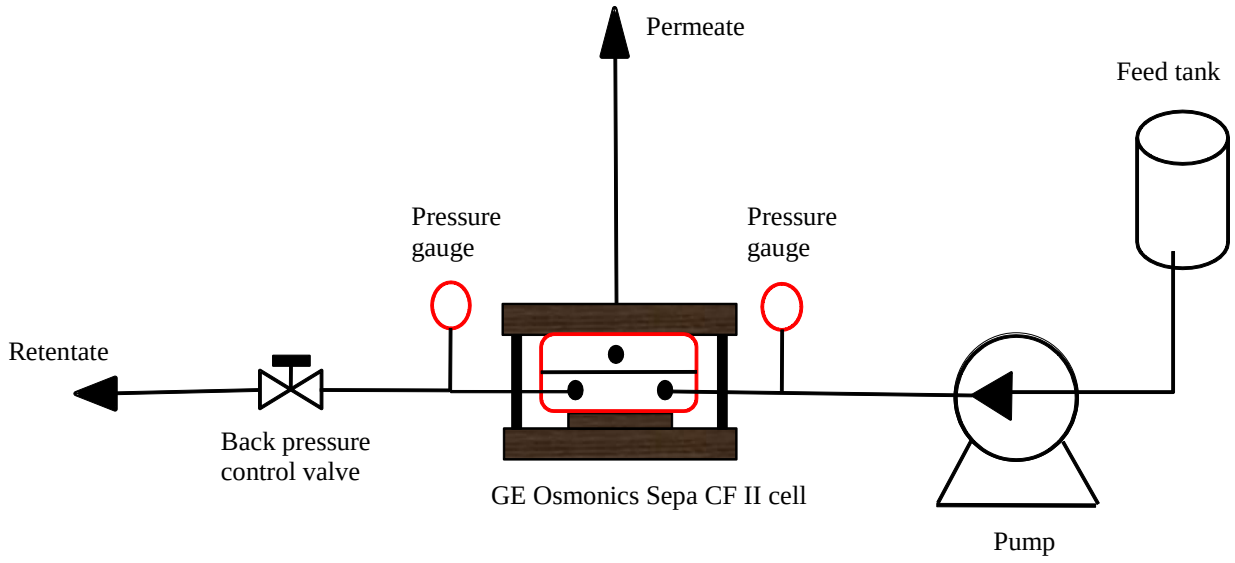

Figure 3-1 Schematic view of the membrane unit used

$$J = \frac{V}{At} \tag{3-1}$$

where V is the volume of the permeate, A the membrane area and t the time over which the volume V was collected. Permeance (P) is calculated by normalizing the flux with the transmembrane pressure and is given by

$$P = \frac{J}{\Delta p} \tag{3-2}$$

where Δp is the transmembrane pressure. The observed retention, R_{obs}, of solute can be used to describe membrane performance and was calculated from Equation (3-3), where C_p and C_f are the permeate and feed concentrations of solute, respectively.

$$R_{obs} = \left(1 - \frac{C_p}{C_f}\right) \times 100\% \tag{3-3}$$

The value of R lies between 100 % (ideal semipermeable membrane; complete retention of the solute) and 0% (completely unselective membrane; solute and solvent pass through the membrane freely). While the permeance and observed retention serve to describe the throughput and selectivity achieved in a given experiment, they do not entirely characterize the membrane/solution system. The observed retention is measured directly from the experiments and may strongly depend on concentration polarization which in turn changes with the hydrodynamic conditions near the membrane. Therefore one must consider some further details of the mass transfer process, as described in the next section.

3.3 Concentration Polarization

Concentration polarization is due to the accumulation of rejected species within a thin boundary layer adjacent to the membrane surface. The polarization hampers the transport

because of increase in the resistance to flow and thus reduces the flux. Also it enhances solute leakage resulting in the loss of membrane retention. As a result of concentration polarization, the actual concentration of solute near the membrane surface is different from the feed or bulk concentration. A parameter other than R_{obs} can be used to evaluate membrane retention which is termed as intrinsic retention (R_{int}) and is defined by

$$R_{int} = \left(1 - \frac{C_p}{C_m}\right) \times 100\ \% \tag{3-4}$$

where C_m is the solute concentration in the liquid feed evaluated at the membrane surface. One could also change the definition of C_p in Equation (3-4), but concentration polarization is typically not important on the permeate side. Since it is difficult to experimentally probe concentrations close to the surface, R_{int} is calculated theoretically from a set of R_{obs}. A combination of film theory and velocity variation method [86] is frequently used to calculate intrinsic retention.

Using film theory, the concentration profile under steady state conditions is shown in Figure 3-2 [5]. The solute concentration (C_f) is assumed constant at distances greater than δ from the membrane surface. However, in most cases the solvent is being transported across the membrane at a greater rate than the solute. This results in a local increase in solute concentration near the membrane surface. Thus, the concentration in the boundary layer increases and reaches a maximum value at the membrane surface (C_m). The concentration gradient also leads to a diffusive back flow towards the bulk of the feed. The following is a mass balance for solute at the feed side membrane interface under steady state conditions

$$J.C = -D\frac{dc}{dx} + J.C_p \tag{3-5}$$

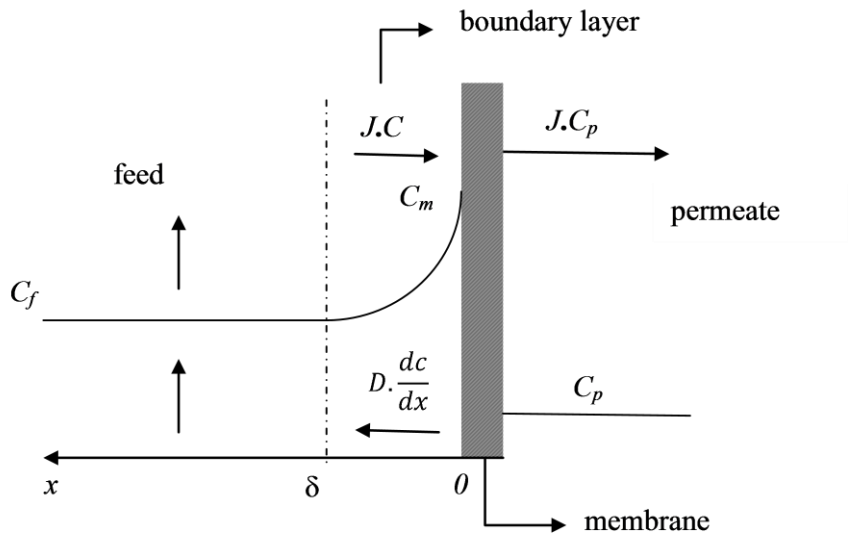

Figure 3-2 Concentration polarization; concentration profile under steady-state conditions. Adapted from [5].

where D is the solute diffusion coefficient. The boundary conditions are

$C = C_m$ at $x = 0$

$C = C_f$ at $x = \delta$

Solving Equation (3-5) using the boundary conditions results in

$$\frac{C_m - C_p}{C_f - C_p} = \exp\left(\frac{J}{k}\right) \tag{3-6}$$

where $k = D/\delta$ is called the mass transfer coefficient. Combining Equations (3-3), (3-4) and (3-6), we obtain

$$\ln\left(\frac{1-R_{obs}}{R_{obs}}\right) = \ln\left(\frac{1-R_{int}}{R_{int}}\right) + \frac{J}{k} \tag{3-7}$$

If one had information about k, R_{int} could be calculated from the experimental observations of J and R_{obs}. For laminar flow conditions (in our case Re~20), the mass transfer coefficient, k, can be calculated using Sherwood's relation [5]

$$Sh = \frac{kd_h}{D} = 1.86\left(Re.Sc.\frac{d_h}{L}\right)^{0.33} \tag{3-8}$$

where d_h is the hydraulic diameter, L is the channel length, Sh is the Sherwood number, Re is the Reynolds number and Sc is the Schmidt number.

From Equation (3-8), the dependence of the mass transfer coefficient k on the cross flow velocity v can be written as

$$k = \frac{v^{0.33}}{c} \tag{3-9}$$

where $c = 0.537\, D^{-0.67}\, d_h^{0.34}\, L^{0.33}$.

Combining Equations (3-5) and (3-7) gives

$$\ln\left(\frac{1-R_{obs}}{R_{obs}}\right)=\ln\left(\frac{1-R_{int}}{R_{int}}\right)+c\frac{J}{v^{0.33}} \quad (3\text{-}10)$$

This is the basic equation for concentration polarization which shows in a simple form the two factors (the flux *J* and the mass transfer coefficient *k*) responsible for polarization. Also it is assumed that the diffusion coefficient, *D*, is independent of extent of polarization and hence c can be considered as constant and is independent of flux and cross-flow velocity. At a constant flux *J* and different cross flow velocities, $\ln\left(\frac{1-R_{obs}}{R_{obs}}\right)$ is plotted against $\frac{J}{v^{0.33}}$. The result is a straight line of slope *c*. From the intercept, R_{int} is calculated. The intrinsic retention, R_{int}, provides a more direct characterization of a given membrane/solution, as compared to R_{obs}, because the effects of feed flow velocity have been factored out. van der Berg et al showed that this model is sensitive to chosen values of parameters and large range of observed retentions and fluxes is required to obtain reliable mass transfer coefficients [87].

3.4 Model Aqueous Solutions

Since the complete chemical analysis of AFBO is difficult, studies containing model compounds are helpful to understand its processing. Model compound studies also help in understanding the interaction between different components in the bio-oil. Based on the composition of bio-oil and literature data, Vispute and Huber [24] suggested a model solution to represent AFBO. Initial experiments were run with single and binary solute solutions of acetic acid and glucose to test the performance of the membranes. The model solutions used were: single solute solutions of 7 wt% acetic acid, 3.5 wt% glucose, and 15 wt% glucose, binary solute solutions of 5 wt% acetic acid & 10 wt% glucose and 7wt% acetic acid & 15wt% glucose and a model AFBO whose composition is given in Table 3-2.

3.5 Membrane Pretreatment

It has been observed that pretreatment by pressure impacts the flux and retention of NF membranes [88]. Also it is important to know how membranes are treated before the actual experiments in particular if fouling of the membranes is assessed by comparing their pure water permeances. Therefore most of the NF membranes need to be pretreated, before actual experiments, at high pressure in order to fully utilize their permeance. The membranes were pressurized by filtering water at pressures 25 and 35 bar for 10 min. Permeation measurements were made with water at different pressures, ranging from 5 to 35 bar, before and after each successive pretreatment step. The results are shown in Figure 3-5 for Desal DK membrane. The permeance at low pressures is increased dramatically after the first pretreatment while there is not much change at high pressures. Second pretreatment has very little effect on the permeance at all pressures. So we conclude that exposing the membrane to high pressure (~ 25 bar) resulted in an increase in permeance. Similar experiments were conducted with the other three membranes but the effect of pretreatment is negligible on water permeance. So it is believed that Desal DK membranes are sensitive to pretreatment effects. Hence permeation experiments with model aqueous bio-oil were conducted with treated and untreated membranes to see the effect of pretreatment on flux and retention and the results are described in section 4.10.

3.6 Chemical Analyses

High performance liquid chromatography (HPLC) and gas chromatography (GC) were used for the analysis of feed and permeate samples. HPLC was equipped with Aminex HPX-87 H column and two detectors; refractive index (RI) and ultraviolet (UV) were used to analyze glucose and acetic acid respectively. The mobile phase was 0.005 M H_2SO_4. For all other compounds, a RTx®-VMS capillary column was used in a Agilent Technologies 7980A

Table 3-2 Composition of model aqueous fraction of bio-oil

Compound	Weight , %	Water solubility (g/100 ml)
Water	65	-----
Glucose	15	91
Acetic acid	7	100 (miscible)
Hydroxyacetone	4.65	100 (miscible)
Formic acid	2.3	100 (miscible)
Furfural	2.3	8.3
Guaiacol	2.3	2.9
Catechol	1.45	43

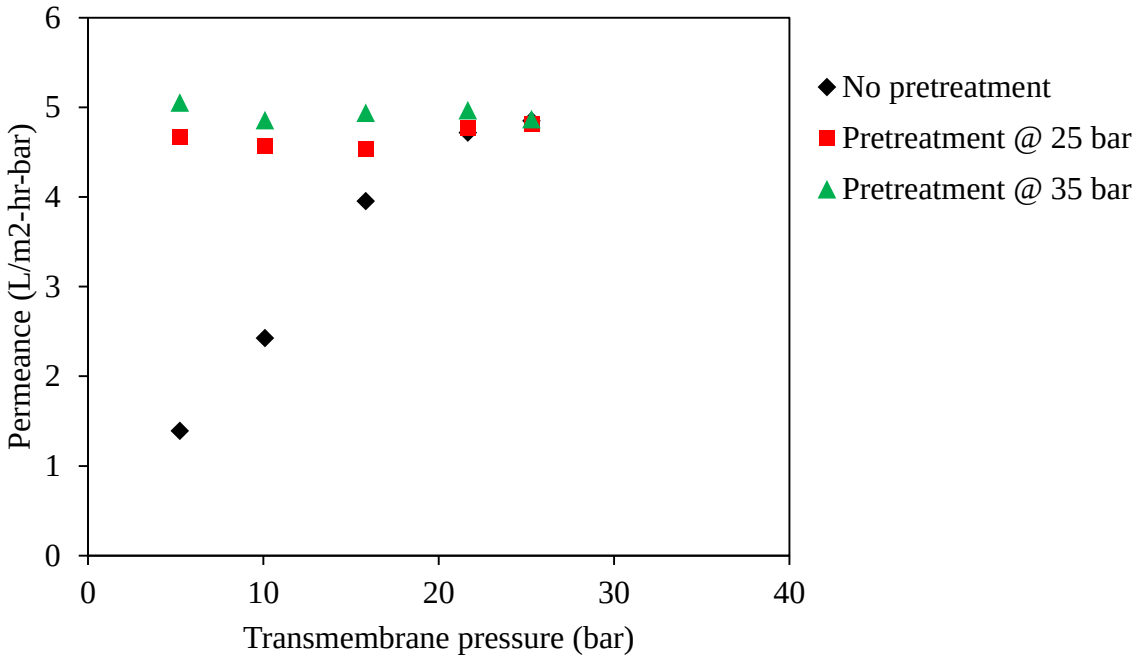

Figure 3-3 Effect of pretreatment on pure water permeance for Desal DK membrane

chromatograph equipped with a flame ionization detector (FID). The carrier gas was helium and a single temperature programming profile was used. Feed samples were diluted by a factor of 10 to reduce the degradation of glucose in the detector. Optical microscopy was used to characterize the membrane surface.

CHAPTER 4

RESULTS AND DISCUSION

In this chapter results of the nanofiltration and reverse osmosis experiments are presented and discussed. The key performance metrics were retention of specific species, especially acetic acid and glucose, and total flux. Experiments were conducted to see the effect of cross flow velocity, transmembrane pressure and total feed concentration on these metrics. The chemical stability of these membranes against different phenolics was also studied. All the results presented in this chapter were obtained without pretreating the membranes unless specified explicitly.

4.1 Pure Water Flux

Pure water flux data for all four membranes used in our study are shown in Table 3-1 in terms of the water permeability constant, *A*, which was obtained from the slope of pressure- flux data as shown in Equation (4-1). The osmotic pressure ($\Delta\pi$) is zero, so $A = J/\Delta P$ for pure water. From Table 3-1, it is clear that the values measured in our lab (shown in parentheses) are consistent with the values provided by the manufacturers.

$$J = A\,(\Delta P - \Delta\pi) \tag{4-1}$$

4.2 Effect of Cross Flow Velocity on Retention

Experiments with 3.5 wt% glucose solution were conducted at different cross flow velocities to study its impact on glucose retention. In addition we also calculated intrinsic retentions using a combination of film theory and velocity variation method which was explained in detail in section 3.3.3. Figure 4-1 shows calculation of the intrinsic retention using Equation (3-10). At a given flux, *J*, the variation of $\ln\left(\frac{1-R_{obs}}{R_{obs}}\right)$ plotted against $\frac{J}{v^{0.33}}$ (i.e. at different

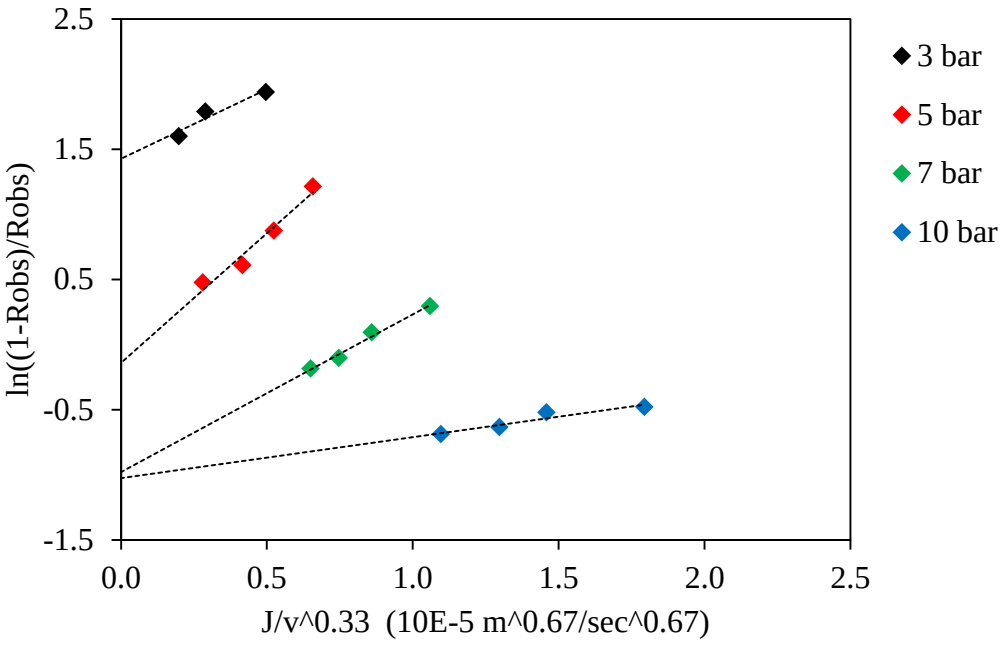

Figure 4-1 Use of velocity variation method to calculate the intrinsic retention R_{int}

cross flow velocities) should give a straight line of slope c, from the y-intercept from which R_{int} is calculated. The results are summarized in Table 4-1. It is evident from the data that increasing the cross flow velocity increased the observed retention. Therefore we confirmed that the observed retention, R_{obs}, is strongly dependent on the concentration polarization and accordingly changes with the hydrodynamic conditions near the membrane. Concentration polarization is undesirable as it exposes the membrane to an increased solute concentration, which increases the resistance to flow and thus reduces the flux. It also decreases the observed solute retention. The intrinsic retention, R_{int}, deals directly with the concentration at the membrane surface, C_m, and is always higher than the observed retention. As the cross flow velocity increases the observed retention approaches the intrinsic retention because concentration polarization is decreased and $C_m \approx C_f$. This agrees with the theory presented in the previous chapter. So we performed all the experiments at the highest cross-flow velocity (0.026 m/sec) achievable with our system, but we expect that there may still be concentration polarization effects. Note that the observed retention increased as the transmembrane pressure is increased. A straightforward explanation is given in the next section.

4.3 Single-solute Solutions

Experiments were carried out with single solute solutions of acetic acid (7 wt %) and glucose (15 wt %) using all four membranes listed in Table 3-1. The effect of transmembrane pressure on flux and solute retention was explored. The variation of flux with transmembrane pressure is shown in Figure 4-2. In all experiments, the flux was a nearly-linear function of transmembrane pressure and was lower than that of pure water. For example, with Desal DK membrane at 36 bar, the fluxes of 7 wt% acetic acid and 15 wt% glucose feed solutions were 85

Table 4-1 Variation of observed retention, R_{obs}, with cross flow velocity

Transmembrane pressure, Δp (bar)	Cross flow velocity, m/sec	**R_{obs} , %**	**R_{int} , %**
3	0.0015 0.0047 0.0097	0.126 0.143 **0.168**	**20**
5	0.0028 0.0045 0.0086 0.0272	22.9 29.4 35.2 **38.3**	**54**
7	0.0034 0.0066 0.0097 0.0139	42.7 47.6 52.6 **54.6**	**73**
10	0.0039 0.0078 0.0120 0.0205	61.7 62.7 65.3 **66.6**	**76**

and 5 L m^{-2} hr^{-1} respectively as compared to the pure water flux of 164 L m^{-2} hr^{-1}. For both single solute solutions, Desal DK and RO AG membrane have the highest and lowest fluxes, respectively. Figure 4-3 shows the effect of transmembrane pressure on acetic acid and glucose retention. Glucose retentions up to 90% and acetic acid retentions down to -4% were observed. For a particular membrane, glucose retention is always higher than that of acetic acid. Evidently, the higher glucose retention is due to the larger size of the glucose molecule, which is in accordance with the sieving effect [89, 90]. Negative retention (i.e., permeate enrichment) is unusual but it is not an entirely new phenomenon. Weng et al [85] observed negative retentions of acetic acid (varied between -2.3 % to 6.6%) with spiral wound Desal DK membrane module. Lonsdale et al. [91] also observed negative retention of phenol in aqueous mixtures with cellulose acetate membranes. Possible explanations for negative retention are charge effects and intermolecular interactions between solvent and solute. In case of acetic acid, there is an inverse relation between flux and retention. The flux of acetic acid solution through the membranes decreased in the sequence DK > CE > MPF 34 > AG whereas the retention of acetic acid followed the reverse order (although DK and CE membranes showed essentially identical retentions). However, there is no such trend with glucose solution. In general, both flux and solute retention increased as the transmembrane pressure increased. This can be explained using the solution-diffusion model for solvent and solute transport through the membrane [46]. According to this model, as pressure is increased the solvent (water) flux increases faster than solute flux and thus retention increases.

4.4 Mixed-solute Solutions

Figures 4-4 and 4-5 show, respectively, the acetic acid and glucose retentions obtained with all the membranes for one mixture composition (7 wt% acetic acid and 15 wt% glucose).

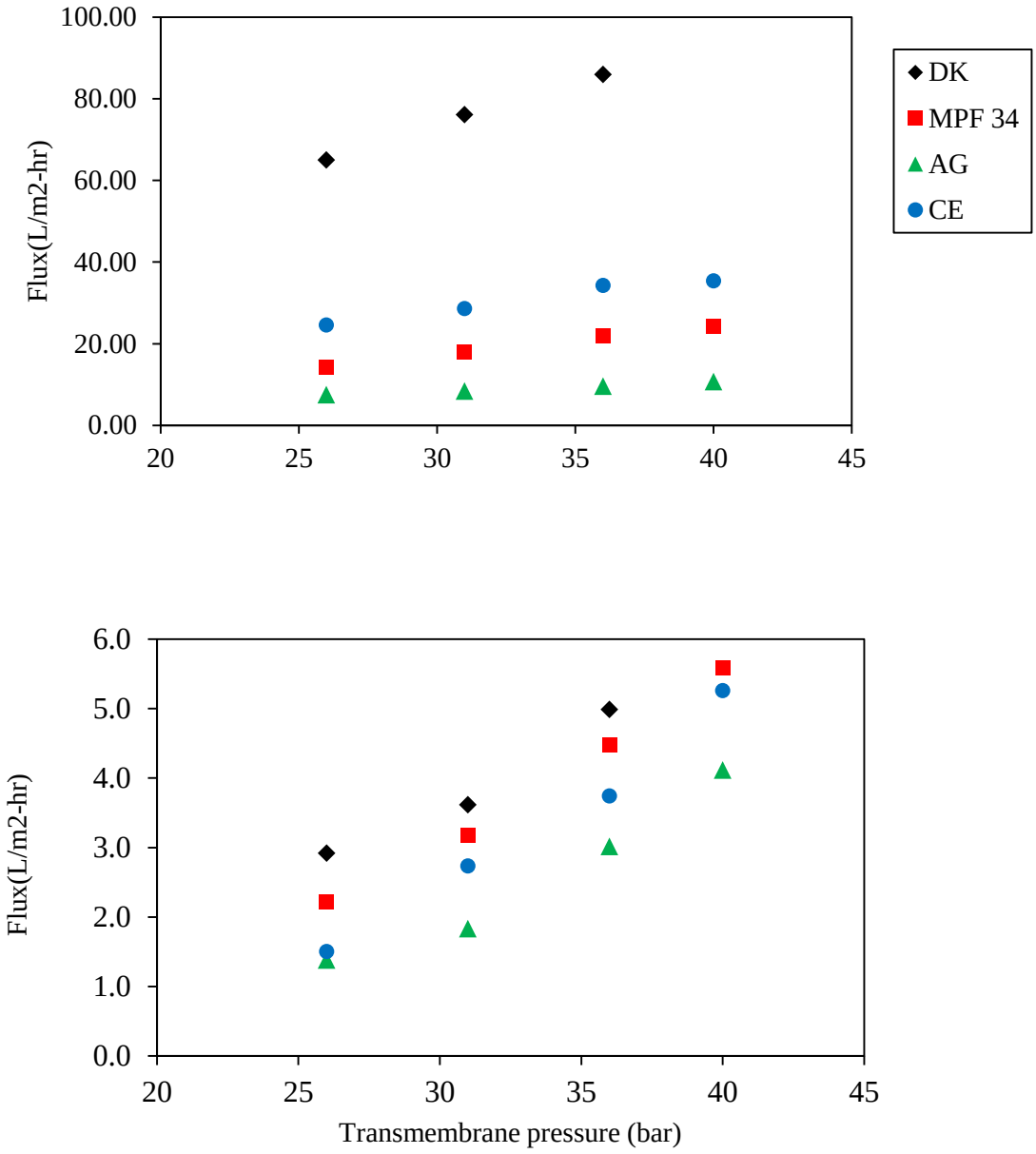

Figure 4-2 Influence of applied pressure on permeate flux. (Top) 7 wt% acetic acid, and (bottom) 15 wt% glucose solutions

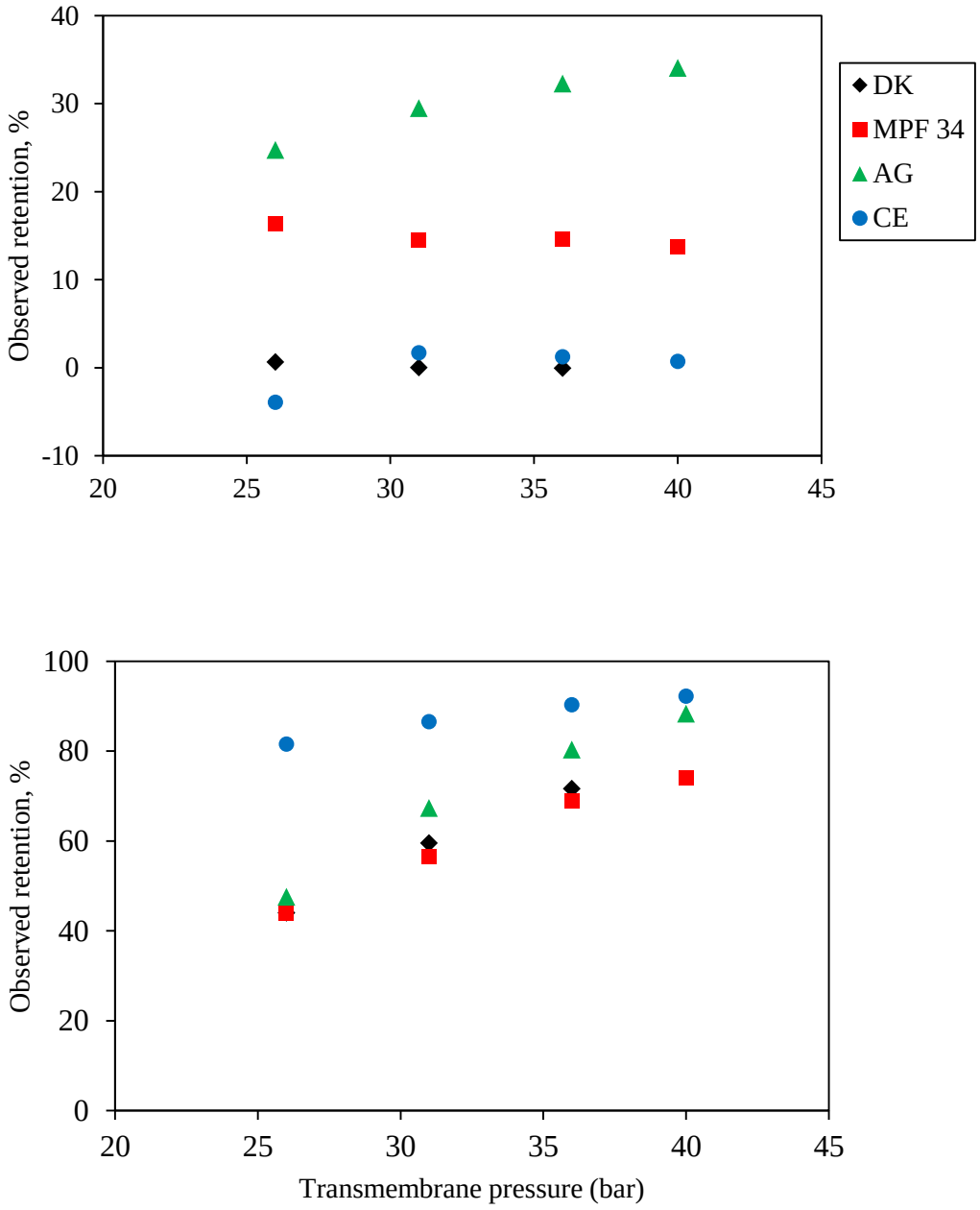

Figure 4-3 Observed retention as a function of transmembrane pressure. (Top) 7 wt% acetic acid (Bottom) 15 wt% glucose solutions

The data for the single-solute solutions at the same concentrations are also shown for comparison. For acetic acid, the retentions in mixed-solute solutions are significantly lower than those in single-solute solutions. This is favorable for the separation process proposed here. A similar phenomenon was reported by Weng et al [85]. They investigated the separation of xylose and acetic acid by nanofiltration and observed that the acetic acid retention was significantly lower in the presence of xylose than that in single-solute solution. Laufenberg et al [92] studied retention characteristics of multicomponent organics by reverse osmosis. They observed that acetic acid retention could be lower or higher in the presence of other organic acids. In both the cases, it was concluded that the alteration in acetic acid retention may be attributed to intermolecular interactions between acetic acid and other components, although further studies are required to understand the link between the intermolecular interactions and the observed changes in retention. Other studies showed that in binary mixtures of salt and sugar, the salt retention was decreased as the sugar concentration increased [93]. This was explained as a result of viscosity increase in the concentration polarization layer due to high retention of sugar, which hampered the back diffusion of the salt. In contrast, Figure 4- 5 shows that the retention of glucose is not much affected by the presence of acetic acid, except for CE membrane for which the retention of glucose in mixed-solute solution is slightly lower than that in single-solute solutions. The observed flux is also slightly higher than that obtained with single-solute glucose solution (not shown). This implies that CE membranes might be swollen in the presence of acetic acid.

4.5 Membrane Stability

Experiments were conducted with the model AFBO, as given in Table 3-2, using Desal DK membrane. A permeance that was unexpectedly high for this concentrated multicomponent

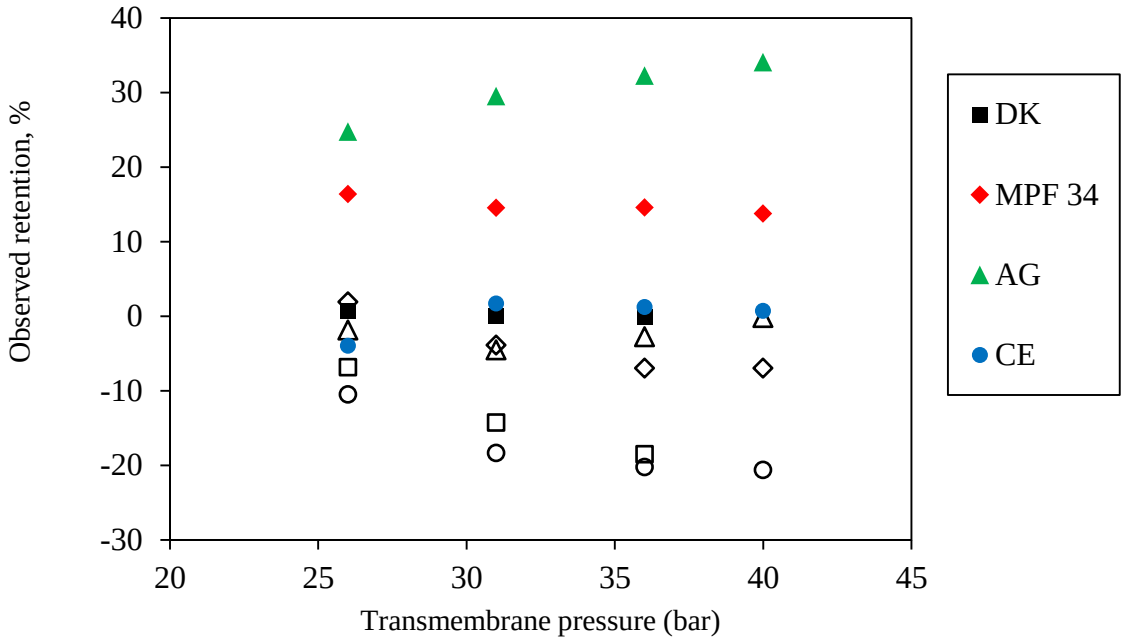

Figure 4-4 Acetic acid retention vs. transmembrane pressure for mixed-solute solution of 7 wt% acetic acid and 15wt % glucose, compared to 7 wt% acetic acid retention in single-solute solution. Closed and open symbols represent single and mixed solute retentions, respectively

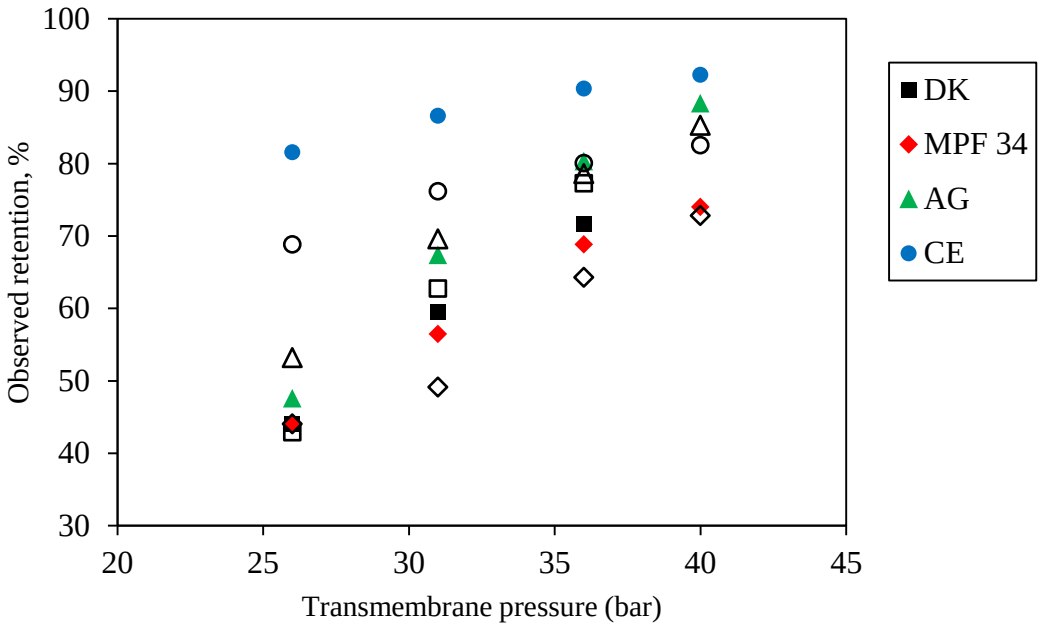

Figure 4-5 Glucose retention vs. transmembrane pressure for mixed-solute solution of 7 wt% acetic acid and 15wt % glucose, compared to 15 wt% glucose retention in single-solute solution. Closed and open symbols represent single and mixed solute retentions, respectively

mixture was observed, indicating that the model AFBO may have damaged the membrane. The membrane was tested again with pure water, and the flux was higher by a factor of 22 as compared to the data in Table 3-1, strongly indicating that irreversible damage had occurred. The results are summarized together with the permeances of single solute solutions of 7 wt% acetic acid and 15wt% glucose in Figure 4-6. Most NF membranes are designed for treating aqueous systems that have low levels of contaminants. Past studies have shown that exposing such membranes to organic compounds at higher concentrations resulted in loss of structural integrity and separation performance [73, 94]. The DK membranes were observed to curl after the permeation experiments with AFBO, which was not the case with binary solutions of glucose and acetic acid. These visual observations on the membranes also support the findings of Yang et al. [94], who observed curling of NF membranes when exposed to different organic solvents. Since the binary mixtures of glucose and acetic acid didn't cause any damage to these membranes, one or more of the new components of the multicomponent mixture likely were responsible.

Permeation experiments were done with different feed solutions to further investigate the cause of damage. Initially, an aqueous solution of furfural was filtered through the membrane. After that catechol, hydroxyacetone, and guaiacol were added step by step. The individual component concentrations were maintained close to those in model AFBO. At each step, the membranes were exposed to feed solution for 30 min and the permeances were measured. The results are shown in Figure 4-7. The permeance declined with addition of new components until guaiacol was introduced into the feed solution. Then the permeance went up dramatically, as it did in the case of model AFBO.

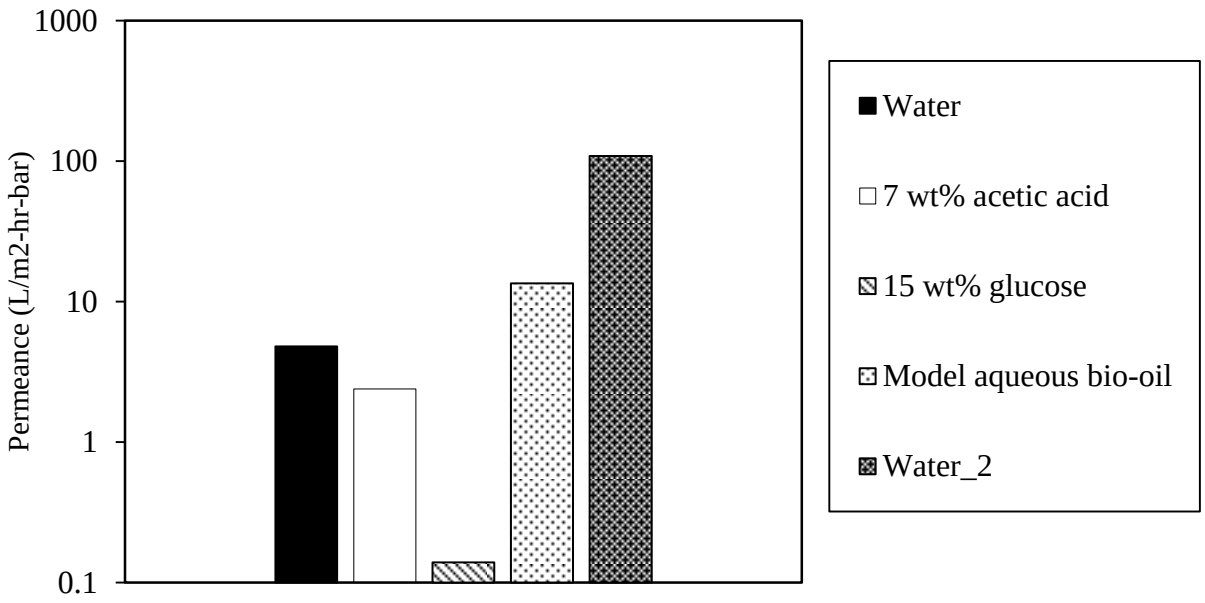

Figure 4-6 Stability test of Desal DK with different feed solutions. The permeance is flux normalized by transmembrane pressure. Water_2 indicates a second pure water test following the model AFBO

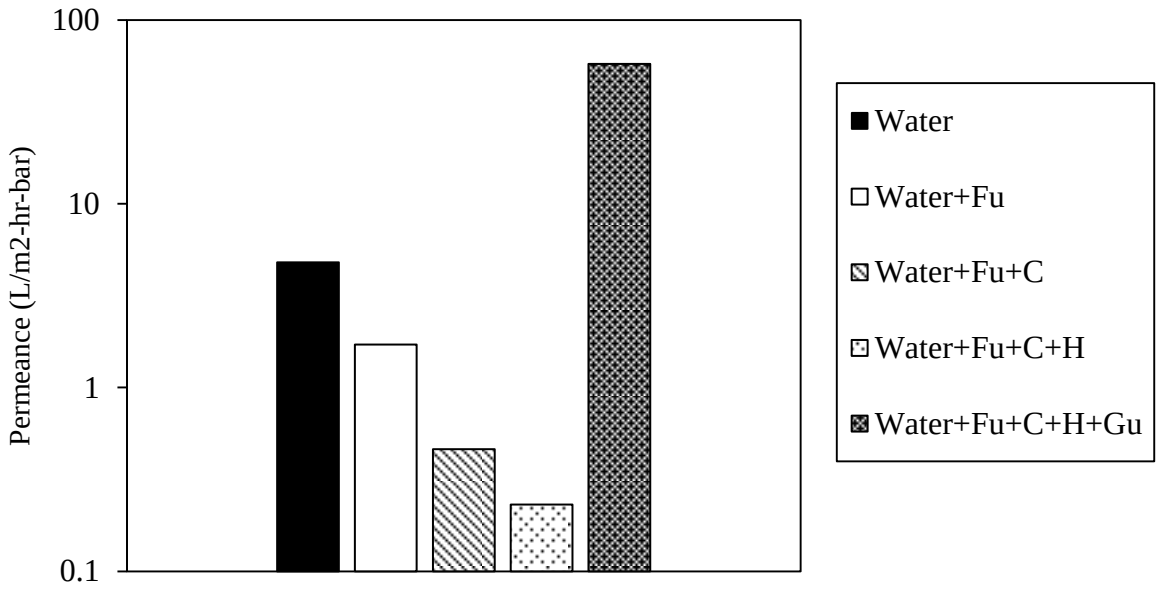

Figure 4-7 Variation in permeance with change in feed components: furfural (Fu), Catechol (C), hydroxyacetone (H), guaiacol (Gu)

Although polyamide membranes are known to be sensitive to chlorine via ring chlorination [54], to our knowledge there exist no literature reports on their sensitivity to phenolic compounds. Polyamide reverse-osmosis membranes were used by Sagehashi et al. [82] to separate phenols and furfural from pyrolysis derived aqueous streams. Bruggen et al studied separation performance of different NF membranes made up of polyamide and polysulfone with a wide variety of organic compounds including phenolics. No membrane damage was reported in either of these studies. However, the concentration of phenolics used in their experiments was an order of magnitude lower than that in our experiments. The effect of solute concentration on membrane compatibility was examined by performing filtration experiments with solutions of guaiacol and phenol at different concentrations using Desal DK and MPF 34 membranes. At each concentration, the feed solutions were filtered for 30 min and the concentration was increased step by step. The results are summarized in Figure 4-8. Both membranes showed similar qualitative behavior with guaiacol and phenol. Permeance initially decreased as the concentration of the phenolic compounds in the feed solution was increased, up to a "critical concentration" at which it started to increase. The critical concentrations at which the membranes started to show signs of damage were different for guaiacol (~1.5 wt%) and phenol (~5 wt%). Above the critical concentration, the active (top) layer of treated membranes developed visible pinches while the bottom layer seemed unaffected. Optical microscopy was carried out to characterize both virgin and guaiacol-treated Desal DK membranes. The images are shown in Figure 4- 9. The images show that the active surface was not uniformly dissolved in guaiacol but was damaged at certain spots. On the other hand, the bottom layer was not affected. Experiments using RO AG and RO CE membranes were also conducted with 1.5 wt% of guaiacol solution. The RO AG membranes developed a very high permeance similar to that of

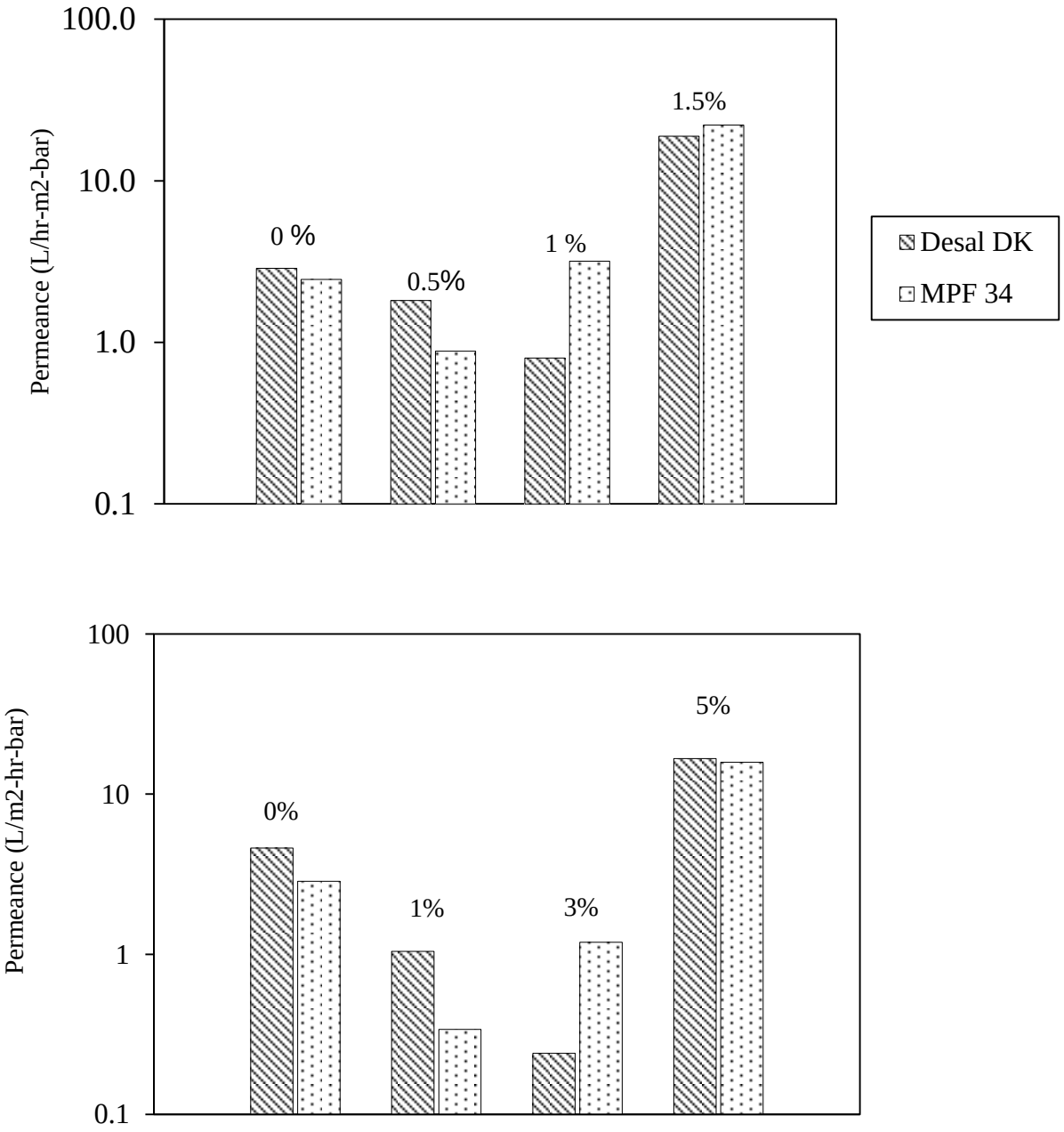

Figure 4-8 Contents in feed solutions for Desal DK and MPF 34. (Top) Guaiacol and (Bottom) Phenol

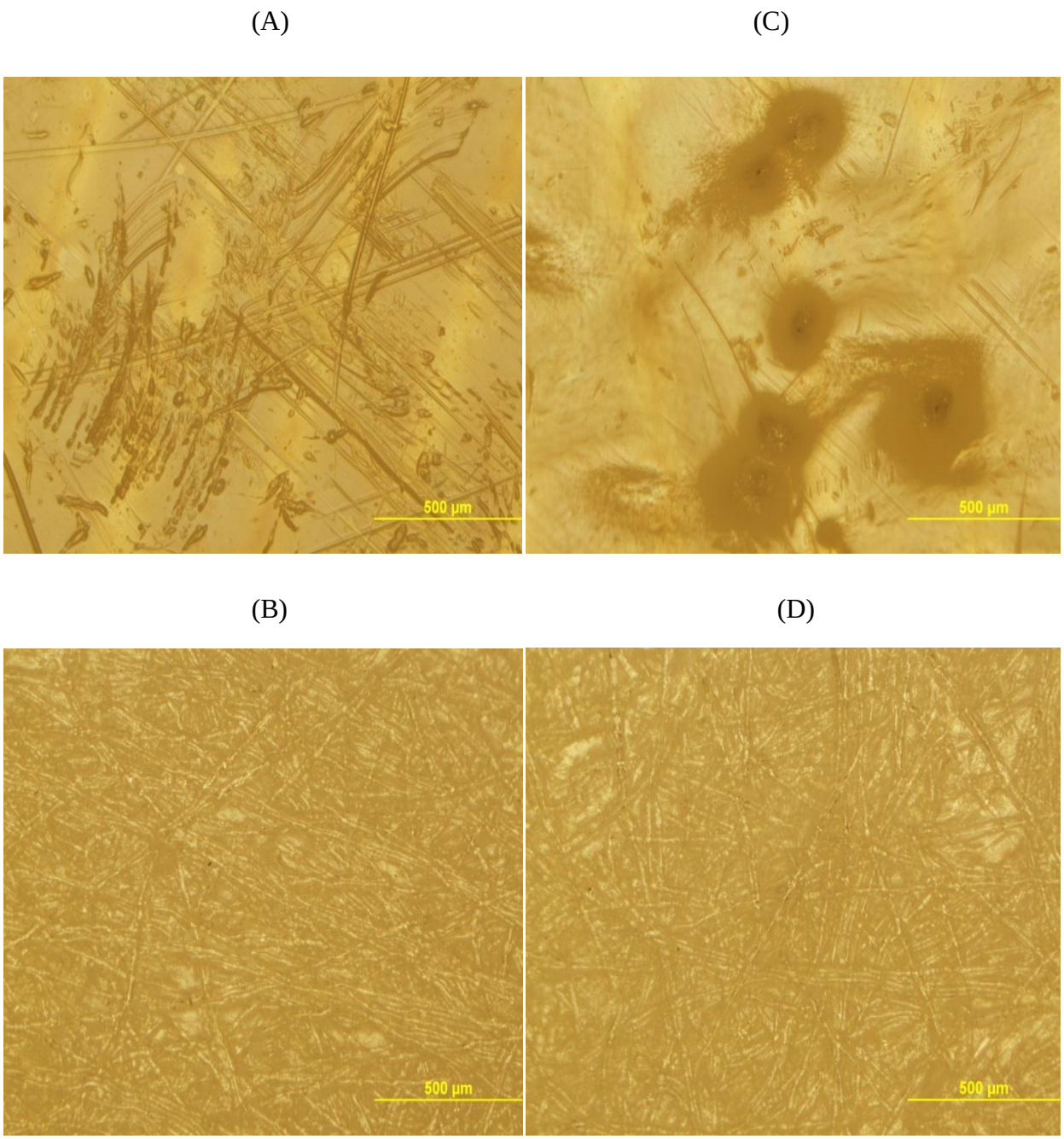

Figure 4-9 Optical microscopic images. (A) Top layer and (B) Bottom layer of virgin membrane (C) Top layer and (D) Bottom layer of guaiacol treated membrane

Desal DK and MPF 34 membranes. In contrast, the flux through the RO CE membrane was seen to drop until it was no longer measurable, suggesting that the mechanism of damage may be different for this membrane.

Experiments with aliphatic alcohols, methanol and ethanol, were also conducted. Both the membranes, Desal DK and MPF 34, were very stable up to alcohol concentrations as high as 18 wt%. Compared to aliphatic alcohols (p*K*a ~ 15), phenolics (p*K*a~10) have a greater tendency to deprotonate, resulting in highly water-soluble phenoxide ions, *e.g.* $C_6H_5O^-$. (One explanation for the greater acidity of phenolics is the delocalization of negative charge over the aromatic ring). These phenoxide anions might react with an amide group on the membrane and convert it to a corresponding ester, providing a possible explanation for the observation that membrane damage occurred with phenolics but not with aliphatic alcohols. However, comparing the two phenolics, membrane damage occurred at a lower solute concentration with guaiacol as compared to phenol, though the pKa values of both are almost equal. At this point further investigation is needed to explain the chemical mechanism behind the damage.

4.6 Modified Model Aqueous Fraction of Bio-oil

Due to membrane damage by guaiacol, experiments with model AFBO excluding guaiacol were conducted using all four types of membranes at a transmembrane pressure of 40 bar. Both the RO membranes failed to yield meaningful results. With the RO CE membrane there was no measurable flow. The active layer of RO AG membranes turned pink after treating with model AFBO and glucose retention was very low (~ 20%). The permeate solution was believed to be contaminated due to the chemical changes that took place in the active layer; therefore the data for RO AG is not presented here. Data at 40 bar were obtained with the two NF membranes, Desal DK and MPF 34, and was averaged over two membrane samples in each

case. Solute retentions are summarized in Table 4-2 (Columns 2 and 4). Formic acid and catechol had very low signals in the feed and permeate and were almost undetected by GC, so they are not shown in the table. Glucose retention is positive and all other solutes have negative retentions. However the glucose retention is lower than that in single and binary solutions. This result is consistent with the findings of Goulas et al. [95] who found that in mixtures of oligosaccharides, individual sugar retentions decreased as the total sugar concentration increased. Another possible explanation is that there might be positive coupling between glucose and other components present in the model AFBO that in turn reduced the glucose retention.

Since the glucose retentions achieved at 40 bar with model AFBO were moderate, experiments were performed with the Desal DK membrane at a higher pressure, 58 bar. The results are also shown in Table 4-2 (Column 3). Glucose retention is increased from 47% to 83% as the transmembrane pressure increased from 40 to 58 bar. Furthermore, the retentions of all other compounds became more negative. These results indicate that the separation of acids and other low molecular weight organic compounds from glucose is operationally feasible at high transmembrane pressures.

4.7 Effect of Concentration on Flux

The effect of total feed concentration on flux is shown in Figure 4-10. Our results indicate that higher the concentration of the feed solution the lower the flux. These results are consistent with the findings of Sjöman et al [84]. With Desal DK membranes they found an order of magnitude decrease in flux as the concentration of the feed (binary mixture of xylose and glucose in the mass ratio 1:1) increased from 10 wt% to 30 wt%. Yang et al [94] observed similar behavior with aqueous solutions of dyes. At a pressure of 30 bar, the water fluxes at dye concentrations of 35 and 10000 mg/l were 24 and 18 L m^{-2} h^{-1}, respectively. Due to high feed

Table 4-2 Retention of components present in model aqueous fraction of bio-oil, without guaiacol. Formic acid and catechol were undetectable

	Retention, %		
Compound	Desal DK		MPF 34
	40 bar	58 bar	40 bar
Glucose	**47.4**	**83.1**	**54.7**
Acetic acid	-14	-16.7	-7.7
Hydroxyacetone	-9	-15.9	-1.35
Furfural	-12	-35.6	-14.4

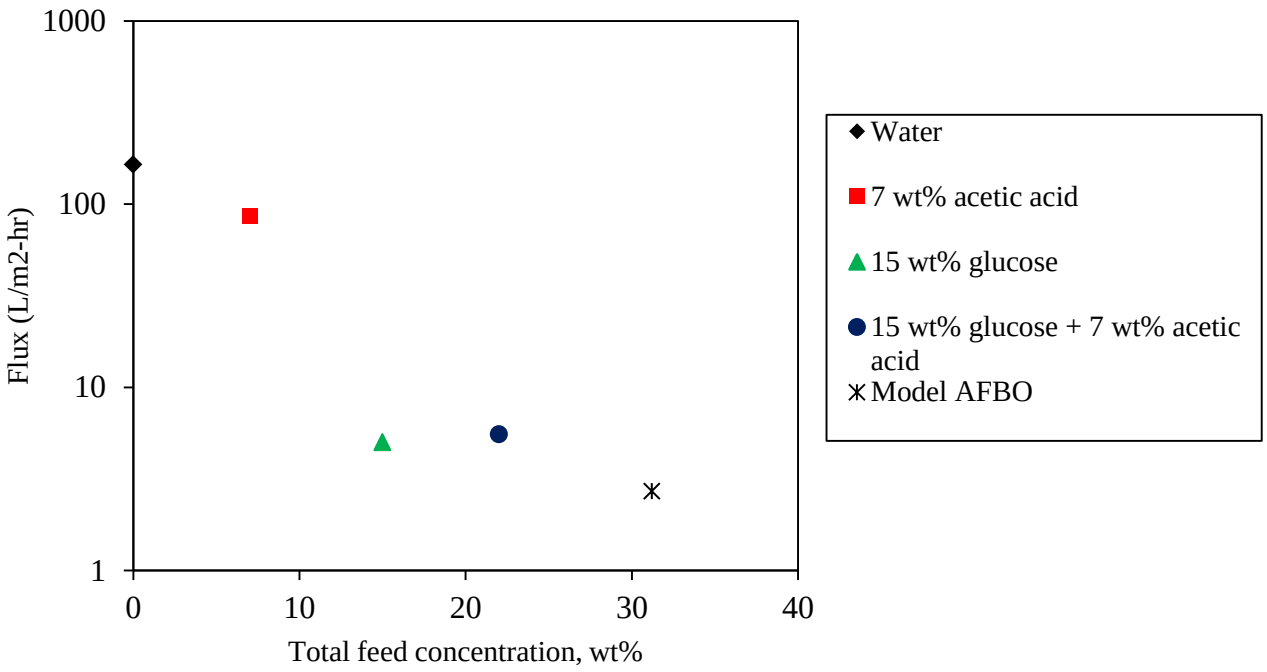

Figure 4-10 Effect of total feed concentration on flux (measurements were made at constant pressure, 36 bar)

concentrations and low cross flow velocities used in our work, concentration polarization cannot be neglected. Accordingly, flux would decrease due to the increased resistance near the membrane surface. Also when a solute is added to the pure water, the driving force for water flux decreases as can be seen from Equation (4- 1); the effective transmembrane pressure that drives the feed is equal to the applied hydraulic pressure minus osmotic pressure difference. Other possible explanations include increase in viscosity, adsorption, or blocking of the membrane pores.

4.8 Effect of Membrane Pretreatment

In section 3.2.4, it is shown that pretreatment by pressure effects pure water permeance of Desal DK membranes. Permeation experiments with modified AFBO were conducting using treated and untreated membranes. The effect of pretreatment (pressurizing membranes with pure water [88]) on membrane performance is evaluated by plotting glucose retention vs. permeance and is shown in Figure 4-11. A trade-off relation was observed between retention and permeance of treated and untreated membranes, i.e. high retentions are accompanied by low permeances and vice versa. Pretreatment by pressure clearly opens up the membrane pore structure which resulted in a subsequent increase in permeance accompanied by reduction in glucose retention. Therefore pretreating the Desal DK membranes is not recommended when higher retentions are required.

4.9 Conclusions

Commercially available NF and RO membranes were used to study the possibility of separating carboxylic acids from sugars in AFBO. Initial experiments were run with single and binary solute model aqueous solutions to test the performance of the membranes. The effects of cross flow velocity, pressure, concentration, and pretreatment on membrane performance were

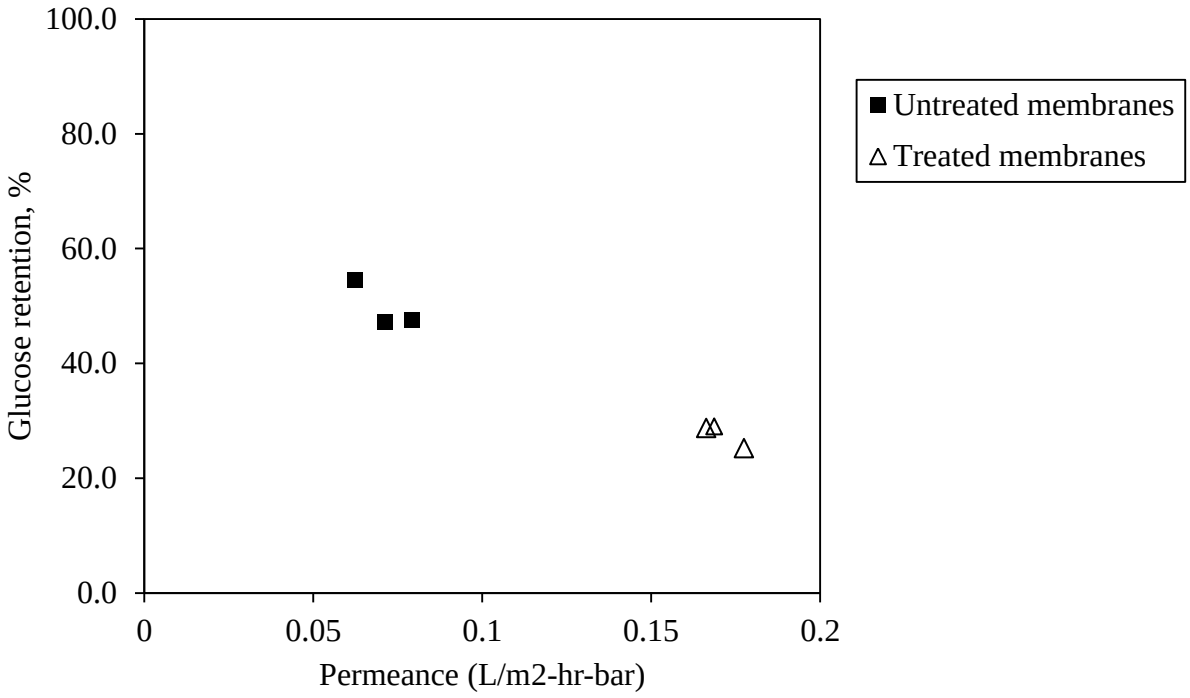

Figure 4-11 Glucose retention vs. permeance of treated and untreated Desal DK membranes. Data is plotted for three treated and untreated membranes

explored. Experiments with glucose solution, conducted at different cross flow velocities, showed that increasing the cross flow velocity increased the observed retention. Therefore it is confirmed that observed retention is strongly dependent on the concentration polarization and hence changes with the flow conditions near the membrane surface.

Experiments with single and binary aqueous solutions of acetic acid and glucose showed that retention factors of glucose above 90% and negative retention factors of acetic acid could be achieved at moderate (~ 40 bar) feed pressures. Fluxes were linearly dependent on transmembrane pressure. In general, both flux and solute retention increased as the transmembrane pressure is increased. This can be explained using solution-diffusion model for solvent and solute transport through the membrane. The binary experiments showed that glucose retention is largely unaffected by the presence of acetic acid (except for the RO CE membrane) but acetic acid retention decreases significantly in the presence of glucose. This might be explained as an effect of viscosity increase of the concentration polarization layer due to high retention of sugar, which hampered the back diffusion of the acetic acid resulting in reduced acetic acid retention. Experiments with the model AFBO resulted in irreversible damage to the membranes. Subsequent experiments identified guaiacol as the detrimental compound and further demonstrated that phenol causes a similar effect. The active (top) layer of guaiacol treated membranes had visible pinches while the bottom layer seemed unaffected. Optical microscopic images of both virgin and guaiacol treated membrane had confirmed the damage. Experiments with guaiacol-free model AFBO showed that high retentions (> 80%) of glucose are possible with NF membranes at higher feed pressures (~ 60 bar). Finally, the effect of pretreatment by pressure on membrane was explored. An inverse correlation was observed

between retention and permeance of treated and untreated membranes, i.e. high retentions are accompanied by low permeances and vice versa.

CHAPTER 5

MODELING MEMBRANE TRANSPORT AND COMPARISION WITH EXPERIMENTAL DATA

Transport of mobile species across a membrane takes place under one or more driving forces. Generally speaking, a gradient in electrochemical potential acts as the driving force. Specifically, the gradient in electrochemical potential may arise from gradients in pressure, concentration, temperature and/or electrical potential. The transmembrane flux, or amount of species per unit cross-sectional area per unit time crossing the membrane, is proportional to the driving force with permeance being the proportionality constant. Both the driving force and the permeance depend on the mechanism of transport. Therefore it is important to understand the nature of transport in membranes. Also models that adequately characterize the membrane performance are needed in the design of membrane processes. In this chapter the discussion is limited to transport of liquid solutions, containing low molecular weight solutes, through the membranes. The goal is to develop mathematical models that explain the experimental data and allow one to predict future experiments.

5.1 Classification of Membrane Models

Many mechanistic and mathematical models have been developed to describe the transport in membranes. These models can be categorized in to two groups: irreversible thermodynamic and structure-related models. In the first type, the membrane is treated as a black box in which the processes are not far from equilibrium. No information regarding the structure of the membrane and the mechanism of transport is needed. The thermodynamics of irreversible processes are useful especially when flow coupling exists between various components. The

coupling may be either positive or negative. In positive (negative) coupling the flux of one component increases (decreases) the flux of a second component.

In structure-related membrane models, some mechanism of transport is assumed and the physiochemical properties of the membrane and the solution are involved. For example, the structure parameters such as pore size, porosity, tortuosity, and the pore size distribution, the membrane thermodynamic properties such solvent and solute solubility and the membrane kinetic properties such as diffusivity of solute and solvent are taken into account. Again, two types of structure-related models are developed: one for porous membranes and the other for nonporous membranes. If all the information regarding the membrane properties is available, one can predict the membrane performance, without having experimental data, under real operating conditions. From this point of view, these models are more useful than the irreversible thermodynamic approach. The individual models are discussed in detail in the following sections.

5.1.1 Irreversible Thermodynamic (IT) Models

5.1.1.1 Basic Principles of Irreversible Thermodynamics

In irreversible or nonequilibrium thermodynamics it is assumed that the system can be divided into small volume elements in which local equilibrium exists and therefore thermodynamic state variables can be written for these elements. For processes near equilibrium, all fluxes (flows) are linearly dependent on all forces. The resulting set of equations, called phenomenological equations, can be written as follows [96]

$$J_i = \sum_j^n L_{ij} X_j \qquad (i = 1, 2, \ldots, n) \tag{5-1}$$

where J_i and X_i are the generalized fluxes and forces, respectively, and L_{ij} is a phenomenological

coefficient. This relation allows the possibility of coupling when multiple fluxes and forces are present.

5.1.1.2 Kedem – Katchalsky Model

Irreversible thermodynamics have been applied to many types of membrane processes and the first practical model was developed by Kedem and Katchalsky [97] for transport of non electrolytes through membranes. For dilute, isothermal and steady state systems consisting of solvent and solute, the transport equations are represented by

$$J_v = L_p (\Delta P - \sigma \Delta \pi) \quad (5\text{-}2)$$

$$J_s = \omega \Delta \pi + (1 - \sigma) (C_{s)ln} J_v \quad (5\text{-}3)$$

where J_v is the volume flux (usually solvent flux), J_s is the solute flux, L_p is the hydraulic permeability, $\omega = (J_s/\Delta\pi)_{Jv=0}$ is solute permeability at zero volume flux, σ is the reflection coefficient, ΔP is the transmembrane pressure, $\Delta\pi$ is the osmotic pressure difference across the membrane and $(C_s)_{ln}$ is the logarithmic mean solute concentration in the membrane. The imperfection of the membrane is defined by the reflection coefficient and usually has a value between 0 and 1.

$\sigma = 1 \rightarrow$ ideal semipermeable membrane, no solute transport

$\sigma < 1 \rightarrow$ not a completely semipermeable membrane; solute transport

$\sigma = 0 \rightarrow$ no retention.

While the thermodynamics of irreversible processes can describe membrane transport, a major drawback is the description of the membrane as a black box from which no insight is provided about the transport mechanisms of the membrane. Therefore, these models are not useful for predicting separations based on membrane structure and properties. Also when there

are larger gradients in the driving forces across the membrane, the application of linear laws is limited.

5.1.2 Structure-related Models

Membranes can be macroporous, microporous or dense (nonporous). In the porous membranes, components are permeated by convection and/or diffusion through pores and the transport is described using pore flow models, whereas the mechanism of transport in dense membranes is described by solution-diffusion model. The difference between these mechanisms lies in the relative pore size and associated modes of transport in the pores. Although mechanisms of liquid and gas transport are similar, the governing equations are slightly different and hence they are explained separately. The models used to describe the mechanism of liquid transport are illustrated in Figure 5-1.

5.1.2.1 Pore Models

Transport mechanisms of liquids through porous membranes are shown in Figure 5-2 a, b, and c. These membranes have pore sizes in the range of 2 nm to 10 μm. The governing equation for one dimensional liquid transport through membranes is often expressed as follows [98]

$$N_i = \rho_i \upsilon - D_{ei} \frac{d\rho_i}{dx} \tag{5-4}$$

where N_i is the mass flux of component i, ρ_i is the mass density of component i, υ is the mass average velocity of liquid, D_{ei} is the effective diffusion coefficient of component i. The first term in the above equation represents flux due to pressure-driven convection and the second term represents flux due to diffusion.

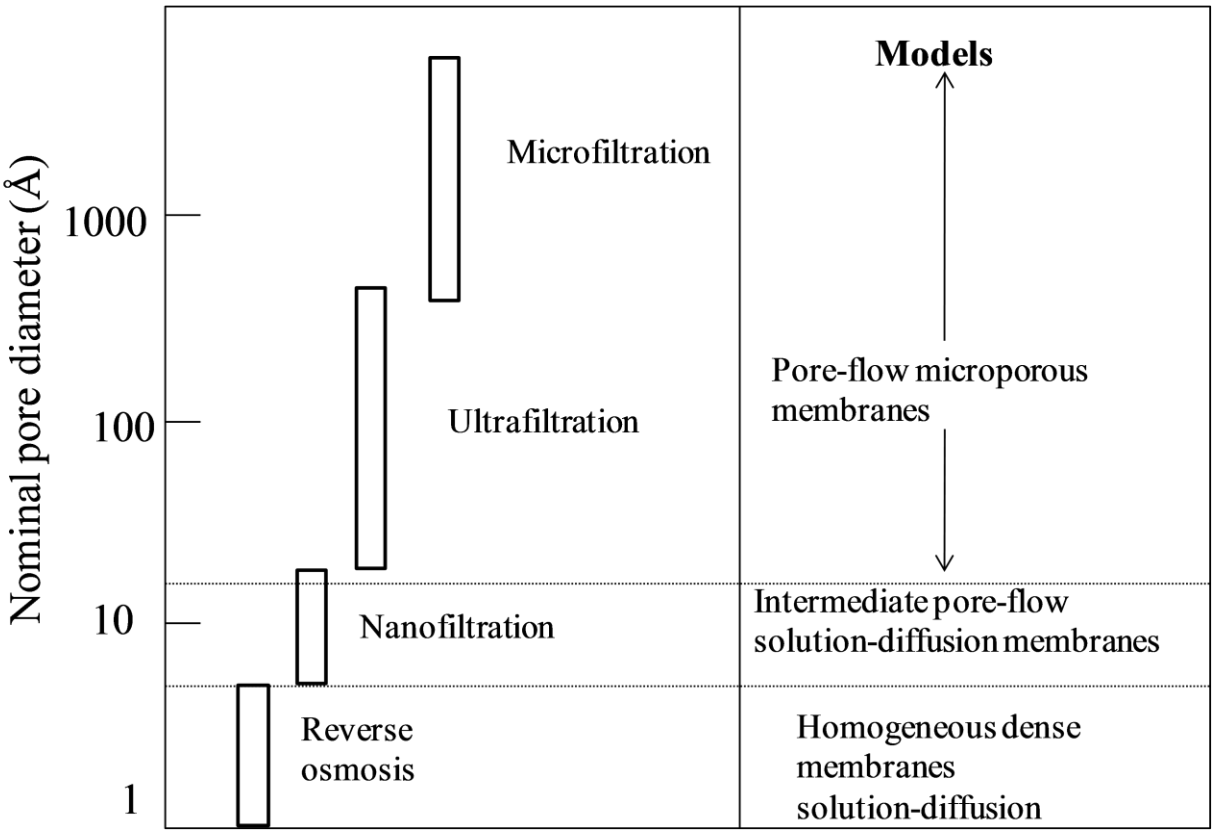

Figure 5-1 Schematic representation of the nominal pore size and the best theoretical model for the principal membrane separation processes. Adapted from [46].

5.1.2.2 Convective Flow

If the pore size is large compared to the molecular diameter and a pressure gradient exists across the membrane, bulk or convective flow occurs through the pores as depicted in Figure 5-2 a. In this case, diffusion is typically negligible relative to bulk flow. Both ultrafiltration and microfiltration operate in this regime and the separation occurs mainly by sieving of particles larger than the pore size. Different pore flow models have been developed to characterize the flow velocity, υ, due to the existence of different pore geometries. The bulk flow of a liquid due to pressure gradient, through an ideal membrane consisting of cylindrical pores with orientation perpendicular to the surface is given by the Hagen-Poiseuille law [99]. Assuming that all the pores have the same dimension, the volumetric flux through the membrane is given by

$$J = \frac{\varepsilon r^2}{8\eta\tau}\frac{\Delta P}{\Delta x} \tag{5-5}$$

where ΔP is the pressure difference across a membrane of thickness Δx, r is the pore radius, η is the viscosity, ε is the surface porosity, which is the fractional area of the membrane occupied by the pores and τ is the pore tortuosity (For cylindrical perpendicular pores, τ = 1). In the real membranes pores may not be cylindrical and the flux equation given by Equation (5-5) should be modified.

5.1.2.3 Diffusion

When identical pressures but different component concentrations exist on both sides of the membrane, the transport of liquid is via diffusion. In that case, there is no or little bulk flow through the membrane and permselective diffusion of components through the pores results in an effective separation as shown in Figure 5-2 b. If the pore size and molecular sizes of some components in the feed mixture are of the same order, the diffusion of those components will be

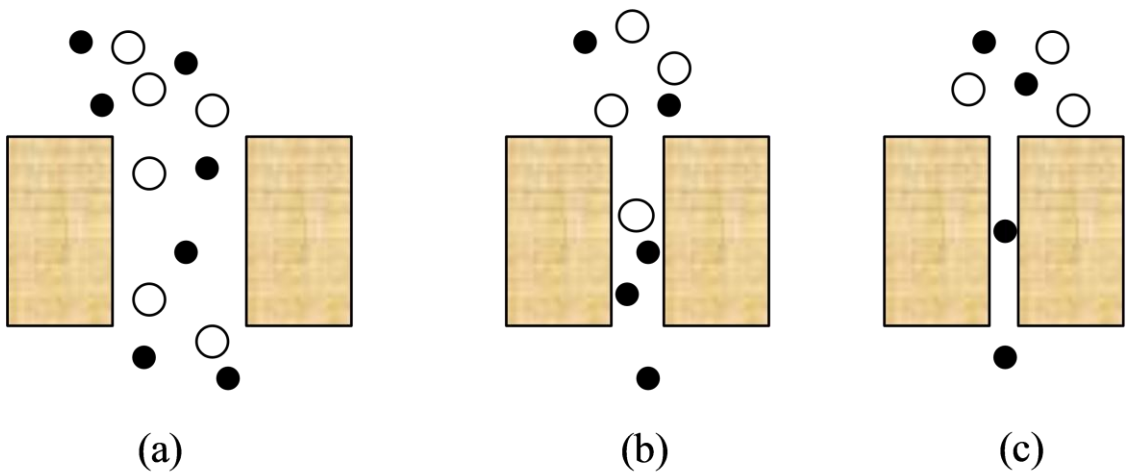

Figure 5-2 Mechanisms of molecular transport through porous membranes. (Flow is downward.) (a) Convective or bulk flow through pores; (b) diffusion through pores; (c) restricted diffusion through pores.

restricted as shown in Figure 5-2 c. Molecules larger than the pores will be excluded from diffusing through the membrane, resulting in enhanced separation. In a feed mixture of solvent and solutes *i*, the flux for each species is given by a modified form of Fick's law [100]

$$J_i = \frac{D_{ei}}{l_m}(C_{if} - C_{ip}) \tag{5-6}$$

where D_{ei} is the effective diffusion coefficient, C_{if} and C_{ip} are the concentrations of species *i* in the pores at the feed and permeate membrane interfaces, respectively, and l_m is the thickness of the membrane. Generally, the effective diffusivity depends, often in a complex way, on factors such as the porosity and tortuosity of the membrane and the ratio of molecular diameter to pore diameter.

5.1.2.4 Solution-diffusion (SD) Model

The transport through nonporous (dense) membranes can be described in terms of solution-diffusion mechanism as indicated in Figure 5-3. It is assumed that liquid components (solvent and solutes) are transported under the chemical potential gradient in an uncoupled manner. These gradients are the result of pressure and concentration differences across the membrane. Transport usually consists of three steps: (1) absorption of liquid components into the membrane at the upstream face, (2) activated diffusion through the solid membrane, and (3) desorption from the downstream face. The permeated components are separated because of the differences in solubilities and diffusivities of the components in the membrane phase. This model is widely used to describe the transport through nonporous membranes. In this section the SD transport model is applied to nanofiltration and reverse osmosis membranes. According to this model, the water transport across the membrane is only by diffusion and the flux is given by Fick's law [101]

$$J_w = -D_{wm}\frac{dC_{wm}}{dx} \tag{5-7}$$

where D_{wm} and C_{wm} are the concentration and diffusivity of water in the membrane, respectively. Assuming the water-membrane solution obeys Henry's law, $d\mu_w = RTd\left(\ln C_{wm}\right)$, Equation (5-7) becomes

$$J_w = -\frac{D_{wm}C_{wm}}{RT}\frac{d\mu_w}{dx} \approx \frac{D_{wm}C_{wm}}{RT}\frac{\Delta\mu}{l_m} \tag{5-8}$$

The chemical potential of any component at any temperature and pressure, $\mu_i\ (T, P)$ can be defined as

$$\mu_i(T,P) = \mu_i^{\,0}(T,P^{ref}) + v_i\ (P - P^{ref}) + RT\ln a_i \tag{5-9}$$

where $\mu_i^0\ (T, P^{ref})$ is the chemical potential in some standard compositional state (usually pure i) and some reference pressure P^{ref}, v_i is molar volume, a_i is chemical activity, R is gas constant and T is absolute temperature. For ideal dilute solutions, where the volume fraction of the solute is small and using Equation (5-9), $\Delta\mu_w$ can be redefined as

$$\Delta\mu_w = v_w\left(\Delta P - \Delta\pi\right) \tag{5-10}$$

where π is the osmotic pressure and is given by

$$\pi = \frac{-RT}{v_w}\ln a_w \tag{5-11}$$

Substituting Equation (5-10) into Equation (5-8), one gets

$$J_w = \frac{D_{wm}C_{wm}v_w}{RT\,l_m}\left(\Delta P - \Delta\pi\right) \equiv A\left(\Delta P - \Delta\pi\right) \tag{5-12}$$

where A is the water permeability coefficient and is defined by the second equality in Equation (5-12). In deriving this result, it has been assumed that D_{wm}, C_{wm}, and v_w are independent of

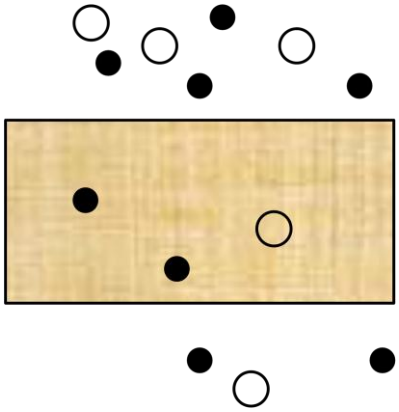

Figure 5-3 Mechanism of transport in dense membranes.

pressure. For the solute flux it is assumed that the chemical potential difference due to pressure is negligible and the flux is almost entirely due to concentration differences and is given by Fick's law

$$J_s = -D_{sm}\frac{dC_{sm}}{dx} \approx D_{sm}\frac{\Delta C_{sm}}{l_m} \tag{5-13}$$

where D_{sm} is the solute diffusion coefficient in the membrane and ΔC_{sm} is the solute concentration difference across the membrane. In Equation (5-13), it is assumed that the concentration profile within the membrane is linear which may not be valid at higher concentrations. Since it is difficult to measure the solute concentration in the membrane, it is related to the liquid phase feed and permeate concentrations using the partition coefficient, K_{sm}. When this is done, Equation (5-13) becomes

$$J_s = \frac{D_{sm}K_{sm}}{l_m}\left(C_{smi} - C_{spi}\right) \equiv B\left(C_{smi} - C_{spi}\right) \tag{5-14}$$

where B is defined as the solute permeability coefficient and C_{smi}, and C_{spi} are solute concentrations in the liquid feed and permeate at the membrane interface, respectively. Note that the approximation that diffusion and partition coefficients are constant may not be valid at higher concentrations, and this model doesn't include the effect of pressure on solute transport. Equation (5-12) predicts that water flux will be in opposite direction if $\Delta P < \Delta\pi$, then will flow in conventional direction when $\Delta P > \Delta\pi$, whereas according to Equation (5-14) solute flow is independent of pressure. Furthermore, the solute flux, J_s, is related to the water flux by

$$J_s = J_w \, .C_{spi}/C_{wpi} \tag{5-15}$$

where C_{wpi} is the water concentration in the membrane on the permeate side. The selectivity of a membrane for a given solute is expressed by retention coefficient R

$$R = 1 - \frac{C_{spi}}{C_{smi}} \tag{5-16}$$

By combining Equations (5-12), (5-14), (5-15) and (5-16), the retention coefficient can be written as

$$\frac{1}{R} = 1 + \frac{B}{A}\left(\frac{C_{wpi}}{\Delta P - \Delta\pi}\right) \tag{5-17}$$

Equation (5-17) expresses the retention in terms of the physical properties of the membrane and the driving force $\Delta P - \Delta\pi$. Note that when $A\ (\Delta P - \Delta\pi) >> B\ C_{wpi}$, the water flux will be much greater than solute flux resulting in almost complete retention of the solute ($R = 1$). Comparison of Equations (5-2) and (5-3) with Equations (5-12) and (5-14) shows that SD model is equivalent to irreversible thermodynamic model for a membrane with perfect solute retention ($\sigma = 1$). Equation (5-17) allows one to predict membrane performance based on the experimental data and membrane properties.

In the above models, only the resistance of membrane is involved. In practice external mass resistances in the boundary layers exist and should be included where appropriate. As described in section 3.3, in case of concentration polarization, the solute concentration at the membrane interface is higher than the bulk feed solute concentration. Therefore, in evaluating Equations (5-12), (5-14) and (5-16), the solute concentration in the liquid feed at the membrane interface, calculated using film theory model, should be used.

5.2 Comparison of Experimental and Theoretical Data

Some of the results described in chapter 4 were used to develop the solution –diffusion (SD) model for the systems we studied.

5.2.1 Estimation of Model Parameters

Osmotic pressures of feed and permeate were calculated using two different methods: van't Hoff equation and OLI Stream Analyzer software (OLI systems, New Jersey). The van't Hoff equation, appropriate for dilute solutions, is given by

$$\pi = i\,C\,R\,T \tag{5-18}$$

where C is molar concentration of solute, R is gas constant, T is absolute temperature and i is van't Hoff factor that accounts for the degree of association or dissociation of solute. Since glucose and acetic acid neither associate nor dissociate at the given experimental conditions, i = 1. OLI Stream Analyzer calculates the osmotic pressure of solutions based on the activities of water. The pure water permeance, A, was determined from flux vs. pressure data by linear regression using Equation (5-12). In case of pure water, the osmotic pressure ($\Delta\pi$) is zero. Figure 5-4 shows the pure water flux data of Desal DK NF membrane. The slope of the fitted line, which is the constant A, is 1.32E-11 m-sec^{-1}-Pa^{-1}. The same procedure is applied to calculate pure water permeances of different membranes. Measured values are compared with manufacturer's data and are shown in Table 5-1. It can be seen that there is a good agreement between them. The parameter B was calculated from the solute flux data using Equation (5-14). Because of the high concentrations and low cross flow velocities used it was not possible to eliminate concentration polarization (CP). In this case, solute concentration evaluated at the membrane surface, C_{smi}, is used in Equation (5-14) to include the effects of CP.

Film theory model, explained in chapter 3, was used to calculate C_{smi} and is explained below

1. At a given pressure drop, ΔP, and feed concentration, C_{sf}, permeate flux, J_w, and permeate concentration, C_{spi}, were determined experimentally.

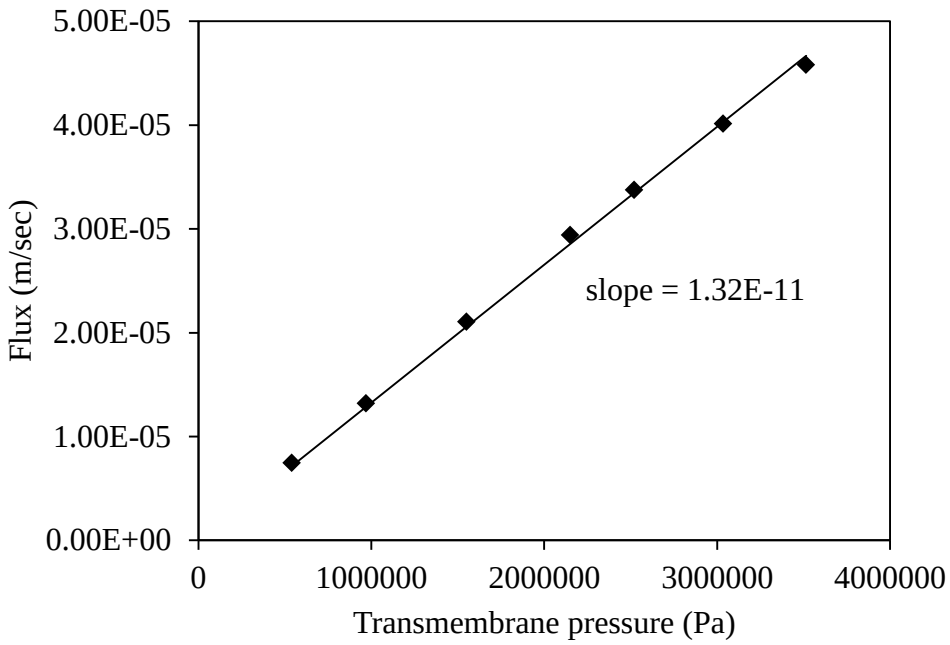

Figure 5-4 Pure water flux versus pressure drop of Desal DK NF membrane. ♦ represents experimental data. – represents fitted line

Table 5-1 Pure water permeances of different membranes calculated from experiments. Manufacturers' data is provided in parenthesis for comparison.

Membrane	Permeance (10^{-12} m-sec^{-1}-Pa)
Desal DK (NF)	13.3 (15.1)
MPF 34 (NF)	4.75 (5.42)
GE AG (RO)	7.97 (7.92)
GE CE (RO)	3.66 (3.83)

2. Solute flux, J_s, was calculated using Equation (5-15) and the mass transfer coefficient, k, was calculated using Equation (3-8).

3. From Equation (3-6), C_{smi} can be calculated which in turn was used in the Equation (5-14) to calculate solute permeability, B.

Once A and B as a function of transmembrane pressure are known, flux and retention can be predicted using Equations (5-12) and (5-17).

5.2.2 Glucose – water Mixture

The effect of transmembrane pressure on water flux is shown in Figure 5-5. As confirmed by the SD model, the water flux increased with increasing transmembrane pressure for all the membranes tested. However, there is no good match between the experimental and theoretical data. The model was unable to match the slope of the experimental flux against pressure and also over-predicted the flux. This deviation might be due to large pressure and concentrations gradients across the membrane. At high concentrations, film theory model, which is an idealized model, cannot give accurate predictions of concentration polarization which in turn results in inaccurate predictions of glucose concentration at the membrane interface. In our experiments, the concentration polarization (CP) modulus, defined as C_{smi}/C_{sf}, ranged from 1.04 to 1.17 as calculated from the film theory using Equation (3-6). Weng et al [27] used the combined model, film theory and velocity variation method, to calculate the concentration polarization modulus of xylose at different cross flow velocities and at a lower feed concentration (xylose = 100 g/l and acetic acid =10 g/l). A detailed description of this model is discussed in section 2.2.2. They observed that xylose CP modulus decreased from 2.38 to 1.62 when the cross flow velocity changed from 0.09 m/s to 0.27 m/s. According to their results, we should obtain higher CP modulus because we performed experiments at higher concentrations (glucose = 150 g/l) and at

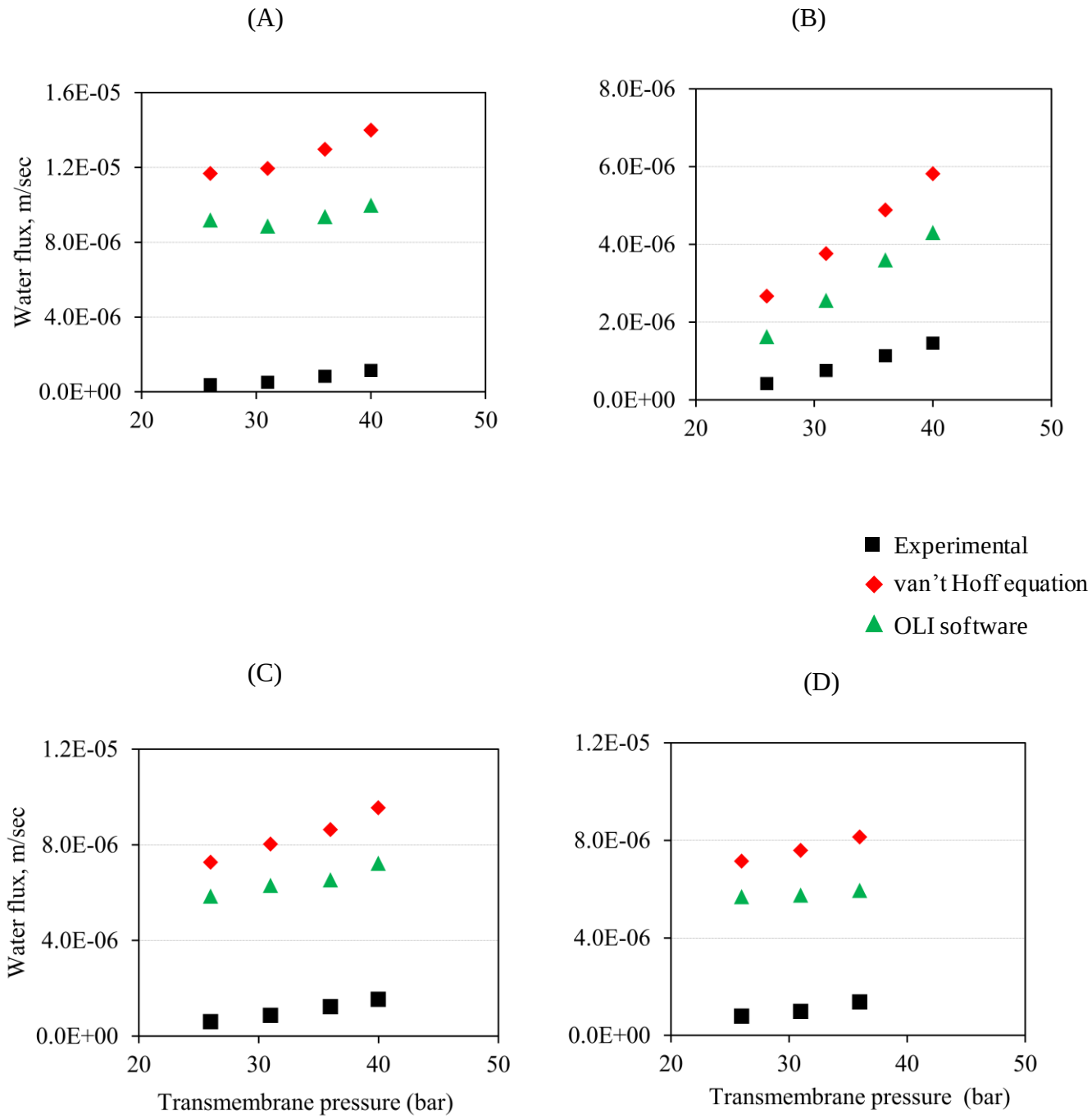

Figure 5-5 Influence of transmembrane membrane pressure on the water flux. Glucose concentration is 15 wt%. (A) RO_AG (B) RO_CE (C) MPF 34 and (D) Desal DK

lower cross flow velocity (0.026 m/s). The inconsistency might also be due to slightly different methods used to calculate surface concentrations. From Equation (5-12) it is clear that the water flux depends on both the applied hydraulic pressure and osmotic pressure difference. Based on glucose surface concentration calculated from film theory model, the osmotic pressure difference is calculated. Hence the evaluation of surface concentration is very critical in modeling highly concentrated solutions. We expect that C_{smi}/C_{sf} should be bigger for our experiments, this will increase $\Delta\pi$ and thus decrease the predicted flux, bringing it closer to the experimental data. The effect of concentration on the ideality of the system can also be seen from the modeling data. Data obtained from OLI software is closer to the experimental data than that of obtained by van't Hoff equation. OLI software, as claimed by the provider, uses the water thermodynamic data, without any assumptions regarding the nature of the solution, to calculate the osmotic pressures and can be used in case of concentrated solutions where as the van't Hoff equation is valid only for dilute systems.

Figure 5-6 provides the retention profiles of glucose at different transmembrane pressures. According to the SD model the water flux increases with pressure but the solute flux does not. Hence, the solute retention increases with pressure. The same trend is observed with the experimental data. However there is a quantitative mismatch between the experimental and theoretical data. In contrast to water flux data, both the theoretical model predictions are almost equal. At higher concentration gradients across the membrane, the application of Equation (5-14) is limited. It is assumed that the solute permeability is constant across the membrane and there is a linear gradient in the concentration across the membrane which may not be true at higher concentration gradients.

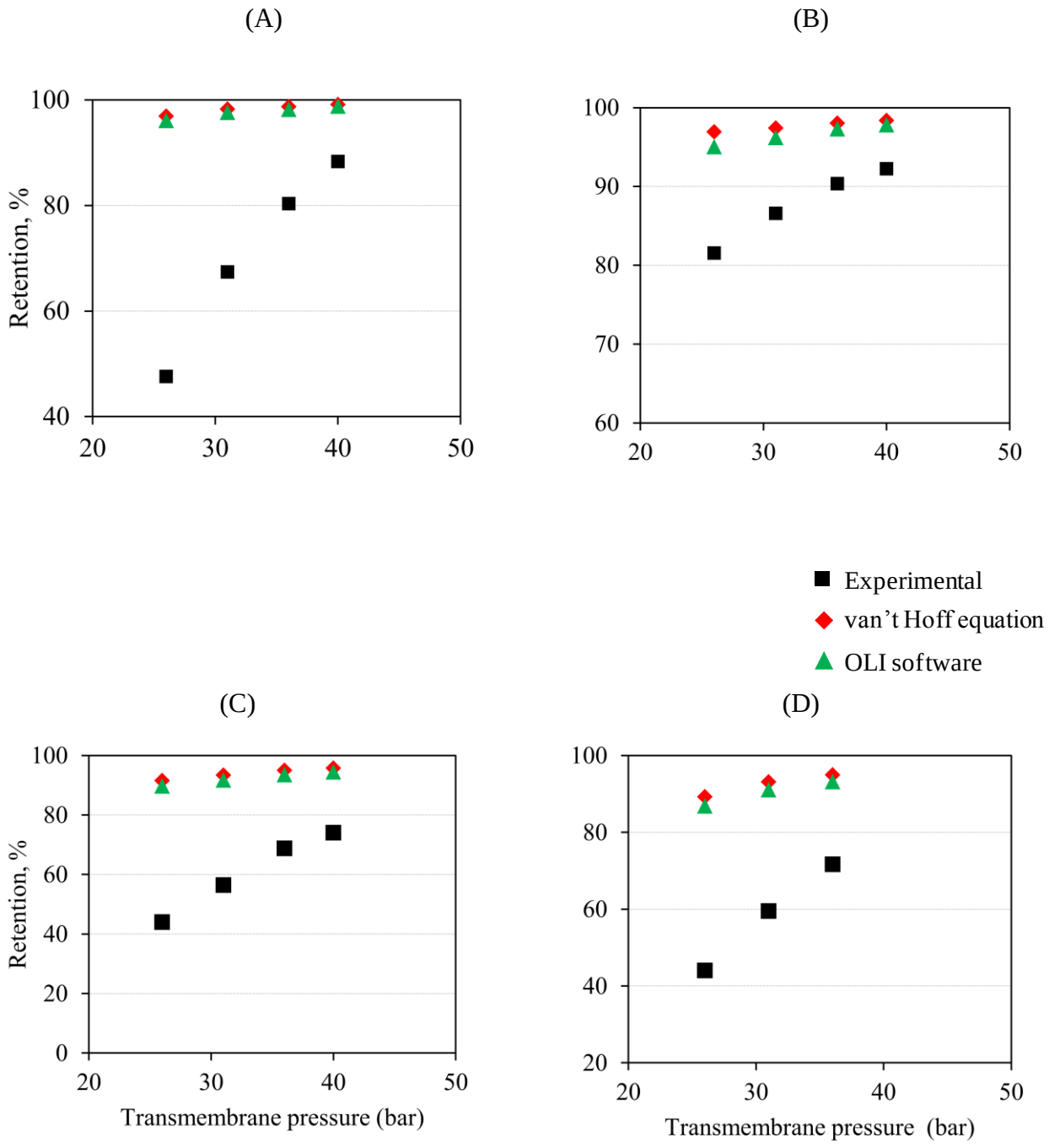

Figure 5-6 Retentions as a function of transmembrane pressure. Glucose concentration is 15 wt%. (A) RO_AG (B) RO_CE (C) MPF 34 and (D) Desal DK

Both diffusion coefficient and solubility coefficient in Equation (5-14) become functions of concentration and vary across the membrane. Rosenbaum and Skiens [102] performed experiments by using cellulose acetate membranes in aqueous solutions of NaCl at different concentrations. At low concentrations (< 0.5M), there is a good agreement between the experimental and theoretical flux data. But at higher concentrations, the data set is highly irregular and non linear. The concentrations used in this experiment (~ 0.8 M) are higher and falls in the non linear regime. Therefore both SD model and film theory model should be modified to account for the non-idealities introduced due to higher concentration gradients. Also in order to reduce the concentration polarization, experiments can be performed at higher cross flow velocities. In that case, film theory model can be used without any ambiguity.

5.2.3 Acetic acid - water Mixture

Similar trends were obtained with fluxes of acetic acid water mixtures. Figure 5-7 shows the variation of flux with transmembrane pressure. As expected, water flux increased with transmembrane pressure. The difference between the experimental and theoretical fluxes is decreased compared to that glucose mixture but agreement is still not good. Figure 5-8 provides the retention profiles of glucose at different transmembrane pressures. Since the retentions of acetic acid, Figure 4-3, are low compared to that of glucose, the effect of concentration polarization should also be low. Hence there is a better match between the experimental and theoretical data. On average, the flux of glucose was over-predicted by a factor of 15 but the flux of acetic acid was over-predicted by a factor of 4. In contrary to flux data, retention data of acetic acid are not in good agreement with modeling data. At this point it is not clear whether the concentration polarization or variation of water and solute permeability coefficients across the membrane is responsible for the inconsistency between experimental and theoretical data.

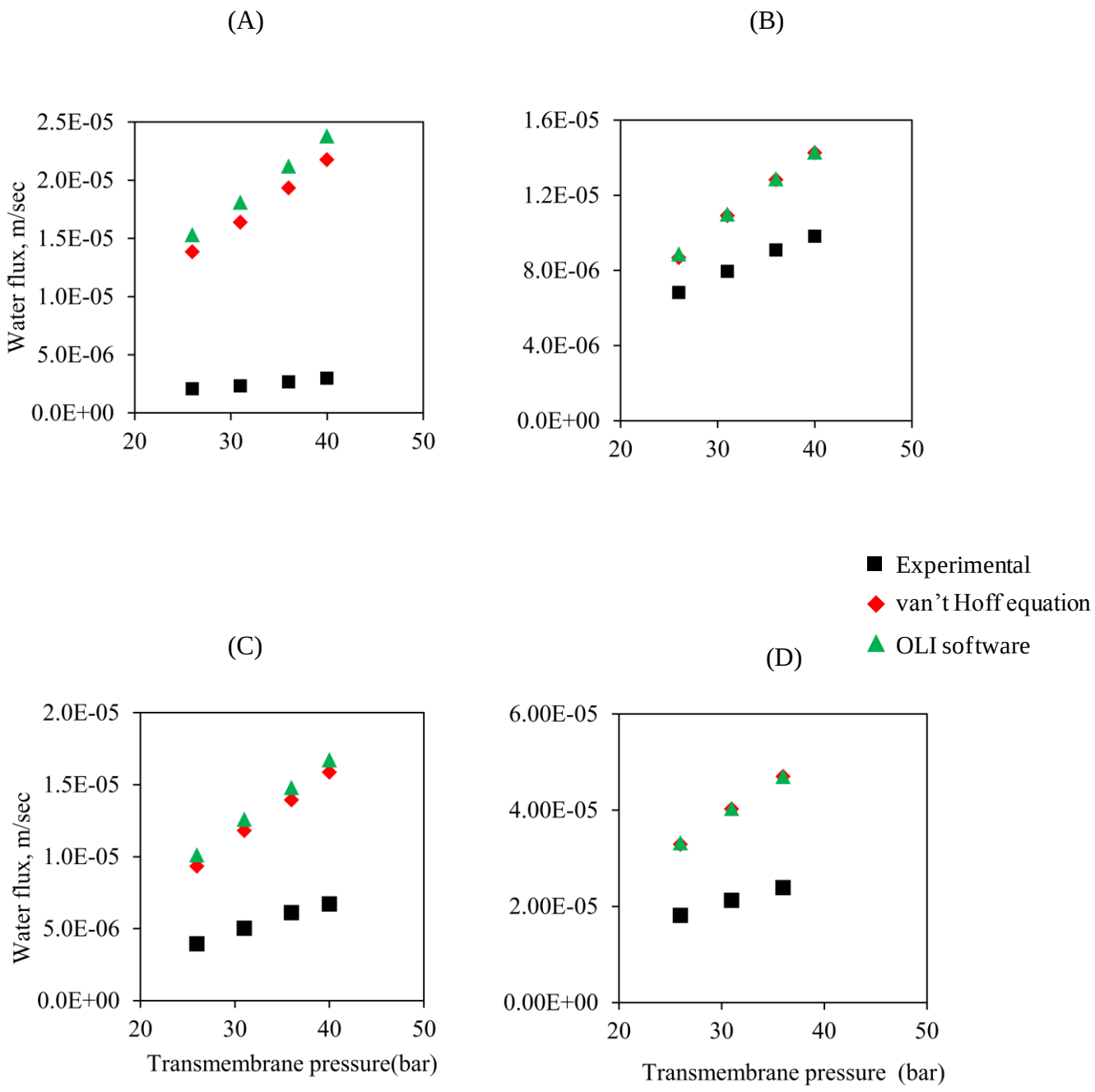

Figure 5-7 Influence of transmembrane membrane pressure on the water flux. Acetic acid concentration is 7 wt%. (A) RO_AG (B) RO_CE (C) MPF 34 and (D) Desal DK.

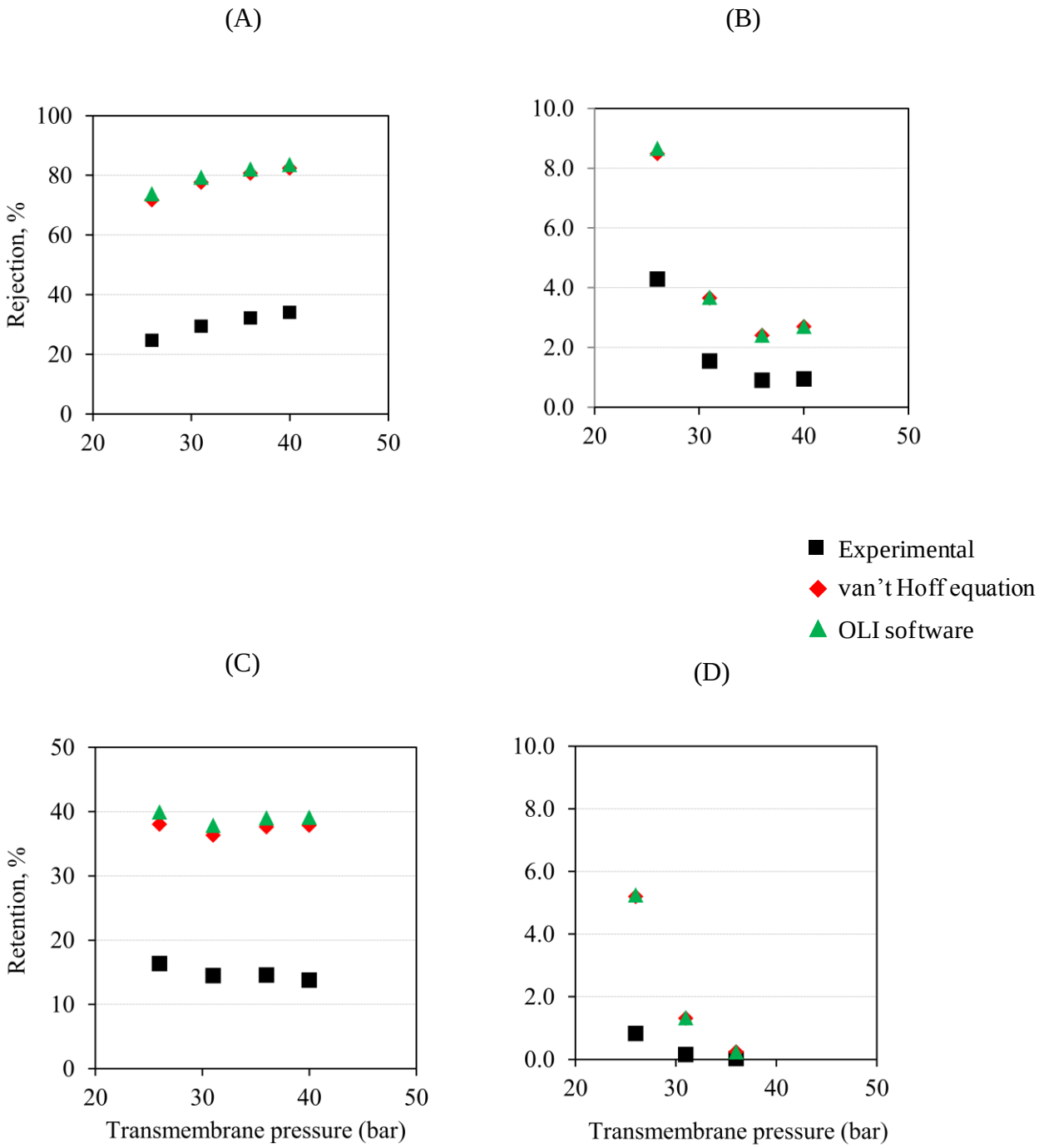

Figure 5-8 Retentions as a function of transmembrane pressure. Acetic acid concentration is 7 wt%. (A) RO_AG (B) RO_CE (C) MPF 34 and (D) Desal DK

5.3 Conclusions

Solution-diffusion model (SD) was employed to the experimental results obtained with single solute solutions of glucose and acetic acid. Osmotic pressures of the feed and permeate were calculated using van't Hoff's equation and OLI software. Water permeability coefficients of all the membranes were determined using corresponding pure water flux data. The values obtained are in consistent with the manufacturer's values. Concentration polarization is modeled using film theory. Empirical relations were used to calculate mass transfer coefficients. Experimental solute flux data is used to determine, solute permeability coefficients. Finally, solvent and solute fluxes were calculated using the SD model equations and compared with experimental data. As predicted by the SD model, both solvent flux and solute retention increased with transmembrane pressure. However, there is no good match between the experimental and theoretical data. The model was incapable of matching the slope of the experimental flux against pressure and also over estimated the flux. Both SD and film theory models are applicable in situations where the concentration and pressure gradients across the membrane are low. We think that high concentrations used in our experiments resulted in a mismatch between measured and calculated values.

CHAPTER 6

ORGANIC-INORGANIC NANOCOMPOSITE MEMBRANES FOR GAS SEPARATION

This chapter focuses on the synthesis of organic-inorganic composite membranes and their application to solubility-based gas separations. Composite membranes were prepared by two different methods. In the first one, melamine-based dendrimers were grown directly off the surface of commercially available mesoporous alumina membranes of 5 nm pore size. In the second method, anodisc alumina membranes were modified with polydimethylsiloxane (PDMS) using dip coating method.

6.1 Introduction

Solubility-based gas separations, where the more soluble components preferentially permeates across the membrane, have attracted considerable interest in recent years due to both economic and environmental concerns[103, 104]. This mode is especially advantageous in applications where the heavier components are present in dilute concentration. Examples include the removal of higher hydrocarbons from refinery hydrogen purge streams and recovery of volatile organic compounds (VOCs) from process effluent streams. In gas separation with membranes, the ideal selectivity for component A relative to component B, $\alpha_{A/B}$, is defined as the ratio of the pure component permeabilities (*P*) as given below

$$\alpha_{A/B} \equiv \frac{P_A}{P_B} = \left(\frac{D_A}{D_B} \times \frac{S_A}{S_B} \right) \tag{6-1}$$

where *D* is the diffusivity and *S* is the solubility of a particular component in the membrane.

Freeman and Pinnau summarized the design criteria for solubility-selective polymeric membranes [104]. They point out that for separation of dilute heavy molecular weight

components from light gases the diffusivity selectivity is generally in favor of the smaller mobile species. Therefore, to achieve solubility-based separation, the polymer needs not only to have high solubility selectivity but also a large free volume so that the ratio of diffusivities of the two components is driven close to unity. The solubility-selectivity is greater for the larger species simply due to van der Waals interactions, resulting in an overall higher selectivity for the larger species. For example, to design a membrane separation system for organics/light gas that is more selective for the organics, the ideal membrane would have the ratio of the diffusivity coefficients of the two gases in the membrane close to unity

$$\frac{D_{organics}}{D_{light\ gas}} \approx 1 \tag{6-2}$$

The propane/nitrogen solubility ratio based on the discussion above would be significantly higher than one

$$\frac{S_{organics}}{S_{light\ gas}} >> 1 \tag{6-3}$$

leading to an overall higher propane permeability as given by equation (2-33) below

$$\frac{P_{organics}}{P_{light\ gas}} > 1 \tag{6-4}$$

Both inorganic and organics membranes can be designed to achieve solubility-based gas separations. Both materials have certain advantages and disadvantages. Presently current effort is concentration on designing membranes that provide high permeance and high selectivity. Such membranes can allow a positive correlation between permeability and selectivity, which is in

contrast to conventional diffusivity-based separations where an upper bound is present [105]. Figure 6-1 shows this upper bound for the oxygen/nitrogen selectivity drawn as a function of oxygen permeability. Much of the present research has focused on pushing the polymer performance above the upper bound and into economically attractive region currently enjoyed by inorganic membranes.

Organic-inorganic nanocomposite membranes, that combine the best characteristics of both polymeric and inorganic materials, provide a viable method to improve membrane materials for solubility-selective separations. Polymers fused with inorganic particles are a common approach [106-109]. Merkel et al. doped poly (4-methyl-2-pentyne) with nanoscale fumed silica particles and applied them to a prototype solubility-selective separation: *n*-butane from methane [107]. They observed that with increasing silica wt% in the polymer there was a simultaneous enhancement in both n-butane permeability and *n*-butane/methane selectivity. This was mainly attributed due to silica-induced disruption of polymer packing and an accompanying slight increase in the size of free volume elements.

Another approach to generate organic-inorganic nanocomposites is based on depositing organic compounds onto a mesoporous inorganic framework. This approach allows one to synthesize membranes that simultaneously deliver the desired chemistry and the desired free volume for specific applications. Nanocomposite membranes prepared by this approach have shown great promise in solubility-based separations [110-113]. Previous work in our group [110, 112] has led to structure-property relationships for membranes comprising organochlorosilanes attached to porous alumina. This work showed that we can rationally modify permeation properties by selecting pore size, and type and amount of organic compound deposited.

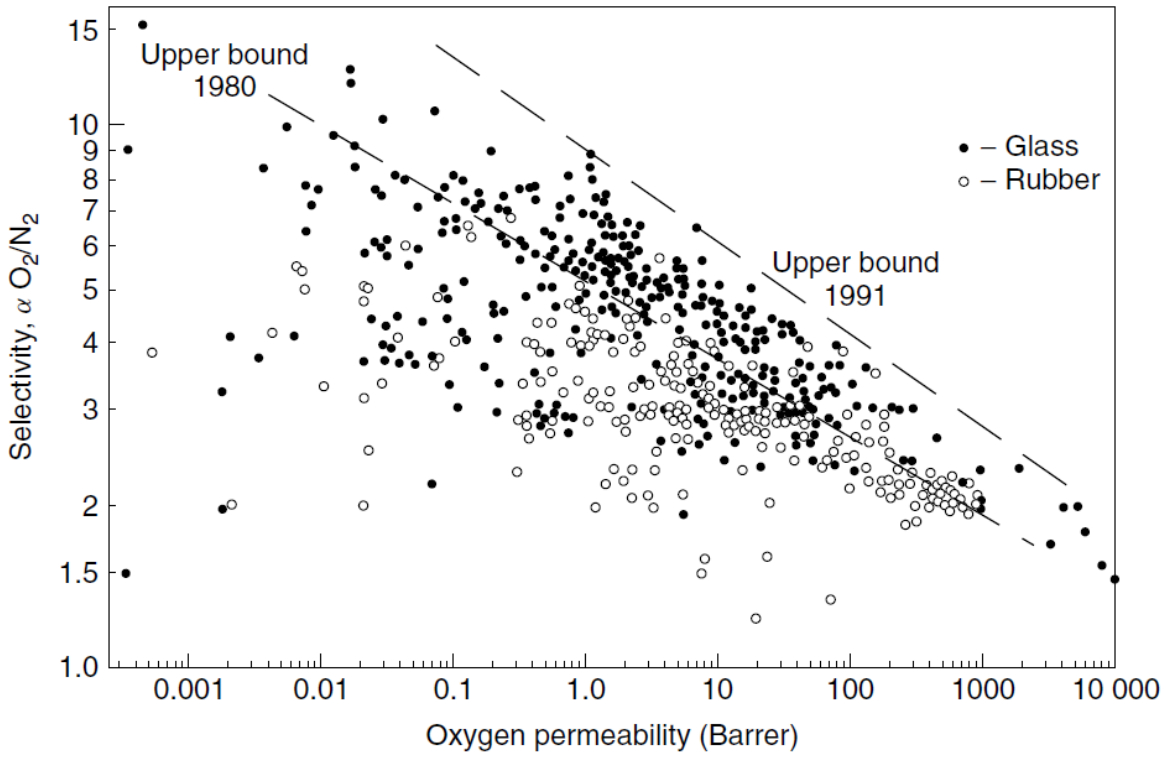

Figure 6-1 Upper bound relation for O_2 / N_2 separation [46]

In this study, we extend this concept of engineering the membrane nano-architecture by exploring a new type of organic compound structure and chemistry, melamine-based dendrimers. Dendrimers are a potential useful class of organic compounds for this purpose due to their wide range of structural and chemical diversity [114-116]. Dendrimer-ceramic nanocomposite membranes were prepared by growing several generations directly off the surface of mesoporous alumina membrane. We achieved reasonable selectivities by engineering the dendrimeric organic phase and carefully screening the effects of the pore size of the mesoporous substrate.

PDMS is a rubbery silicone polymer that has one of the lowest glass transition temperatures. PDMS has been investigated extensively as a suitable material for removal of different solvents from air or nitrogen. The permeabilities of different solvents and gases through PDMS were studied by several groups [117, 118]. Their study showed that solvent permeabilities strongly depend on the solvent concentration and that it is much related with the sorption of the solvent into the polymer. Leemann et al. investigated the performance of PDMS membrane in the removal of toluene from nitrogen [119]. They showed that within certain regimes of purity and flow the PDMS membrane system could be an economical alternative to the conventional processes. However, PDMS has been shown to be prone to plasticization, which may greatly reduce its selectivity when exposed to actual gas mixtures [120]. As discussed earlier, organic-inorganic composite membranes have shown better properties and therefore in our work we synthesized PDMS-ceramic composite membranes using dip coating method and the gas permeance properties of the composite membranes were evaluated.

6.2 Experimental

6.2.1 Synthesis of Dendrimer-ceramic Composite Membrane

Ammonium hydroxide, dichloromethane, ethanol, hydrochloric acid, hydrogen peroxide, methanol, tetrahydrofuran, and toluene (ACS reagent grade) were purchased from Fisher Scientific. 3-aminopropyldimethylethoxysilane (APDMES, 99%) was purchased from Gelest Inc. N, N-diisopropylethylamine (DIPEA, 99%) were purchased from Aldrich. Cyanuric chloride (CC, 99%) was purchased from ACROS. All chemicals were used as received.

The membranes used in this work were Membralox® T1-70-25G-Bare, γ-alumina membranes with an average pore size of 5nm (Part# S700-01227). They were purchased from US Filter Ceramic Membrane Products, Deland, Florida. These membranes have been discussed in detail by Liu and co-workers who have described and characterized them in two part series[121, 122]. The membranes have an extruded tubular macroporous α-alumina support with a thickness of 2nm and an average pore size of 10 μm. The macroporous support is coated by slip casting and firing two more layers of α-alumina with average pore diameters of 0.8 and 0.2 μm, respectively. The final layer, which is 3-5 μm thick, is a γ-alumina layer that is slip cast and fired to yield an average pore size of 5 nm and a porosity of 50 % [121]. Figure 6-2 shows a scanning electron micrograph (SEM) of the membrane cross section. The membrane tube outer and inner diameters were 1cm and 0.7 cm respectively. The tubes were received in 25 cm lengths, and for our experiments we cut them into 1 inch long pieces, using a laboratory glass cutter. After cutting, the membranes were cleaned by soaking in 2:1 ethanol/water solution for 24 hours at ambient temperature. The membranes were dried at 60 °C for 30 min and stored in

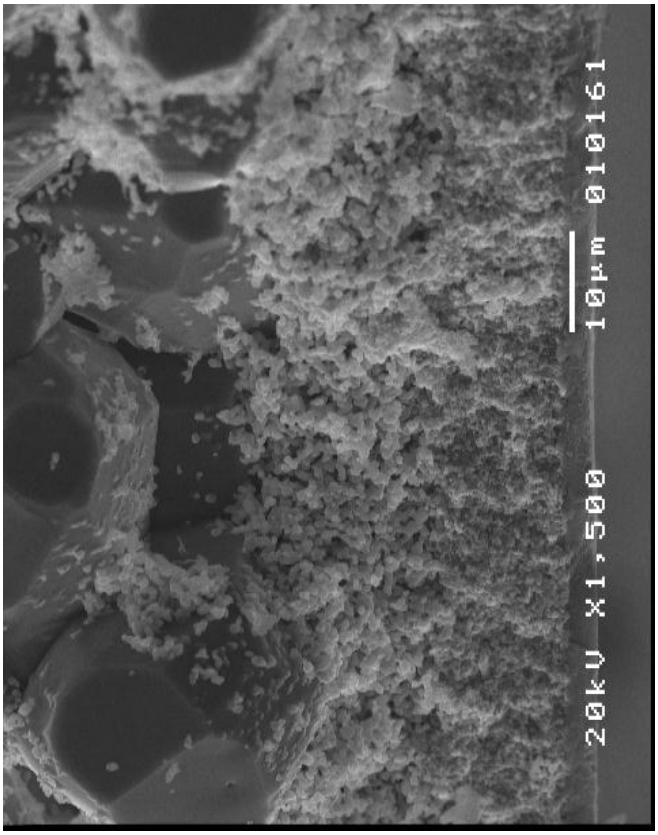

Figure 6-2 SEM image of 5 nm Membralox ® alumina membrane

laboratory environment. Single gas permeation data for nitrogen and propane were obtained according to the procedure described in section 6.2.4.

A stepwise synthesis of dendrons growing divergently from the surface of mesoporous alumina membranes is shown in Figure 6-3. The amine functionalization of membranes was done with a 0.1M solution of 3-animopropyldimethlyethoxysilane in toluene. Prior to treatment, RCA (Radio Corporation of America) cleaning was applied to the membranes. For this purpose the membrane pieces were submerged in 75 ml of 5:1:1 H_2O: H_2O_2: NH_4OH (organic cleaning solution) and then heated to 80 °C for 15 min on a hotplate. After rinsing the membranes with deionized water, membranes were treated in the same manner using 75 ml of 6:1:1 H_2O: H_2O_2: HCl (ionic cleaning solution). The treated membranes were stored in an oven at 100 °C before the amine functionalization. A silane treated membrane was rinsed with toluene and THF and then submerged into 0.15 M solution of cyanuric chloride dissolved in THF. During this step, the surface amines were allowed to react with cyanuric chloride to give dichlorotriazine intermediate, branch-point. The dichlorotriazine was the allowed to react with piperazine by immersing the membranes into 0.3M solution of the piperazine in THF. The treatment with triazine and piperazine was repeated alternately to reach each generation. Dendrimers of third generation (G3) were grown. Finally, dodecyl amine was attached to provide the specific chemical functionality.

6.2.2 Synthesis of Polymer-ceramic Composite Membranes

Tetrahydrofuran (ACS reagent grade) was purchased from Fisher Scientific. Polydimethylsiloxane (PDMS: M_w 92400, M_n 46000 g/mol) was purchased from Aldrich. Anopore ® aluminum oxide membranes were purchased from Whatman and used as received.

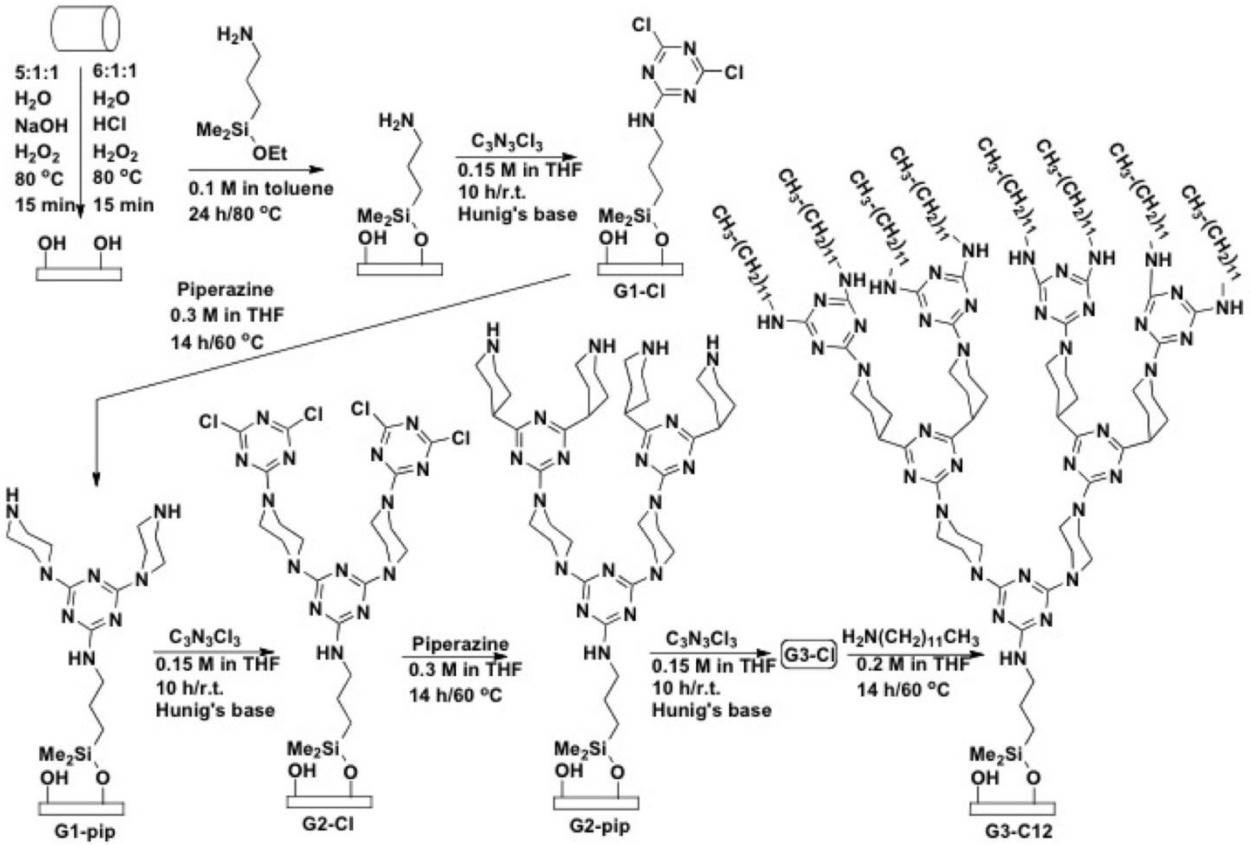

Figure 6-3 Growth of melamine-based dendrimer on the surface of the mesoporous alumina membrane

Anodic aluminum membranes, irrespective of nominal pore size, have an asymmetric structure [123-125]. The structure comprises a relatively thin (0.5 to 1.0 μm) layer on top of a thicker (59 to 59.5 μm) support. The asymmetry appears to be a natural consequence of the way the membranes are made by anodic oxidation [123]. The thin "active" layer generally has the smaller pore size, as compared to the thicker "support" layer. Anopore® membrane of nominal pore size 20 nm has the thin active layer of 25 nm pore size and the thicker support layer of 100 nm pore size. Figure 6-4 shows a scanning electron micrograph (SEM) of the surface of the thicker support layer.

PDMS-anopore composite membranes were prepared by simple dip coating method. Anopore membrane was immersed in a solution of PDMS dissolved in THF and then quickly drawn out. Figure 6-5 is a schematic of how the composite membranes were fabricated. The top and bottom surfaces of the membrane were gently cleaned with THF to remove the PDMS deposited on the surfaces. The dip-coated membranes were dried at 40 °C. As the solvent evaporates, the pores of the membrane are filled with PDMS. Solutions of varying concentrations were prepared to see the effect of PDMS concentration on the membrane performance. Single gas permeation data for nitrogen, carbon dioxide, methane, and propane were obtained according to the procedure described in section 6.2.4.

6.2.3 Single Gas Permeation Set-up

Permeation measurements on the individual gases were performed using an in-house unit. Pure helium, carbon dioxide, methane, and propane gases were used as received from Airgas. The schematic for the single gas permeation experiments is given in Figure 6-6. The membrane was held in a steel module. Two different membrane modules were used for different membrane

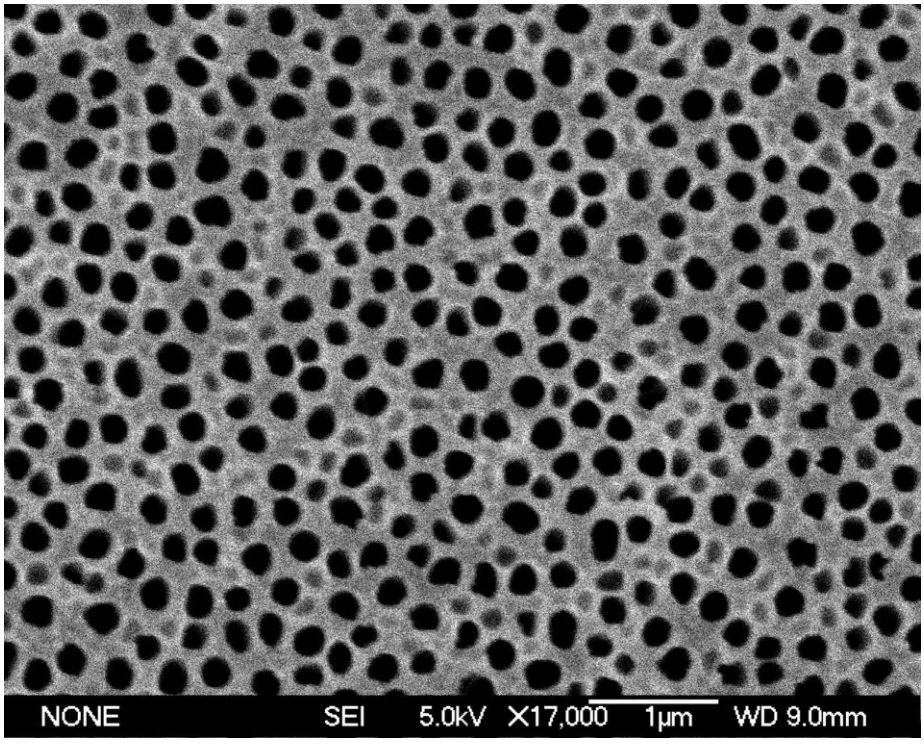

Figure 6-4 SEM image of untreated 20 nm Anopore ® alumina membrane

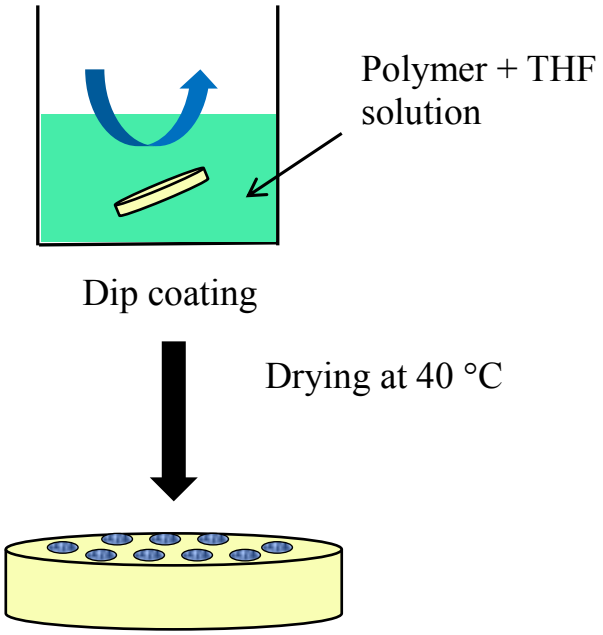

Figure 6-5 Schematic of the synthesis procedure

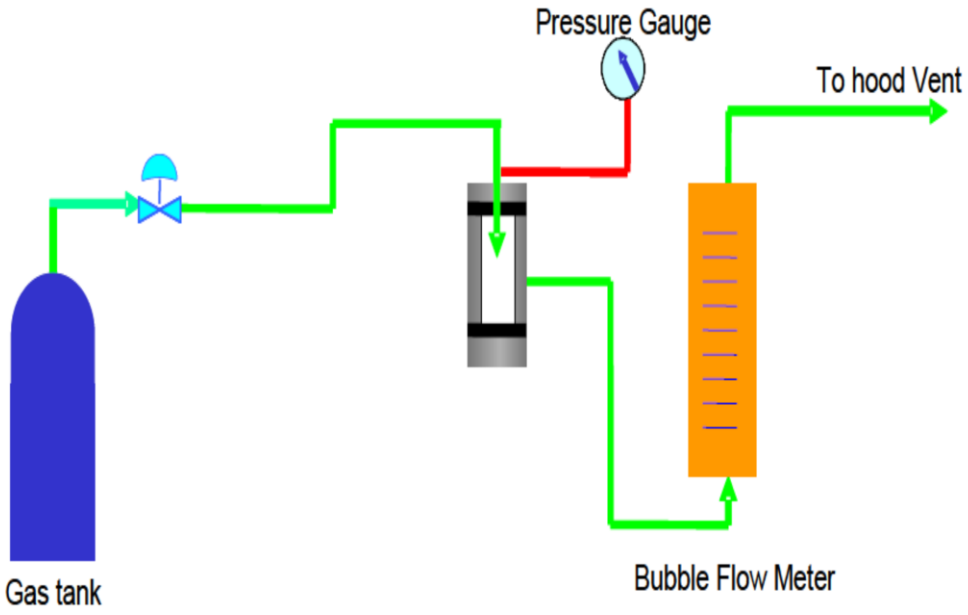

Figure 6-6 Schematic of the dead-end pure gas permeation experiment

types. A shell-tube module was used for the Membralox® cylindrical membrane and a disc module was used for Anopore® disc membrane. Each membrane module has two openings, one for feed and the other for permeate (shell-tube module was dead-ended on one of the tube ends). Screw caps and rubber gaskets were used for proper sealing. Feed gas from the cylinder was supplied to the feed inlet and flowed across the membrane through the outlet. The pressure on the feed side was measured with a digital pressure gauge. Since the outlet was at atmospheric pressure, the gauge pressure reading was considered as the pressure drop across the membrane. The permeate flow was measured using a bubble flow meter that was exhausted to the vent hood. Block valves were placed on feed and permeate outlets.

A leak test was performed prior to each single gas permeation experiment. The membrane was placed inside the module, and with the retentate valve closed, feed gas was introduced to the module. When the pressure drop across the membrane was around 1 bar, the feed and permeate valves were closed to isolate the membrane module. A continuous drop in the pressure would indicate the presence of leak, in which case a soap solution was used to detect the source of the leak. In no pressure drop was observed within a period of five minutes, the apparatus was considered to be free of leaks.

Once the leak test was satisfactorily completed, the feed and the permeate valves were opened. The retentate was closed for a shell-tube module so that a “dead-end” experiment could be done. Pressure drop across the membrane was set to the desired value by adjusting the regulator on the gas cylinder. The pressure drop was monitored until it reached the set-point

value, after which permeate volumetric flow rate was measured using the bubble flow meter and a stopwatch. At least four measurements were taken at each pressure and are averaged to determine the permeate flow rate. Volumetric flow rate was measured for at least three different pressure readings. After completing the set of readings for one gas, the gas flow from the cylinder was stopped and the retentate valve was opened to quickly release the gas from inside the module. The feed tubing was then connected to the next gas cylinder and with the retentate valve open, gas was slowly introduced into the module. The retentate valve was kept open for about 30 seconds after which it was closed. This procedure was done to ensure that no gas from the previous experiment was left inside and the system had been completely flushed with the new gas. Volumetric flow rate was again monitored at different feed pressure readings. This procedure was then repeated until all the data needed for the different gases had been obtained. During the permeation experiment, room temperature and barometric pressure were noted to make the necessary connection for converting volumetric flow rate to molar flow rate using ideal gas equation.

6.2.4 Permeance Calculation

This section describes the procedure for calculating the singe gas permeances. As noted above, volumetric flow rate was measured for different pressure readings. The volumetric flow rates were converted to molar flow rate assuming ideal gas behavior, as given by Equation (6-5) below

$$N\,(gmol/\sec) = Q\left(\frac{ml}{\sec}\right)\times\left(\frac{1l}{1000ml}\right)\times\left(\frac{1gmol}{22.4l}\right)\times\left(\frac{T_0}{T}\right)\times\left(\frac{p}{p_0}\right) \qquad (6\text{-}5)$$

where

T_0 = 273 K

T = ambient room temperature (K)

p_0 = 1.01 bar

p = ambient pressure reading (bar)

The surface area of the membrane, available for flow, was calculated using Equation (6-6)

$$Area\,(m^2) = \pi \times D \times L \qquad \text{for a cylindrical membrane} \tag{6-6}$$

$$\text{or} \quad \pi \times R^2 \qquad \text{for a disc membrane}$$

where

D = internal diameter of the cylindrical membrane (m)

L = length of the cylindrical membrane (m)

R = radius of the disc membrane (m)

The membrane flow area was determined to be 0.000559 m^2 for Membralox® membrane and to be 0.000346 m^2 for Anopore® by using Equation (6-6).

The gas flux J through the membrane was calculated by dividing the molar flow rate with the membrane flow area.

$$J\left(\frac{gmol}{\sec m^2}\right) = \frac{N}{area} \tag{6-7}$$

Permeance is related to flux through Equation (6-8)

$$P\left(\frac{gmol}{\sec m^2\, bar}\right) = \frac{J}{\Delta p} \tag{6-8}$$

where Δp is pressure drop across the membrane (bar).

Permeance was obtained directly using Equation (6-8). The intrinsic property of the membrane is permeability which is the product of the permeance and the thickness of the membrane. We have no direct data on the thickness of the active layer, which controls transport

in our membranes, so therefore we report permeances instead of permeabilities. During the course of this study the room temperature ranged from 18 to 22 °C, while the ambient pressure varied between 0.97 to 1.02 bars.

6.3 Results and Discussion

6.3.1 Dendrimer-ceramic Composite Membranes

Bare membrane single gas permeance and ideal selectivity data for nitrogen and propane for three identical membranes (MM11, MM12, and MM24) are given in Table 6-1. Nitrogen has an average permeance of 0.82 ± 0.13 mol sec^{-1} m^{-2} bar^{-1} for untreated 5nm membranes. This result is in good agreement with the data provided by US Filter in which nitrogen permeance for the 5nm membranes is given as 0.87 ± 0.248 mol sec^{-1} m^{-2} bar^{-1}.

Propane/nitrogen selectivities for the bare membranes are greater than theoretical Knudsen selectivity, which is 0.8. Figure 6-7 shows nitrogen and propane single gas permeances for MM24 untreated membrane. Nitrogen permeance is almost constant with transmembrane pressure. Furthermore the mean free path of nitrogen (under the experimental conditions) is 47 nm, and is greater than the average pore diameter. This result strongly suggests that the Knudsen diffusion is the dominant mechanism of transport for nitrogen. However, propane permeance increased with transmembrane pressure until a maximum was reached at about 5 bar. This corresponds to an absolute feed pressure of about 6 bar. The capillary condensation pressure for propane in the 5 nm pores, as calculated from the "uncorrected" Kelvin equation is 6.4 bar [126-128]. These results strongly suggest that surface effects, and eventually capillary condensation, are important for propane in the membrane. Therefore, propane/nitrogen selectivity is less than the theoretical Knudsen selectivity.

Single gas permeance and selectivity data for dendrimer-modified membranes are given in Table 6-2. For the surface-modified membranes we observed an overall drop of two to three

Table 6-1 Single gas permeance and selectivity data at 1.38 bar transmembrane pressure for three untreated identical membranes

Membrane	Permeance, mol sec^{-1} m^{-2} bar^{-1}		Selectivity
	Nitrogen, N_2	Propane, C_3H_8	C_3H_8/ N_2
MM11	0.95	1.76	1.85
MM12	0.72	1.39	1.93
MM24	0.78	1.6	2.05

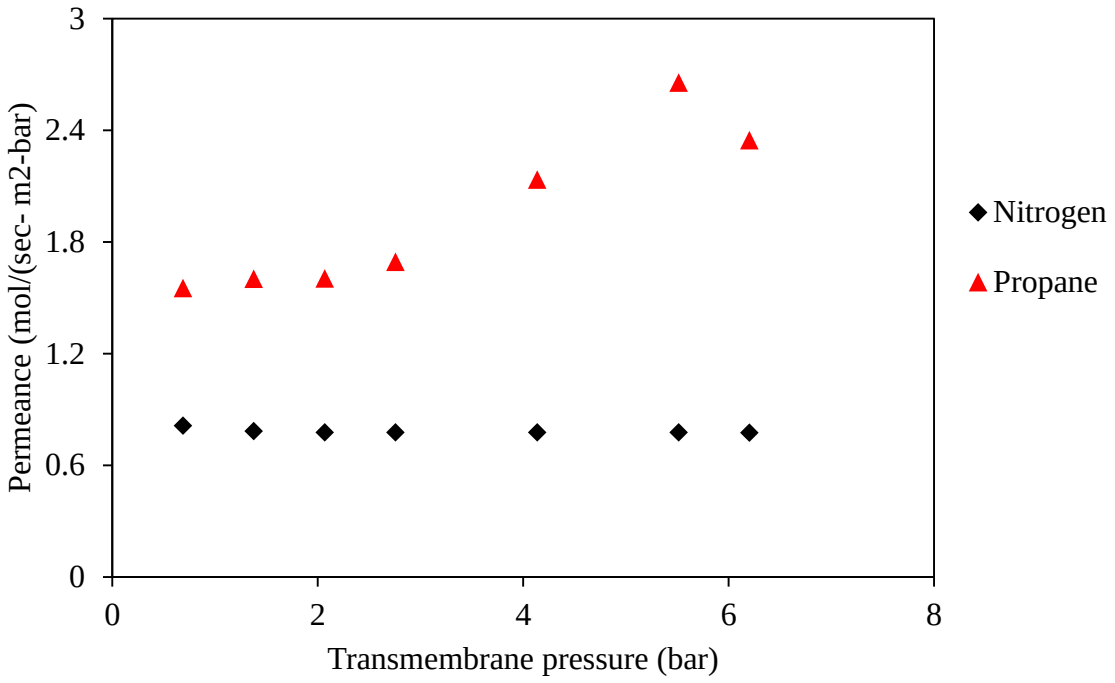

Figure 6-7 Nitrogen and propane permeances for MM24 untreated membrane, as a function of transmembrane pressure

Table 6-2 Single gas permeance and selectivity data for dendrimer-modified membranes at 1.38 bar transmembrane pressure for three identical membranes

Membrane	Permeance, mol sec^{-1} m^{-2} bar^{-1}		Selectivity
	Nitrogen, N_2	Propane, C_3H_8	C_3H_8/ N_2
MM11	0.001012	0.003192762	3.15
MM12	0.001873	0.002879	1.54
MM24	0.001074	0.002243	2.07

orders of magnitude in nitrogen and propane permeances accompanied by a slight or no increase in the propane/nitrogen selectivity. While these results are not promising, previous research in our group, using identical synthesis procedure, showed very wide range of propane/nitrogen selectivities for the G3 membranes and it was found that the pore size variance of the untreated mesoporous substrate and the residual solvent in the membranes appeared to be critical to the membrane performance [116]. To confirm that hypothesis we decided to test for solvent effects by taking existing membranes through a cycle of re-rinsing and drying. Figure 6.8 shows the propane/nitrogen selectivity for MM11 membrane after a series of rinsing/drying treatments. In this figure, *Initial* is the first measurement of permeance and the selectivity after synthesis. After each *THF soaking*, the membrane was dried in ambient condition for 30 min and the permeation measurements were taken. Finally, the membrane was dried at 40 °C before taking final readings. The first THF soaking showed a slight increased selectivity compared to initial result. However, there was a remarkable increase in selectivity after the second THF soaking. Furthermore the membrane performance was back to *Initial* when dried at 40 °C. On the other hand, nitrogen permeance is unaffected by residual THF as shown in Figure 6-8. This indicates that there is an effect caused by residual solvent (THF) in the membrane on propane permeance. Although the adsorbed solvent in the membranes is removed at 40 °C, the adsorption was strong enough not to cause the abrupt change of permeance and selectivity during the permeation test, which was carried out around 20 °C.

6.3.2 PDMS-ceramic Composite Membranes

Figure 6-9 shows single gas permeances of nitrogen, carbon dioxide, methane, and propane and ideal selectivities of different gas pairs for untreated 20 nm Anopore membranes as a function of transmembrane pressure. For this pore size, under the near-ambient conditions

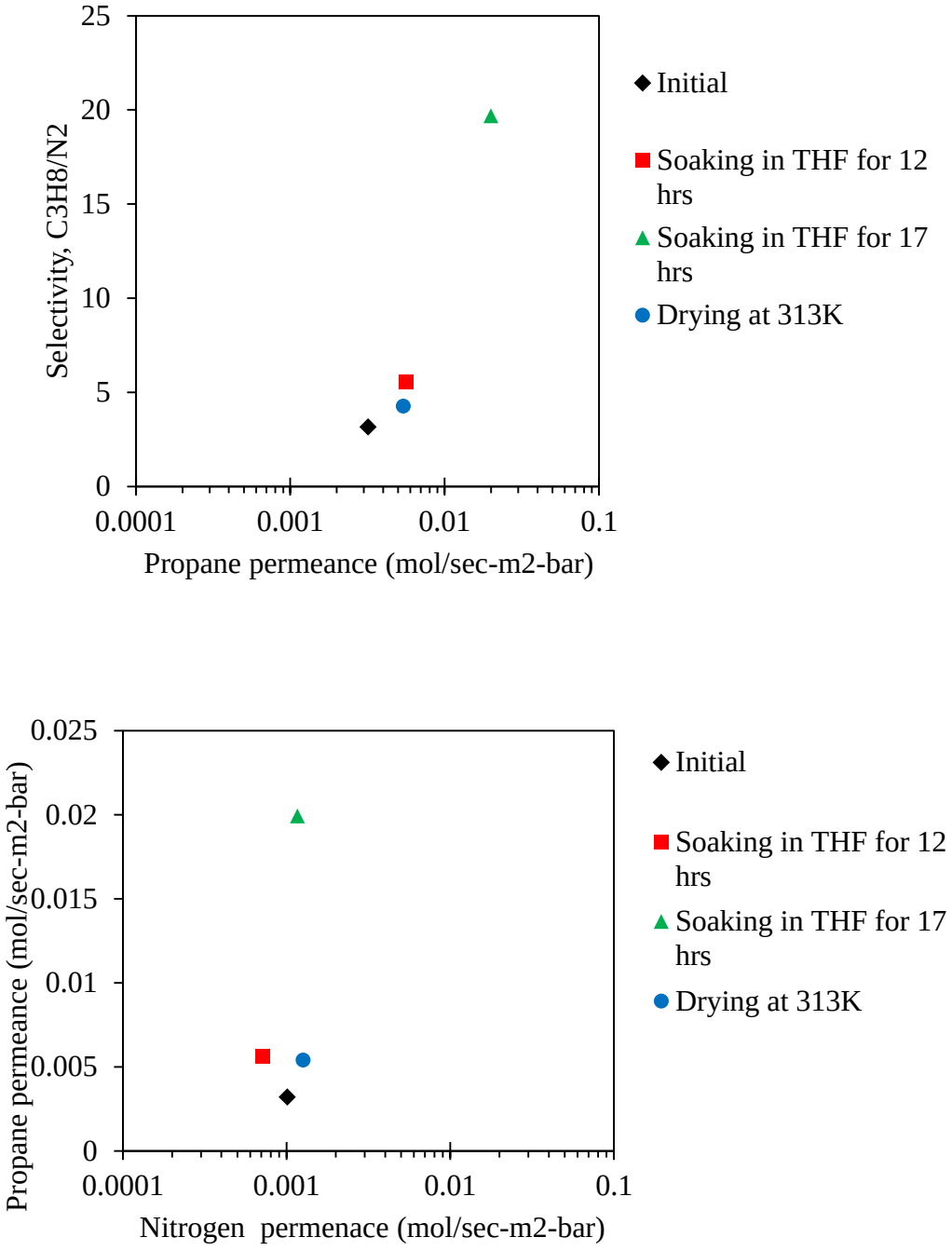

Figure 6-8 Effect of solvent rinsing/drying on propane and nitrogen permeances for modified MM11 membrane. Measurements were taken at 1.38 bar

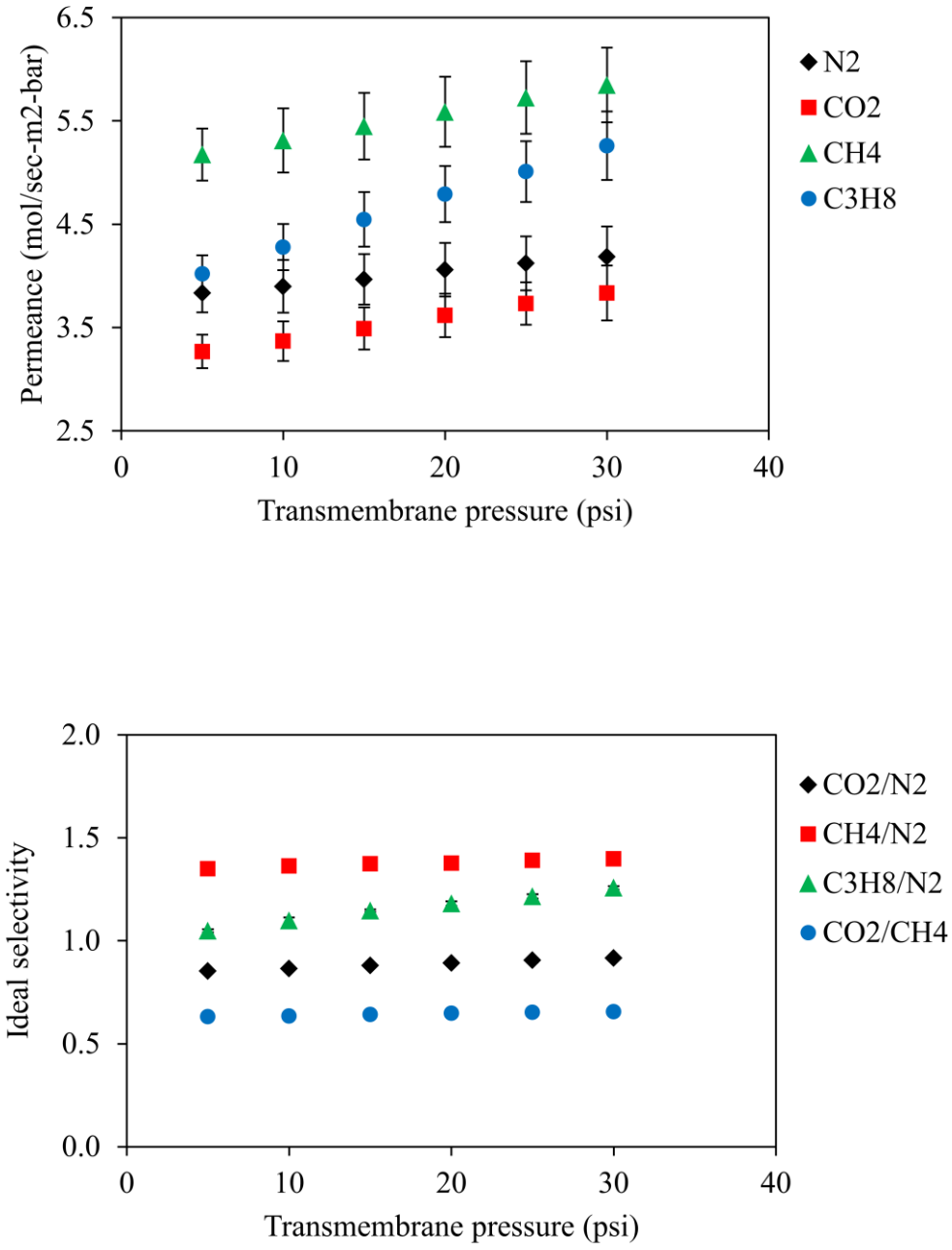

Figure 6-9 Plot of gas permeances and selectivities of different gas pairs for untreated 20 nm Anodisc membrane as a function of transmembrane pressure.

used in the experiments, a combination of Knudsen diffusion and Poiseuille (viscous) flow is expected [126]. At 20 psig, a methane/nitrogen selectivity of 1.38 and a carbon dioxide/nitrogen selectivity of 0.89 are close to what a Knudsen separation (square root of the inverse ratio of molecular weights) would yield, which in both cases would be 1.32 and 0.8 respectively. In case of purely Knudsen diffusion, the permeance is constant and is independent of transmembrane pressure. However, the results for nitrogen, carbon dioxide, and methane show that the permeances increase slightly as the transmembrane pressure is increased. This indicates the presence of some Poiseuille flow, in addition to Knudsen diffusion. Another way of estimating the presence of Knudsen diffusion is by comparing the pore size to the characteristic mean free path of the gas. At 20 psig and 20 °C, the mean free paths of nitrogen, carbon dioxide, and methane are 28, 35, and 26 nm, respectively. The mean free paths are larger than the pore diameter (20 nm) indicating the presence of Knudsen diffusion. Therefore a combination of Knudsen diffusion and viscous flow is the mechanism of transport for nitrogen, carbon dioxide and methane. On the other hand, a propane/nitrogen selectivity of 1.18 is quite contrary to Knudsen separation limit (0.8). In addition, Figure 6-9 shows that propane permeance increased more quickly with transmembrane pressure when compared to other gases. As discussed earlier the situation for propane is more complicated. Under the conditions studied, propane is expected to have significant contributions from surface flow and possibly capillary condensation mechanisms in parallel with Knudsen and Poiseuille.

PDMS solutions of varying concentrations in THF (1 mg/ml, 5mg/ml, and 7.5 mg/ml) were prepared and several PDMS- Anopore® composite membranes were synthesized using the procedure described in the section 6.2.2. Pure gas permeation studies were done with propane and nitrogen. Figures 6-10 and 6-11 show the effect of PDMS concentration on the separation

performance. For comparison bare membrane performance data is also included. Treatment with 1 mg/ml of PDMS solution caused no significant change in the membrane structure. The propane

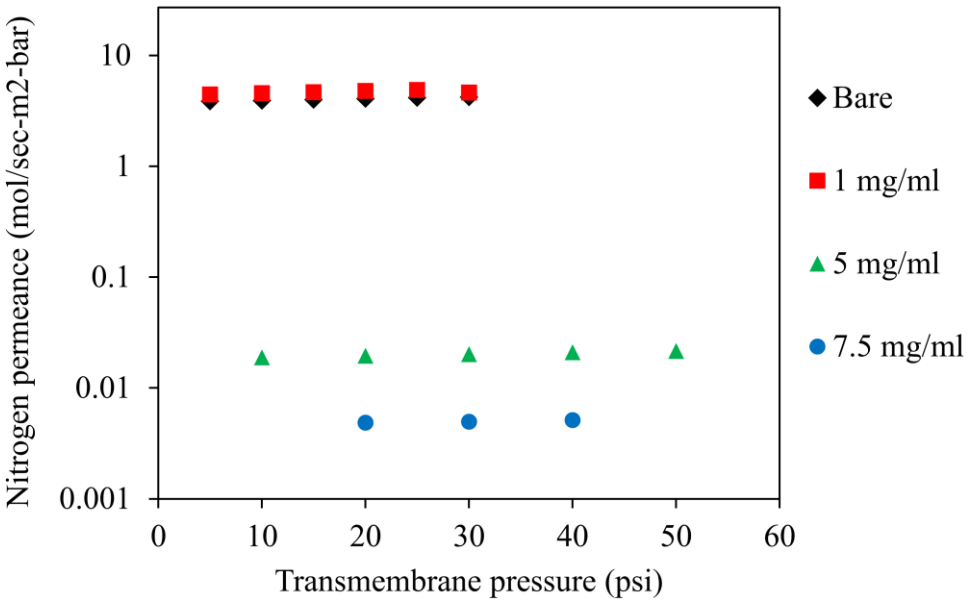

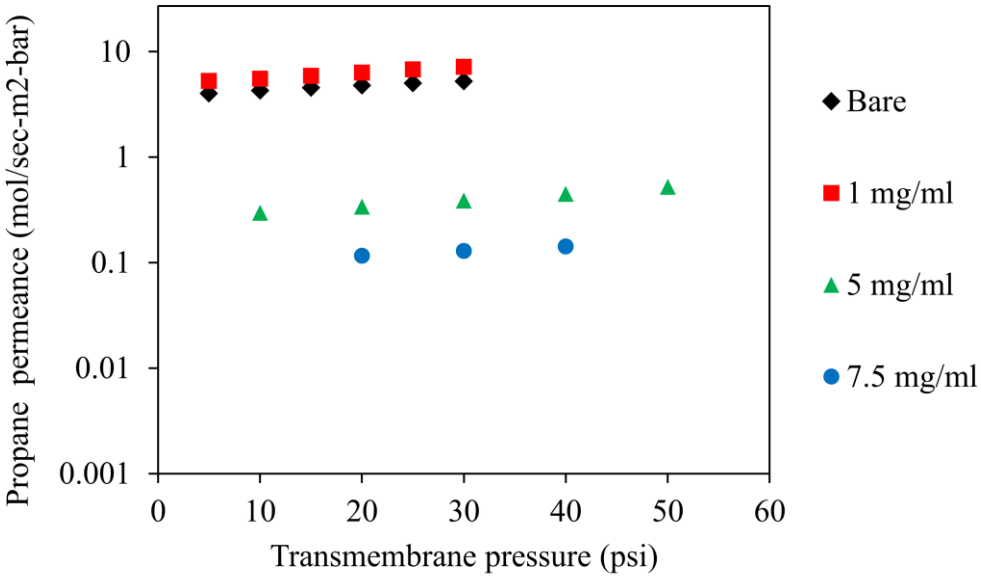

Figure 6-10 Permeances as a function of transmembrane pressure. Effect of PDMS concentration and on nitrogen (Top) and propane (Bottom) permeance.

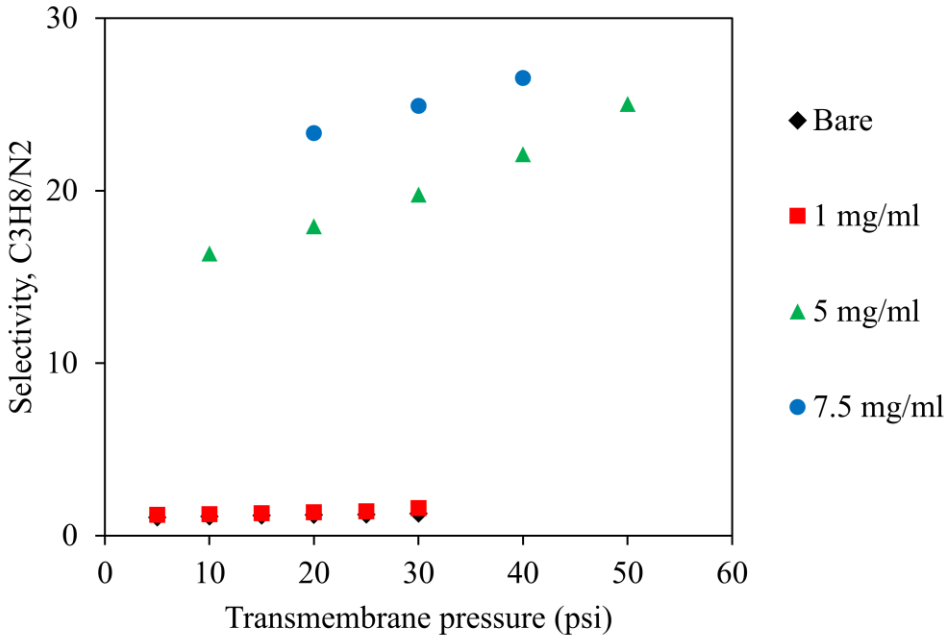

Figure 6-11 Propane/nitrogen selectivity as a function of transmembrane pressure. Effect of PDMS concentration.

and nitrogen permeance and propane/nitrogen selectivity data is statistically similar to bare membrane permeance and selectivity data. The concentration of PDMS is too low to have much effect on transport through the mesopores and thus there is no significant change in the membrane performance. By contrast, there is a substantial decrease in the permeances accompanied by an increase in the selectivity when the concentration of PDMS in the solution is increased to 5mg/ml and 7.5 mg/ml. As the PDMS concentration increases the amount of polymer adsorbed in the mesopores of the inorganic support increases, which increases the membrane performance was observed. So we can conclude that at this concentration, the mesopores are completely filled with polymer and the performance of the membrane is determined by the nature of the polymer. Single gas permeation experiments were also performed with carbon dioxide and methane for these composite membranes. The data is summarized in Table 6-3. After modification, the membranes exhibited solubility-selective separation.

6.4 Conclusions

The current study reports synthesis of organic-inorganic nanocomposite membranes and their application to relevant gas separations. One set of composite membranes was prepared by growing a melamine-based dendrimer directly off a commercial alumina membrane with 5 nm mesopores. Dendrimers are a promising class of organic molecules for this purpose due to wide range of structural and chemical diversity. Although surface modification resulted in a loss of permeance, the permselectivity of propane over nitrogen is not changed much. The effect of residual solvent on composite membrane performance was explored.

We also prepared PDMS-inorganic composite membranes using dip coating method. The permeation data for nitrogen, methane, carbon dioxide, and propane indicates that the effective

Table 6-3 Single gas permeance and selectivity data for composite membranes (modified with 7.5 mg/ml of PDMS in THF) at 30 psi transmembrane pressure. For comparison bare membrane data is also presented.

	Permeance (mol/sec-m2-bar)		Selectivity ($\mathbf{P_{gas}/P_{N2}}$)	
Gas	Bare	Composite	Bare	Composite
Nitrogen	4.186	0.00494	1	1
Methane	5.848	0.01448	1.38	3
Carbon dioxide	3.834	0.04747	0.92	9.72
Propane	5.260	0.1286	1.26	25

pore size of the membrane can be manipulated based on the PDMS concentration. The results indicate that membranes modified with 7.5 mg/ml of PDMS concentration in toluene have propane/nitrogen selectivity values of composite membranes were comparable to polymeric PDMS membranes.

CHAPTER 7

CONCLUSIONS AND SUMMARY

This dissertation focused on investigating the possibility of separation of carboxylic acids from aqueous fraction of fast pyrolysis bio-oils (AFBO) using membrane technology, in particular nanofiltration (NF) and reverse osmosis (RO) processes. A separate project studied modification of the surfaces of mesoporous alumina membranes with a selective organic material that is physically or chemically anchored to the porous surfaces, in order to tune the gas separation properties.

Fast pyrolysis bio-oil, a potential source of sustainable energy, has attracted considerable recent attention due to an increase in energy demand and potential shortages and environmental concerns associated with fossil fuels. However, the direct use of bio-oil is limited due to its high viscosity, corrosiveness, and high char content. AFBO is convenient to process and contains sugars, acids and other low molecular weight organic compounds that can be converted to fuels and/or chemicals. However, the acidity of AFBO is relatively high and the removal of acids is essential to prevent corrosion of processing equipment and for further upgrading. Membrane based separations, generally targeted for aqueous streams containing little or no organic solvents, are extended to separate acids from organic-rich streams.

Commercially available polymeric NF and RO membranes were used to study the feasibility of separating carboxylic acids from sugars in AFBO. Initial experiments were run with single and binary solute model aqueous solutions to test the performance of the membranes. The performance of these membranes was sensitive to cross flow operating parameters (cross flow

velocity, transmembrane pressure, and concentration). Cross flow velocity had a strong effect on glucose retention, due to the well-known concentration polarization effect. In general, increasing the transmembrane pressure resulted in higher permeate flux and higher solute retentions. This can be explained using solution-diffusion mechanism for solvent and solute permeation through the membrane. According to this mechanism the solvent (water) flux increases with the transmembrane pressure but the solute flux doesn't and therefore solute retention increases. Increasing the feed concentration resulted in flux reduction. Possible explanations could include increase in concentration polarization, viscosity, and osmotic pressure, adsorption and blocking of the membrane pores. The effect of pretreatment by pressure on membrane was explored. An inverse correlation was observed between permeance and retention of untreated and treated membranes, i.e. high retentions are accompanied by low permeances and vice versa.

Based on single and binary aqueous solutions data, it appeared that it was possible to separate acetic acid and glucose using nanofiltration and/or reverse osmosis when operated at high pressure and high cross flow velocity. However, all the membranes were permanently damaged when exposed to model AFBO. Subsequent experiments revealed that the membranes are strongly susceptible to damage by phenolic compounds, especially to guaiacol. Optical microscopic images of both virgin and guaiacol treated membrane also confirmed the damage. Experiments with guaiacol-free model AFBO showed that high retentions (> 80%) of glucose are possible with NF membranes at higher transmembrane pressures (~ 60 bar).

The solution-diffusion model (SD) was employed to predict the flux and retention of single solute solutions of glucose and acetic acid. Film theory was used to model concentration polarization. Pure water permeability coefficients obtained are in consistent with the manufacturer's values. However, both solvent flux and solute retention predicted by SD model

are not in good agreement with the experimental data. We assume that high concentrations used in our experiments might be a cause for the mismatch.

This study shows that the separation of acids and other low molecular weight compounds from sugars in AFBO using NF membranes appears to be feasible, with two important caveats. First, the commercial membranes studied here were irreversibly damaged when brought in contact with phenolics, prevalent compounds in AFBO. A practical membrane process would require a different, resistant polymer formulation or a pretreatment to remove phenolics. Second, relatively high transmembrane pressures (~ 60 bar) are needed to achieve reasonably good retention of glucose (> 80%).

We synthesized organic-inorganic composite membranes by growing the melamine-based dendrimer directly off the commercial mesoporous alumina membranes. The permselectivity of the dendrimer-alumina composite membranes for propane over nitrogen is not changed significantly though there was a loss in permeance. PDMS-alumina composite membranes, especially the membranes modified with 7.5 mg/ml of PDMS concentration in toluene, showed propane/nitrogen selectivity values comparable with polymeric PDMS membranes. This study shows that we can modify permeation properties of nanocomposite membranes by rationally choosing selective organic materials to tailor membrane characteristics to the recovery of higher hydrocarbons from air.

BIBLIOGRAPHY

[1] G.W. Huber, S. Iborra, A. Corma, Synthesis of Transportation Fuels from Biomass: Chemistry, Catalysts, and Engineering, Chem. Rev., 106 (2006) 4044-4098.

[2] S. Czernik, a.V. Bridgwater, Overview of Applications of Biomass Fast Pyrolysis Oil, Energy & Fuels, 18 (2004) 590-598.

[3] A.V. Bridgwater, D. Meier, D. Radlein, An overview of fast pyrolysis of biomass, Org. Geochem., 30 (1999) 1479-1493.

[4] D. Mohan, C.U. Pittman, P.H. Steele, Pyrolysis of Wood/Biomass for Bio-oil: A Critical Review, Energy & Fuels, 20 (2006) 848-889.

[5] M. Mudler, Basic Principles of Membrane Technology, Kulwer Academic Publishers, 1996.

[6] W.S.W. Ho, K.K. Sirkar, Membrane Handbook, Kluwer Acedemic Publishers, 1992.

[7] T. Rachwal, S. Judd, A synopsis of membrane technologies in UK municipal potable water treatment: histroy, status and prospects, Water and Environmental Journal, 20 (2006) 110-113.

[8] B. Van der Bruggen, C. Vandecasteele, Distillation vs. membrane filtration: overview of process evolutions in seawater desalination, Desalination, 143 (2002) 207-218.

[9] G. Wade Miller, Integrated concepts in water reuse: managing global water needs, Desalination, 187 (2006) 65-75.

[10] M. Into, A.-S. Jönsson, G. Lengdén, Reuse of industrial wastewater following treatment with reverse osmosis, Journal of Membrane Science, 242 (2004) 21-25.

[11] L.R. Raman, M. Cheryan, N. Rajagopalan, Solvent recovery and partial deacidification of vegetable oils by membrane technology, Fett/Lipid, 98 (1996) 10-14.

[12] M.J. Bridge, K.W. Broadhead, V. Hlady, P.A. Tresco, Ethanol treatment alters the ultrastructure and permeability of PAN-PVC hollow fiber cell encapsulation membranes, Journal of Membrane Science, 195 (2002) 51-64.

[13] R. Subramanian, M. Nakajima, T. Kawakatsu, Processing of vegetable oils using polymeric composite membranes, Journal of Food Engineering, 38 (1998) 41-56.

[14] L.S. White, I.-F. Wang, B.S. Minhas, Polyimide membranes for separation of solvents from lube oil, in, US Patent 5, 264, 166, 1993.

[15] L.S. White, A.R. Nitsch, Solvent recovery from lube oil filtrates with a polyamide membrane, Journal of Membrane Science, 179 (2000) 267-274.

[16] A.V. Bridgwater, G.V.C. Peacocke, Fast pyrolysis processes for biomass, Renewable Sustainable Energy Rev., 4 (2000) 1-73.

[17] A.V. Bridgwater, Fast Pyrolysis of Biomass: A Handbook, in, CPL Press, 2002.

[18] T.P. Vispute, H. Zhang, A. Sanna, R. Xiao, G.W. Huber, Renewable chemical commodity feedstocks from integrated catalytic processing of pyrolysis oils, Science, 330 (2010) 1222-1227.

[19] Q. Lu, W.Z. Li, X.F. Zhu, Overview of fuel properties of biomass fast pyrolysis oils, Energy Convers. Manage., 50 (2009) 1376-1383.

[20] P. Badger, S. Badger, M. Puettmann, P. Steele, J. Cooper, Techno-Economic Analysis: Preliminary Assessment of Pyrolysis Oil Production Costs and Material and Energy Balance Associated with a Trasportable Fast Pyrolysis System, BioResources, 6 (2010) 34-47.

[21] M. Ringer, V. Putsche, J. Scahill, Large-Scale Pyrolysis Oil Production: A Technology Assessment and Economic Analysis, in, 2006.

[22] S.M. Ryan, P. Alexandru, J.A. Satrio, R.C. Brown, Techno-economic analysis of biomass-to-liquids production based on gasification, Fuel, 89 (2010) S11-S19.

[23] R.P. Anex, A. Aden, F.K. Kazi, J. Fortman, R.M. Swanson, M.M. Wright, J.A. Satrio, R.C. Brown, D.E. Daugaard, A. Platon, G. Kothandaraman, D.D. Hsu, A. Dutta, Techno-economic comparison of biomass-to-transportation fuels via pyrolysis, gasification, and biochemical pathways, Fuel, 89 (2010) S29-S35.

[24] T.P. Vispute, G.W. Huber, Production of hydrogen, alkanes and polyols by aqueous phase processing of wood-derived pyrolysis oils, Green Chem., 11 (2009) 1433-1445.

[25] G.W. Huber, R.D. Cortright, J.A. Dumesic, Renewable alkanes by aqueous-phase reforming of biomass-derived oxygenates, Angew. Chem., 116 (2004) 1575-1577.

[26] R.D. Cortright, R.R. Davda, J.A. Dumesic, Hydrogen from catalytic reforming of biomass-derived hydrocarbons in liquid water, Nature, 418 (2002) 964-967.

[27] D.C. Elliott, T.R. Hart, G.G. Neuenschwander, L.J. Rotness, A.H. Zacher, Catalytic hydroprocessing of biomass fast pyrolysis bio-oil to produce hydrocarbon products, Environmental Progress & Sustainable Energy, 28 (2009) 441-449.

[28] P.J. Dauenhauer, B.J. Dreyer, N.J. Degenstein, L.D. Schmidt, Millisecond Reforming of Solid Biomass for Sustainable Fuels, Angew. Chem. Int. Ed., 46 (2007) 5864-5867.

[29] I.M. de Manchilha, M.N. Karim, Evaluation of ion exchange resins for removal of inhibitory compounds from corn stover hydrolyzate for xylitol fermentation, Biotechnol. Prog., 19 (2003) 1837-1841.

[30] J.C. Parajo, H. Dominguez, J.M. Dominguez, Biotechnological production of xylitol. Part 3. Operation in culture media made from lignocellulosic hydrolysates, Bioresour. Technol., 66 (1998) 25-40.

[31] S.I. Musssatto, I.C. Roberto, Alternatives for detoxification of diluted-acid lignocellulosic hydrolysates for use in fermentative processes: a review, Bioresour. Technol., 93 (2004) 1-10.

[32] H.J. Huang, S. Ramaswamy, U.W. Tschirner, R.B. V., A review of separation technologies in current and future biorefineries, Sep. Purif. Technol., 62 (2008) 1-21.

[33] B. Han, W. Carvalho, L. Canilha, S.S. da Silva, J.B. Almeida e Silva, J.D. McMillan, S.R. Wickramasinghe, Adsorptive membranes vs. resins for acetic acid removal from biomass hydrolysates, Desalination, 193 (2006) 361-366.

[34] D.L. Grzenia, D.J. Schell, S.R. Wickramasinghe, Membrane extraction for removal of acetic acid from biomass hydrolysates, Journal of Membrane Science, 322 (2008) 189-195.

[35] A. Fick, Über diffusion, Annalen der Physik Chemie, 94 (1855) 59-86.

[36] T. Graham, On osmotic force, Philosophical Transactions of the Royal Society of London, 144 (1854) 177-228.

[37] T. Graham, On the absorption and dialytic separation of gases colloid septa, Philosophical Magazine, 32 (1866) 401-420.

[38] H.K. Lonsdale, The growth of membrane technology, Journal of Membrane Science, 10 (1982) 81-181.

[39] H. Bechhold, Investigations on colloids by filtration method, Biochem. Z., 6 (1907) 379-408.

[40] R. Zsigmondy, W. Bachmann, Über neue Filter, Z. Anorg. Chem., 103 (1918) 119-128.

[41] W.J. Elford, Principles governing the preparation of membranes having graded porosities. The properties of “gradocol” membranes as ultrafilters, Trans. Faraday. Soc., 33 (1937) 1094-1104.

[42] J.D. Ferry, Ultrafilter membranes and ultrafiltration, Chem. Rev., 18 (1936) 373-455.

[43] S. Loeb, S. Sourirajan, Sea water demineralization by means of an osmotic membrane, Advances in Chemistry Series, 38 (1962) 117-132.

[44] J.M.S. Henis, M.K. Tripodi, A novel approach to gas separation using composite hollow fiber membraes, Separation Science and Technology, 15 (1980) 1059-1068.

[45] E. Drioli, L. Giorno, Membrane operations: Innovative separations and transformation, in, Wiley-VCH Verlag GmbH & Co. KGaA, Weinheim, 2009.

[46] R.W. Baker, Membrane Technology and Applications, John Wiley & Sons, Ltd, West Sussex, England, 2004.

[47] R. Mahajan, W.J. Koros, Mixed matrix membrane materials with glassy polymers. Part 1, Polymer Engineering & Science, 42 (2002) 1420-1431.

[48] B. Van Der Bruggen, C. Vandecasteele, T. Van Gestel, W. Doyen, R. Leysen, A review of pressure-driven membrane processes in wastewater treatment and drinking water production, Environmental Progress, 22 (2003) 46-56.

[49] C.E. Reid, J.R. Kuppers, Physical characteristics of osmotic membranes of organic polymers, Journal of Applied Polymer Science, 2 (1959) 264-272.

[50] C.E. Reid, E.J. Breton, Water and ion flow across cellulosic membranes, Journal of Applied Polymer Science, 1 (1959) 133-143.

[51] J.E. Cadotte, Evolution of Composite Reverse Osmosis Membranes, in: Materials Science of Synthetic Membranes, American Chemical Society, 1985, pp. 273-294.

[52] T. Kawaguchi, H. Tamura, Chlorine-resistant membrane for reverse osmosis. I. Correlation between chemical structures and chlorine resistance of polyamides, Journal of Applied Polymer Science, 29 (1984) 3359-3367.

[53] J. Glater, S.-k. Hong, M. Elimelech, The search for a chlorine-resistant reverse osmosis membrane, Desalination, 95 (1994) 325-345.

[54] S. Avlonitis, W.T. Hanbury, T. Hodgkeiss, Chlorine degradation of aromatic polyamides, Desalination, 85 (1992) 321-334.

[55] G.M. Geise, H.-S. Lee, D.J. Miller, B.D. Freeman, J.E. McGrath, D.R. Paul, Water purification by membranes: The role of polymer science, Journal of Polymer Science Part B: Polymer Physics, 48 (2010) 1685-1718.

[56] C.S. Slater, R.C. Ahlert, C.G. Uchrin, Applications of reverse osmosis to complex industrial wastewater treatment, Desalination, 48 (1983) 171-187.

[57] A.H. Ghabris, M. Abdel-Jawad, G.S. Aly, Municipal wastewater renovation by reverse osmosis state of the art, Desalination, 75 (1989) 213-240.

[58] A.S. Jönsson, R. Wimmerstedt, The application of membrane technology in the pulp and paper industry, Desalination, 53 (1985) 181-196.

[59] S. Basu, V.S. Sapkal, Membrane technique in simplification of soda recovery process in pulp and paper industry, Desalination, 67 (1987) 371-379.

[60] M.E. Williams, D. Bhattacharyya, R.J. Ray, S.B. McCray, Selected applications of reverse osmosis, in: W.S.W. Ho, K.K. Sirkar (Eds.) Membrane Handbook, Van Nostrand reinhold, New York, 1992, pp. 312-354.

[61] F.G. Donnan, The Theory of Membrane Equilibria, Chem. Rev., 1 (1924) 73-90.

[62] J. Schaep, B. Van der Bruggen, S. Uytterhoeven, R. Croux, C. Vandecasteele, D. Wilms, E. Van Houtte, F. Vanlerberghe, Removal of hardness from groundwater by nanofiltration, Desalination, 119 (1998) 295-301.

[63] B.M. Watson, C.D. Hornburg, Low-energy membrane filtration for removal of color, organics and hardness from drinking water supplies, Desalination, 72 (1989) 11-22.

[64] A. Wahab Mohammad, R. Othaman, N. Hilal, Potential use of nanofiltration membranes in treatment of industrial wastewater from Ni-P electroless plating, Desalination, 168 (2004) 241-252.

[65] B. Van der Bruggen, I. De Vreese, C. Vandecasteele, Water Reclamation in the Textile Industry: Nanofiltration of Dye Baths for Wool Dyeing, Industrial & Engineering Chemistry Research, 40 (2001) 3973-3978.

[66] J.M.K. Timmer, J. Kromkamp, T. Robbertsen, Lactic acid separation from fermentation broths by reverse osmosis and nanofiltration, Journal of Membrane Science, 92 (1994) 185-197.

[67] M.I. González, S. Alvarez, F.A. Riera, R. Álvarez, Lactic acid recovery from whey ultrafiltrate fermentation broths and artificial solutions by nanofiltration, Desalination, 228 (2008) 84-96.

[68] Y. Pouliot, M.C. Wijers, S.F. Gauthier, L. Nadeau, Fractionation of whey protein hydrolysates using charged UF/NF membranes, Journal of Membrane Science, 158 (1999) 105-114.

[69] B. Van der Bruggen, C. Vandecasteele, Removal of pollutants from surface water and groundwater by nanofiltration: overview of possible applications in the drinking water industry, Environmental Pollution, 122 (2003) 435-445.

[70] P. Berg, G. Hagmeyer, R. Gimbel, Removal of pesticides and other micropollutants by nanofiltration, Desalination, 113 (1997) 205-208.

[71] K. Ebert, F.P. Cuperus, Solvent resistant nanofiltration membranes in edible oil processing, Membrane Technology, 1999 (1999) 5-8.

[72] B. Van der Bruggen, J. Geens, C. Vandecasteele, Fluxes and rejections for nanofiltration with solvent stable polymeric membranes in water, ethanol and n-hexane, Chemical Engineering Science, 57 (2002) 2511-2518.

[73] Y. Zhao, Q. Yuan, Effect of membrane pretreatment on performance of solvent resistant nanofiltration membranes in methanol solutions, Journal of Membrane Science, 280 (2006) 195-201.

[74] D.R. Machado, D. Hasson, R. Semiat, Effect of solvent properties on permeate flow through nanofiltration membranes. Part I: investigation of parameters affecting solvent flux, Journal of Membrane Science, 163 (1999) 93-102.

[75] D.R. Machado, D. Hasson, R. Semiat, Effect of solvent properties on permeate flow through nanofiltration membranes: Part II. Transport model, Journal of Membrane Science, 166 (2000) 63-69.

[76] D. Bhanushali, S. Kloos, C. Kurth, D. Bhattacharyya, Performance of solvent-resistant membranes for non-aqueous systems: solvent permeation results and modeling, Journal of Membrane Science, 189 (2001) 1-21.

[77] R. Subramanian, M. Nakajima, K. Raghavarao, T. Kimura, Processing vegetable oils using nonporous denser polymeric composite membranes, Journal of the American Oil Chemists' Society, 81 (2004) 313-322.

[78] H. Zwijnenberg, A. Krosse, K. Ebert, K. Peinemann, F. Cuperus, Acetone-stable nanofiltration membranes in deacidifying vegetable oil, Journal of the American Oil Chemists' Society, 76 (1999) 83-87.

[79] J.P. Sheth, Y. Qin, K.K. Sirkar, B.C. Baltzis, Nanofiltration-based diafiltration process for solvent exchange in pharmaceutical manufacturing, Journal of Membrane Science, 211 (2003) 251-261.

[80] P. Vandezande, L.E.M. Gevers, I.F.J. Vankelecom, Solvent resistant nanofiltration: separating on a molecular level, Chemical Society Reviews, 37 (2008) 365-405.

[81] I.S. Han, M. Cheryan, Nanofiltration of model acetate solutions, J. Membr. Sci., 107 (1995) 107-113.

[82] M. Sagehashi, T. Nomura, H. Shishido, A. Sakoda, Separation of phenols and furfural by pervaporation and reverse osmosis membranes from biomass-superheated steam pyrolysis-derived aqueous solution, Bioresour. Technol., 98 (2007) 2018-2026.

[83] Y.-H. Weng, H.-J. Wei, T.-Y. Tsai, T.-H. Lin, T.-Y. Wei, G.-L. Guo, C.-P. Huang, Separation of furans and carboxylic acids from sugars in dilute acid rice straw hydrolyzates by nanofiltration, Bioresour. Technol., 101 (2010) 4889-4894.

[84] E. Sjöman, M. Mänttäri, M. Nyström, H. Koivikko, H. Heikkilä, Separation of xylose from glucose by nanofiltration from concentrated monosaccharide solutions, Journal of Membrane Science, 292 (2007) 106-115.

[85] Y.H. Weng, H.J. Wei, T.Y. Tsai, W.H. Chen, T.Y. Wei, W.S. Hwang, C.P. Wang, C.P. Huang, Separation of acetic acid from xylose by nanofiltration, Sep. Purif. Technol., 67 (2009) 95-102.

[86] V.G.B. Berg, I.G. Rácz, C.A. Smolders, Mass transfer coefficients in cross-flow ultrafiltration, Journal of Membrane Science, 47 (1989) 25-51.

[87] G.B. van den Berg, I.G. Rácz, C.A. Smolders, Mass transfer coefficients in cross-flow ultrafiltration, Journal of Membrane Science, 47 (1989) 25-51.

[88] M. Mänttäri, A. Pihlajamäki, E. Kaipainen, M. Nyström, Effect of temperature and membrane pre-treatment by pressure on the filtration properties of nanofiltration membranes, Desalination, 145 (2002) 81-86.

[89] V.B. Bruggen, J. Schaep, D. Wilms, C. Vandecasteele, Influence of molecular size, polarity and charge on the retention of organic molecules by nanofiltration, J. Membr. Sci., 156 (1999) 29-41.

[90] P. Pontalier, A. Ismail, M. Ghoul, Mechanisms for the selective rejection of solutes in nanofiltration membranes, Sep. Purif. Technol., 12 (1997) 175-181.

[91] H.K. Lonsdale, U. Merten, T. Tagami, Phenol transport in cellulose acetate membranes, J. Appl. Polym. Sci., 11 (1967) 1807-1820.

[92] G. Laufenberg, S. Hausmanns, B. Kunz, The influence of intermolecular interactions on the selectivity of several organic acids in aqueous multicomponent systems during reverse osmosis, J. Membr. Sci., 110 (1996) 59-68.

[93] E. Vellenga, G. Trägårdh, Nanofiltration of combined salt and sugar solutions: coupling between retentions, Desalination, 120 (1998) 211-220.

[94] X.J. Yang, A.G. Livingston, L.F. Santos, Experimental observations of nanofiltration with organic solvents, J. Membr. Sci., 190 (2001) 45-55.

[95] A.K. Goulas, P.G. Kapasakalidis, H.R. Sinclair, R.A. Rastall, A.S. Grandison, Purification of oligosaccharides by nanofiltration, J. Membr. Sci., 129 (2002) 312-335.

[96] A. Katchalsky, P.F. Curran, Nonequilibrium thermodynamics in biophysics, Harvard University Press, Cambridge, MA, 1965.

[97] O. Kedem, A. Katchalsky, Thermodynamic analysis of the permeability of biological membranes to non-electrolytes, Biochim. Biophys. Acta, 27 (1958) 229-246.

[98] R.B. Bird, W.E. Stewart, E.N. Lightfoot, Transport phenomena, J. Wiley, 2007.

[99] W.L. McCabe, J.C. Smith, P. Harriott, Unit operations of chemical engineering, McGraw-Hill, 2005.

[100] M. Perry, C. Linder, Intermediate reverse osmosis ultrafiltration (RO UF) membranes for concentration and desalting of low molecular weight organic solutes, Desalination, 71 (1989) 233-245.

[101] M. Soltanieh, W.N. Gill, REVIEW OF REVERSE OSMOSIS MEMBRANES AND TRANSPORT MODELS, Chemical Engineering Communications, 12 (1981) 279 - 363.

[102] S. Rosenbaum, W.E. Skiens, Concentration and pressure dependence of rate of membrane permeation, Journal of Applied Polymer Science, 12 (1968) 2169-2181.

[103] M.B. Rao, S. Sircar, Performance of pore characterization of nanoporous carbon membranes for gas separation, J. Membr. Sci., 85 (1993) 253-264.

[104] B.D. Freeman, I. Pinnau, Separation of gases using solubility-selective polymers, Trends in Polymer Science, 5 (1997) 167-173.

[105] L.M. Robeson, Polymer membranes for gas separation, Current Opinion in Solid State and Materials Science, 4 (1999) 549-552.

[106] M. Moaddeb, W.J. Koros, Gas transport properties of thin polymeric membranes in the presence of silicon dioxide particles, J. Membr. Sci., 125 (1997) 143-163.

[107] T.C. Merkel, B.D. Freeman, R.J. Spontak, Z. He, I. Pinnau, P. Meakin, A.J. Hill, Ultrapermeable, reverse-selective nanocomposite membranes, Science, 296 (2002) 519-522.

[108] M. Smaihi, T. Jermoumi, J. Marignan, R.D. Noble, Organic-inorganic gas separation membranes: Preparation and characterizzation, J. Membr. Sci., 116 (1996) 211-220.

[109] I.F.J. Vankelecom, E. Merckx, M. Luts, J.B. Uytterhoeven, Incorporation of zeolites in polyimide membranes, J. Phys. Chem., 99 (1995) 13187-13192.

[110] A. Javaid, M.P. Hughey, V. Varutbangkul, D.M. Ford, Solubility-based gas separation with oligomer-modified inorganic membranes, Journal of Membrane Science, 187 (2001) 141-150.

[111] J. Randon, R. Paterson, Preliminary studies on the potential for gas separation by mesoporous ceramic oxide membranes surface modified by alkyl phosphonic acids, Journal of Membrane Science, 134 (1997) 219-223.

[112] A. Javaid, S.O. Gonzalez, E.E. Simanek, D.M. Ford, Nanocomposite membranes of chemisorbed and physisorbed molecules on porous alumina for environmentally important separations, Journal of Membrane Science, 275 (2006) 255-260.

[113] K.C. McCarley, J.D. Way, Development of a model surface flow membrane by modification of porous γ-alumina with octadecyltrichlorosilane, Separation and Purification Technology, 25 (2001) 195-210.

[114] O.A. Matthews, A.N. Shipway, J.F. Stoddart, Dendrimers-branching out from curiosities into new technologies, Progress in Polymer Science, 23 (1998) 1-56.

[115] W. Zhang, E.E. Simanek, Dendrimers based on melamine. Divergent and convergent synthesis of a G3 dendrimer, Organic letters 2(2000) 843-845.

[116] S. Yoo, S. Yeu, R.L. Sherman, E.E. Simanek, D.F. Shantz, D.M. Ford, Reverse-selective membranes formed by dendrimers on mesoporous ceramic supports, Journal of Membrane Science, 334 (2009) 16-22.

[117] W.R. Baker, N. Yoshioka, M.J. Mohr, J.A. Khan, Separation of organic vapors from air, Journal of Membrane Science, 31 (1987) 259-271.

[118] I. Blume, P.J.F. Schwering, M.H.V. Mulder, C.A. Smolders, Vapour sorption and permeation properties of poly (dimethylsiloxane) films, Journal of Membrane Science, 61 (1991) 85-97.

[119] M. Leemann, G. Eigenberger, H. Strathmann, Vapour permeation for the recovery of organic solvents from waste air streams: separation capacities and process optimization, Journal of Membrane Science, 113 (1996) 313-322.

[120] J. Schultz, K.V. Pienemann, Membranes for separation of higher hydrocarbons from methane, Journal of Membrane Science, 110 (1996) 37-45.

[121] G.R. Gallaher, P.K.T. Liu, Characterization of ceramic membranes I. Thermal and hydrothermal stabilities of commercial 40 Å membranes, Journal of Membrane Science, 92 (1994) 29-44.

[122] C.L. Lin, D.L. Flowers, P.K.T. Liu, Characterization of ceramic membranes II. Modified commercial membranes with pore size under 40 Å, Journal of Membrane Science, 92 (1994) 45-58.

[123] R.C. Furneaux, W.R. Rigby, A.P. Davidson, The formation of contorlled-porosity membranes from anodically oxidized membrane, Nature, 337 (1989) 147-149.

[124] A. Hernandez, J.I. Calvo, P. Pradanos, L. Palacio, M.L. Rodriguez, J.A. de Saja, Surface structure of microporous membranes by cmputerized SEM image analysis applied to anopore filters, Journal of Membrane Science, 137 (1997) 89-97.

[125] M. Platt, R.A.W. Dryfe, E.P.L. Roberts, Voltammetry with liquid/liquid microarrays: Characterization of membrane materials, Langmuir, 19 (2003) 8019-8025.

[126] J. Karger, D.M. Ruthven, Diffusion in zeolites and other microporous solids, New York, 1992.

[127] K. Keizer, R.J.R. Uhlhorn, R.J. Van Vuren, A.J. Burggraaf, Gas separation mechanism in microporous modified γ-Al_2O_3 membranes, Journal of Membrane Science, 39 (1988) 285-300.

[128] R.J.R. Uhlhorn, K. Keizer, A.J. Burggraaf, Gas transport and separation with ceramic membranes. Part I. Multilayer diffusion and capillary condensation, Journal of Membrane Science, 66 (1992) 259-269.